

Synthesis of Zeolite 13X and 4A Monolith for CO₂ Adsorption



By

Mamoona Safeer

(Registration No: 00000364018)

School of Chemical and Materials Engineering

National University of Sciences & Technology (NUST)

Islamabad, Pakistan

(2024)

Synthesis of Zeolite 13X and 4A Monolith for CO₂ Adsorption



By

Name: Mamoona Safeer

(Registration No: 00000364018)

A thesis submitted to the National University of Sciences and Technology, Islamabad,

in partial fulfillment of the requirements for the degree of

**Master of Science in
Chemical Engineering**

ⁱSupervisor Name: Dr. Tayyaba Noor

Co Supervisor: Dr. Sher Ahmad

School of Chemical and Materials Engineering

National University of Sciences and Technology (NUST)

Islamabad, Pakistan

(2024)



THESIS ACCEPTANCE CERTIFICATE

Certified that final copy of MS Thesis written by Ms **Mamoona Safeer** (Registration No 00000364018), of School of Chemical & Materials Engineering (SCME) has been vetted by undersigned, found complete in all respects as per NUST Statues/Regulations, is free of plagiarism, errors, and mistakes and is accepted as partial fulfillment for award of MS degree. It is further certified that necessary amendments as pointed out by GEC members of the scholar have also been incorporated in the said Thesis.

Signature: *Tayyaba*

Name of Supervisor: Dr Tayyaba Noor

Date: 25/3/24

Signature (HOD): *SB*

Date: 25/3/24

Signature (Dean/Principal): *AS*

Date: 25.3.2024



Form: TH-04

National University of Sciences & Technology (NUST)

MASTER'S THESIS WORK

We hereby recommend that the dissertation prepared under our supervision by
Regn No & Name: 00000364018 Mamoona Safer

Title: Synthesis of Zeolite 13X and 4A Monoliths for CO₂ Adsorption.

Presented on: 21 Mar 2024 at: 1200 hrs in SCME Seminar Hall

Be accepted in partial fulfillment of the requirements for the award of Master of Science degree
in Chemical Engineering.

Guidance & Examination Committee Members

Name: Dr Sarah Farrukh

Signature: Sarah Farrukh

Name: Dr Erum Pervaiz

Signature: EB

Name: Dr Sher Ahmad (Co-Supervisor)

Signature: SA

Supervisor's Name: Dr Tayyaba Noor

Signature: Tayyaba

Dated: 22.03.2024

EB
Head of Department

Date 22/3/24

AG
Dean/Principal

Date 22-3-2024

School of Chemical & Materials Engineering (SCME)

AUTHOR'S DECLARATION

I Mamoona Safeer hereby state that my MS thesis titled "Synthesis of Zeolite 13X and 4A Monolith for CO₂ Adsorption" is my own work and has not been submitted previously by me for taking any degree from National University of Sciences and Technology, Islamabad or anywhere else in the country/ world.

At any time if my statement is found to be incorrect even after I graduate, the university has the right to withdraw my MS degree.

Name of Student: Mamoona Safeer

Date: 25/3/24

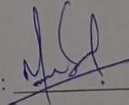
PLAGIARISM UNDERTAKING

I solemnly declare that research work presented in the thesis titled "Synthesis of Zeolite 13X and 4A Monolith for CO₂ Adsorption" is solely my research work with no significant contribution from any other person. Small contribution/ help wherever taken has been duly acknowledged and that complete thesis has been written by me.

I understand the zero tolerance policy of the HEC and National University of Sciences and Technology (NUST), Islamabad towards plagiarism. Therefore, I as an author of the above titled thesis declare that no portion of my thesis has been plagiarized and any material used as reference is properly referred/cited.

I undertake that if I am found guilty of any formal plagiarism in the above titled thesis even after award of MS degree, the University reserves the rights to withdraw/revoke my MS degree and that HEC and NUST, Islamabad has the right to publish my name on the HEC/University website on which names of students are placed who submitted plagiarized thesis.

Student Signature: _____



Name: Mamoonah Safeer

DEDICATION

Dedicated to Almighty Allah, my beloved family, and my supervisor. It could not have been possible without them.

ACKNOWLEDGEMENTS

Blessings foremost, I extend my utmost gratitude to **Allah Almighty**, whose unwavering blessings and guidance have illuminated my path and fueled my determination. Your divine guidance has been my source of strength and inspiration, and for that, I am eternally grateful.

My deepest gratitude to Principal SCME Dr. Amir Azam Khan for helping to facilitate our research project and serving as a wonderful source of inspiration.

I would like to express my sincere appreciation to my supervisor, Dr. Tayyaba Noor, for her exceptional mentorship, unwavering encouragement, and profound insights. Your expertise and dedication have been pivotal in shaping my research and fostering my growth as a scholar. I am truly fortunate to have had the privilege to learn from you. I am equally indebted to my co-supervisor, and my sincere gratitude to Dr. Sher Ahmad for her invaluable guidance, which has been instrumental in refining and broadening my perspectives. I also extend heartfelt appreciation to the esteemed members of the GEC, Dr. Sarah Farrukh, and Dr Erum Pervaiz, whose constructive feedback and dedication to academic excellence have greatly enhanced the quality of my research.

My gratitude extends to my Parents and Siblings whose unwavering love, encouragement, and sacrifices have been the cornerstone of my journey. Your belief in me has been my driving force, and I am humbled by your constant support. I appreciate my family a great deal for their unwavering affection. I appreciate your confidence in me, your desire for my success, and your encouragement to pursue my passion. I appreciate your financial and emotional assistance. I appreciate all my friends' help, counsel, and inspiration.

I would like to acknowledge Muhammad Munib-ul-Hassan for your contributions have played a significant role in shaping this achievement, and I am deeply thankful for everything you have done. I would also like to acknowledge the support and assistance of the lab support staff at SCME, whose dedication has ensured a conducive research environment. My heartfelt thanks to my fellow lab mates and colleagues who have shared in this journey. Your camaraderie, exchange of ideas, and collaborative spirit have enriched my experience and made this journey memorable.

TABLE OF CONTENTS

ACKNOWLEDGEMENTS	viii
TABLE OF CONTENTS.....	ix
LIST OF FIGURES	xiii
LIST OF TABLES.....	xv
LIST OF SYMBOLS, ABBREVIATIONS AND ACRONYMS.....	xvi
ABSTRACT.....	xvii
1. CHAPTER 1 INTRODUCTION.....	1
1.1 Background	1
1.2 Carbon Dioxide: A Greenhouse Gas	2
1.3 Carbon Capture and Storage.....	4
1.4 Pre combustion technology	6
1.5 Post Combustion Technology	7
1.6 Oxy-Flame Combustion Technology	7
1.7 Chemical Looping Combustion Technology.....	8
1.8 Separation Techniques.....	11
1.8.1 Absorption.....	12
1.8.2 Adsorption.....	13
1.8.3 Membrane Separation	14
1.8.4 Cryogenic Distillation.....	15
1.9 Adsorbents for Carbon Dioxide Capture.....	16
1.10 Introduction to Zeolites	17
1.11 Synthesis of Zeolites.....	19
1.11.1 Hydrothermal Synthesis.....	19
1.11.2 Solvothermal method	20

1.11.3	Ionothermal method	22
1.11.4	Sol-gel method	22
1.12	Applications of Zeolites	23
1.12.1	Catalytic Properties	24
1.12.2	Adsorption.....	25
1.12.3	Ion Exchange Properties of Zeolites	26
1.12.4	Purification of Water	26
2.	CHAPTER 2 LITERATURE REVIEW	28
3.	CHAPTER 3 EXPERIMENTATION	32
3.1	Synthesis of Zeolite 13X.....	32
3.1.1	Materials	32
3.1.2	Method of Preparation	33
3.2	Synthesis of zeolite 4A	33
3.2.1	Materials	34
3.2.2	Method of Preparation	34
3.3	Synthesis of Zeolite 13x Monolith.....	35
3.3.1	Materials	36
3.3.2	Method of Preparation	36
3.4	Synthesis of zeolite 4A monolith	36
3.4.1	Materials	36
3.4.2	Method of Preparation	37
3.5	Synthesis of zeolite 13X and 4A monolith.....	37
3.5.1	Materials	37
3.5.2	Method of Preparation	38
4.	CHAPTER 4 CHARACTERIZATION TECHNIQUES.....	39

4.1	Scanning Electron Microscope	39
4.2	X-Ray Diffraction.....	40
4.3	Fourier Transform Infrared spectroscopy (FTIR)	41
4.4	BET.....	42
4.5	CO₂ Capture Study	43
4.6	Particle Size Analyzer	45
5.	CHAPTER 5 RESULTS AND DISSCUSIONS	46
5.1	Characterization Techniques	46
5.2	Scanning Electron Microscope	46
5.2.1	SEM Image of zeolite 13X	46
5.2.2	SEM Image of Zeolite 4A.....	47
5.2.3	SEM Image of zeolite monolith 13X at 0.5 μ m, 1 μ m, 5 μ m.	48
5.2.4	SEM Image of zeolite monolith 4A, at 0.5 μ m, 1 μ m, 5 μ m.	49
5.2.5	SEM Image of zeolite monolith 13X+4A, at 0.5 μ m, 1 μ m, 5 μ m.	50
5.3	BET.....	51
5.4	Particle Size Analyzer	53
5.5	Fourier Transform Infrared spectroscopy (FTIR)	54
5.6	X-Ray Diffraction.....	55
5.7	CO₂ Adsorption study.....	57
5.7.1	Adsorption & Desorption Isotherms of Zeolite 13X	58
5.7.2	Adsorption & Desorption Isotherms of Zeolite 4A	59
5.7.3	Adsorption & Desorption Isotherms of Zeolite 13X Monolith	61
5.7.4	Adsorption & Desorption Isotherms of Zeolite 4A Monolith.....	62
5.7.5	Adsorption & Desorption Isotherms of Zeolite 13X + 4A Monolith	63
5.7.6	Comparison with literature	65

6. CHAPTER 6	CONCLUSIONS AND RECOMMANDATION.....	67
6.1	Future Recommendations	67
REFERENCES.....		69

LIST OF FIGURES

Figure 1-1. Visual heat trapped by carbon dioxide. [15].....	4
Figure 1-2. Overall process of carbon capture and storage. [16].....	4
Figure 1-3. Comparison of different carbon capture technologies[20].....	5
Figure 1-4. Block diagram of pre combustion technology[22].....	6
Figure 1-5. Block diagram of post-combustion technology [22].....	7
Figure 1-6. Block diagram of Oxy-combustion technology [22].....	8
Figure 1-7. Schematic of chemical looping combustion technology [25].....	9
Figure 1-8. Schematic of chemical looping combustion technology [26].....	10
Figure 1-9. Techniques for CO ₂ capture [27].....	11
Figure 1-10. Process flow diagram of amine-based carbon capture through absorption [28].....	13
Figure 1-11. Multistage fluidized bed with downer and heat exchanger. [29].....	14
Figure 1-12. Cryogenic distillation column process. [28].....	15
Figure 1-13. The pores in between the aluminum, silicon, and oxygen atoms in zeolites [32]...	19
Figure 1-14. Hydrothermal method of zeolite synthesis [33].....	19
Figure 1-15. General schematic of all solvothermal methods (including hydrothermal and ionothermal) for the synthesis of zeolite. [34].....	21
Figure 1-16. Sol-gel method for synthesis of zeolite. [34].....	23
Figure 1-17. Brønsted acid sites in zeolites framework [35].....	24
Figure 1-18. Vapor-phase acetic acid esterification with ethanol [35].....	25
Figure 1-19. Zeolites use for water purification.....	27
Figure 3-1. Zeolite 13X.....	32
Figure 3-2. Zeolite 4A.....	34
Figure 3-3. Schematic Of synthesis of zeolites.....	35
Figure 3-4. Schematic of Synthesis of Zeolite Monolith.....	38
Figure 4-1. Schematic of SEM [49].....	40
Figure 4-2. Working principle of XRD[50].....	41
Figure 4-3. Schematic of FTIR [51].....	42
Figure 4-4. Process of CO ₂ adsorption [52].....	44
Figure 4-5. Schematic of Malvern particle size analyzer system.....	45

Figure 5-1. SEM Images Of 13X Zeolite at 0.5 μ m, 1 μ m and 5 μ m	47
Figure 5-2. SEM image of zeolite 4A	48
Figure 5-3. SEM Image of zeolite monolith 13X at 0.5 μ m, 1 μ m,5 μ m.....	48
Figure 5-4. EDX OF Zeolite 13X Monolith	49
Figure 5-5. SEM Image of zeolite monolith 4A at 0.5 μ m, 1 μ m, 5 μ m.	49
Figure 5-6. SEM Image of zeolite monolith 13X, 4A, and combine 13x+4A at 0.5 μ m, 1 μ m, 5 μ m.	50
Figure 5-7. EDX of 13X and 4A monolith.....	51
Figure 5-8. EDX of Activated carbon	51
Figure 5-9. Size distribution of particle sizes of synthesized 4A zeolite	53
Figure 5-10. Size distribution of particle sizes of synthesized 13X zeolite	54
Figure 5-11. Combined FTIR of zeolites and its monoliths.....	55
Figure 5-12. XRD of Zeolites	56
Figure 5-13. XRD of Zeolite Monoliths	57
Figure 5-14. Adsorption/Desorption Isotherm of zeolite 13X	59
Figure 5-15. Adsorption/Desorption isotherm of Zeolite 4A.....	60
Figure 5-16. Adsorption/Desorption Isotherm of zeolite 13X Monolith	61
Figure 5-17. Adsorption/Desorption Isotherm of zeolite 4A monolith	63
Figure 5-18. Adsorption/Desorption Isotherm of zeolite 13X +4A Monolith	64

LIST OF TABLES

Table 3-1. Chemicals used in the synthesis properties.....	33
Table 3-2. Properties of chemicals used in synthesis.....	36
Table 3-3. Chemical properties of materials used in the synthesis of zeolite 4A monolith.....	37
Table 3.4. Chemical properties of materials used in the synthesis of zeolite 13X and 4A monolith.	38
Table 5-1. Physical Properties of adsorbents (SA: surface area, PV: pore volume and APD: average pore diameter).....	52
Table 5-2. Summary of CO ₂ adsorption analysis.....	65
Table 5-3. Comparison table of zeolites and its monoliths.....	66

LIST OF SYMBOLS, ABBREVIATIONS AND ACRONYMS

ZSM	Zeolite Socony Mobil
GHG	Greenhouse gas
CCS	Carbon capture and storage
Na	Sodium
CO₂	Carbon dioxide
Si	Silicon
CH₄	Methane
Na₂O	Sodium Oxide
Al₂O₃	Aluminum Oxide
SiO₂	Silicon Oxide
AC	Activated Carbon
DI	Deionized Water
SEM	Scanning electron microscopy
XRD	X-ray Diffraction
EDX	Energy Dispersive X-ray
PSA	Particle Size Analyzer
BET	Brunauer-Emmett-Teller
FTIR	Fourier Transform Infrared Spectroscopy
NOAA	National Oceanic and Atmospheric Administration
Ads/Des	Adsorption/Desorption

ABSTRACT

Fossil fuels are one of the most abundant fuel resources in the world, the combustion of which fulfills much of our energy needs. Such energy resources with high CO₂ emissions contribute a lot to global climate change. To alleviate the atmospheric concentration of CO₂, some tangible measures are required. Carbon capture and storage is a technique that has presented some promising results toward the reduction of climate change and global warming. Carbon capture is the most important part of the process. Gas separation has made extensive use of solid adsorbents. Nonporous inorganic materials called zeolites have applications as adsorbents in carbon capture. This thesis explores the fabrication, characterization, and adsorption analysis of 13X and 4A zeolites, monolith synthesized using these zeolites and their mixture. Zeolite 13X + 4A monolith had the highest uptake of carbon dioxide. Zeolites have the potential for a wide range of applications, because of their large surface area, specific pore sizes, low cost, and molecular sieving ability.

The zeolite samples were analyzed for adsorption and desorption activities of CO₂ using a high-pressure sorption analyzer, also analyzed their surface characteristics were studied and morphology using SEM analysis, and X-ray diffraction to see the crystallinity of samples, and the presence of different functional groups was confirmed using FTIR spectroscopy. At a temperature of 50°C and a pressure of 0-15 bar, the adsorption and desorption of these samples were investigated.

In general, monoliths are synthesized with high surface area, easy-to-regenerate, defined structure designs, and high pore volume presenting higher adsorption/desorption capacity for carbon dioxide. Zeolite 13X+4A had the highest molar adsorption of 4.90mmol/g amongst the five studied samples. The monolith of zeolite 4A and 13X had the adsorption capacity of 2.50 and 3.68 mmol/g, respectively. While the 4A and 13X had an adsorption capacity of 1.20 and 2.94 mmol/g, respectively. Also, the adsorption of carbon dioxide increased in each case with the increase in pressure because of higher collisions.

Keywords: Greenhouse Effect, Zeolite, Zeolite 13X, Zeolite 4A, Zeolite Monolith, Zeolite 13X Monolith, Zeolite 4A Monolith, Zeolite 13X+4A Monolith, Carbon dioxide Adsorption Study

CHAPTER 1 INTRODUCTION

1.1 Background

According to estimates from the Energy Information Administration, energy consumption will increase by 57% by 2030 [1]. Worldwide, due to the industrial revolution, a large increase in energy use, and greenhouse gas emissions has resulted in numerous environmental problems. CO₂ emissions are responsible for about 60% of environmental issues, such as global temperature rise and climate change [2]. Of all the greenhouse gases caused by human activity, carbon dioxide is the most notable. As of right now, it is estimated that the annual increase in CO₂ concentration is 2 parts per million [3]. Reducing human activity is a crucial way to control the levels of CO₂. In general, a few tactics can be used to reduce the amount of CO₂ released into the atmosphere. By using biomass and H₂ for commercial purposes and substituting fossil fuels—the combustion of fossil fuels is the primary source of CO₂ emissions—efficient and appropriate energy use, and the creation of novel CO₂ capture technologies [4]. To extract the CO₂, a variety of technologies are used, including membrane gas adsorption, amine absorption, and cryogenic distillation. Research is being done on the unique idea of CO₂ collection and adsorption. Adsorbents with a wide range of properties are used to capture CO₂. Because adsorptive materials employ a simple process of physisorption to capture carbon dioxide molecules, they utilize less energy than conventional systems. Because of its low cost, minimal sensitivity, and thermal stability, activated carbon has been employed widely. Alumina, and silica have demonstrated impressive CO₂ adsorption performance; nevertheless, the release of the absorbed carbon dioxide demands a significant amount of energy, resulting in lower energy efficiency and higher costs. One of the main disadvantages of these conventional adsorbents is their limited capacity and challenging regeneration procedure[5]. The primary obstacle for carbon dioxide collecting devices is that the material utilized for capturing CO₂ needs to be readily regenerable. Zeolites' vast surface area, particular pore sizes, inexpensive cost, and molecular sieving capacity make them suitable for a variety of uses, including adsorbents, molecular sieves, and catalysts.[6]. Zeolites have good desorption properties and a high capacity for adsorbing carbon dioxide. It has been demonstrated that zeolite exhibits noticeably higher CO₂ adsorption selectivity[7]. For CO₂ adsorption, a variety of synthesized zeolites, such as A, X, ZSM-5, and beta, are widely utilized [8].

1.2 Carbon Dioxide: A Greenhouse Gas

Also known as a greenhouse gas, carbon dioxide (CO₂) absorbs heat. Fossil fuels, such as coal, oil, and natural gas, as well as wildfires and other natural occurrences like volcanic eruptions, are the sources of it. The atmospheric CO₂ concentrations that NOAA has been monitoring at Hawaii's Mauna Loa Observatory since 1958 are shown in the first graph. [9]

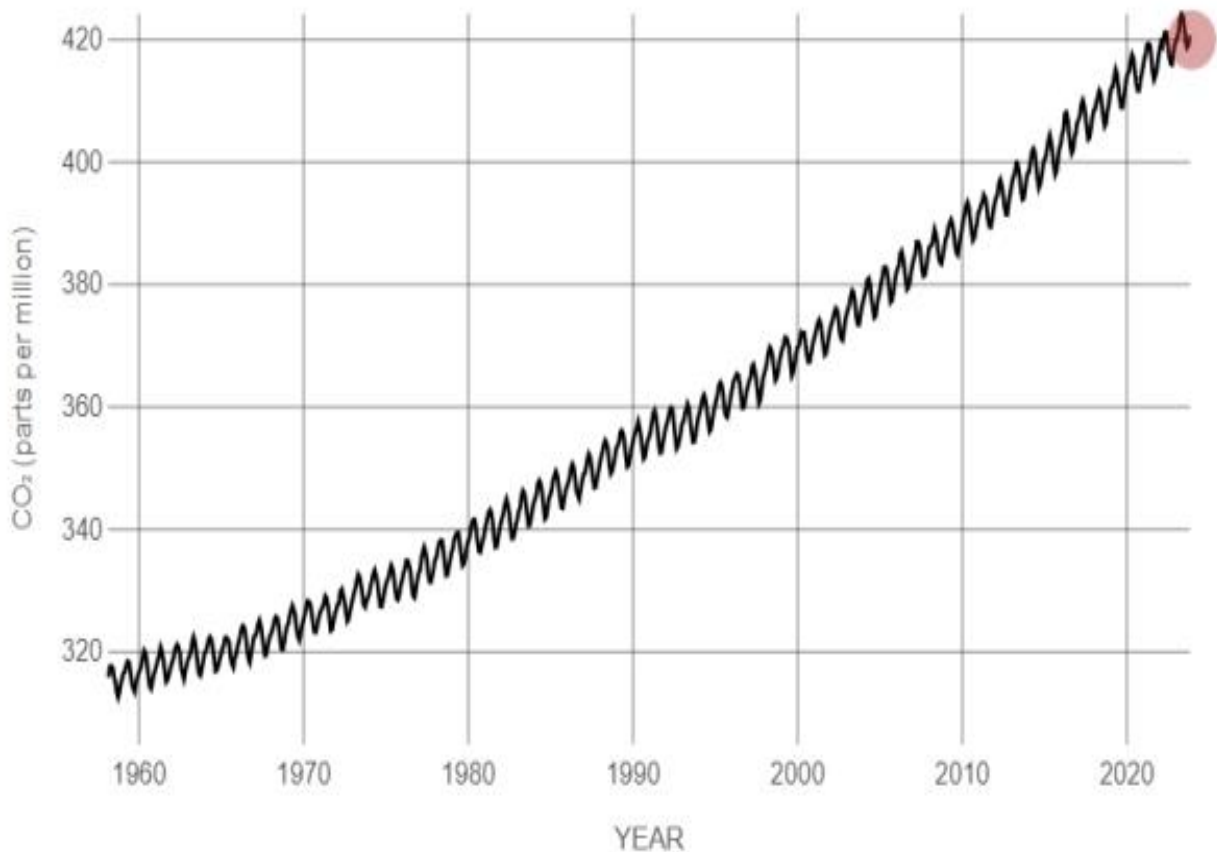


Figure 1-1. Change in concentration of carbon dioxide over the decades.[9]

Since the industrial revolution, there has been a noticeable increase in the atmospheric concentration of carbon dioxide (CO₂) and other greenhouse gases. The main contributor of greenhouse gases released into the atmosphere is CO₂. Since 1989, as public awareness of the effects of climate change has grown, researchers have been interested in lowering greenhouse gas emissions from CO₂. Globally, sequestering carbon dioxide is becoming more and more significant. In Kyoto, several nations signed the United Nations Framework Treaty on Climate

Change (UNFCCC), pledging to cut CO₂ emissions by 6% below 1990 levels. Protection of the climate system must be carried out "on an equitable basis and in agreement with Parties' common but differentiated obligations and various capabilities," according to a UNFCCC statement. Developed nations ought to take the lead in combating climate change and its aftereffects [10]. The human factor is the primary cause of the sharp rise in CO₂ concentration. While some CO₂ is released into the sea, which causes ocean acidification, the majority is discharged into the atmosphere, which leads to greenhouse gas emissions, global warming, and rising sea levels[11]. Climate change policies are attributed to both CO₂ and non-CO₂ emissions in many countries across the world. Carbon taxes and emissions trading schemes (ETSs) are two examples of climate change policies that are now vital instruments for cutting greenhouse gas (GHG) emissions and slowing global warming. For instance, in Tanzania, Cambodia, Bangladesh, Brazil, Philippines, Indonesia, Argentina, Vietnam, Australia, Qatar Mexico and Ethiopia, non-CO₂ emissions made up 40–92 percent of all GHG emissions. This implies that the results of climate change policies in different nations may differ significantly based on methods used to assess greenhouse gas emissions and to implement policies[12]. One of the most urgent problems facing the global world is addressing climate change. Climate change is facilitated by greenhouse gas emissions, particularly carbon dioxide (CO₂). 2018 saw a 2% increase in worldwide CO₂ emissions, which is the highest rate in the previous seven years [13]. 2018 saw a 1-degree Celsius increase in global average surface temperature over the pre-industrial baseline.

The four warmest years on record from 2015 to 2018 served as additional evidence of the long-term warming trend. The Intergovernmental Panel on Climate Change (IPCC) states that in order to keep global warming to 1.5 degrees Celsius over pre-manufacturing levels, significant cuts in CO₂ emissions from the energy, urban infrastructure, and industrial sectors must be made [14]. Reducing CO₂ emissions from industrial processes is crucial in order to mitigate the impact of CO₂ on climate change. The utilization of carbon capture and storage techniques lowers CO₂ emissions. Nowadays, a lot of carbon capture technologies are becoming available for purchase to lower CO₂. Capturing carbon dioxide from large-scale power plants, industrial operations, and transportation is their main goal. The technique known as Carbon Capture Utilization or Storage (CCUS) allows for the capture of carbon and its subsequent use in the production of useful products.

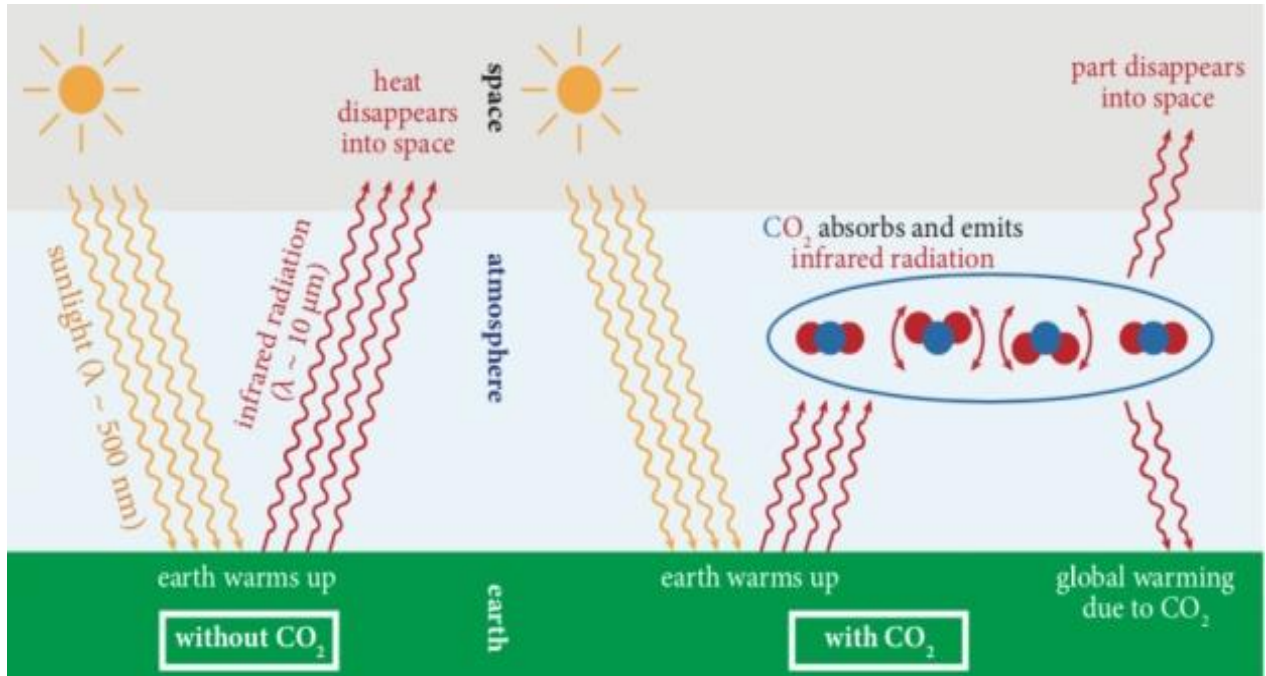


Figure 1-1. Visual heat trapped by carbon dioxide. [15]

1.3 Carbon Capture and Storage

A crucial component of reducing climate change, which is perhaps a challenging threat to our world, is carbon capture and storage. The process of capturing CO₂ is expensive and energy-intensive, and it is made more difficult by the variety of emission sources and their varying amounts, contents, locations, types, and industries or sectors.

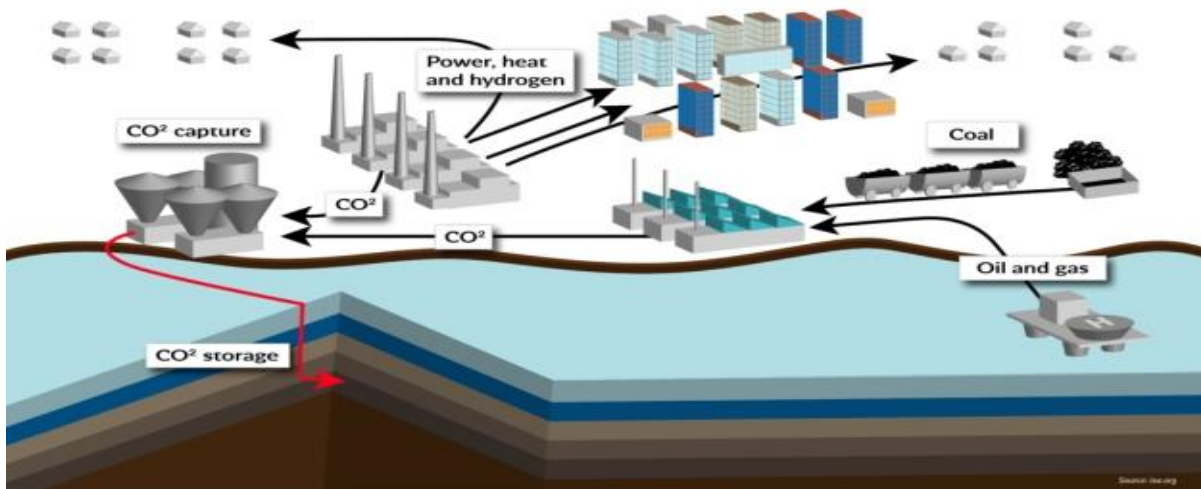


Figure 1-2. Overall process of carbon capture and storage. [16]

When UN Secretary-General Antonio Guterres declared, "We are in trouble," in December 2018, he did not use hyperbole. We face many challenges because of climate change [17]. There were just 800 GWh of total energy storage capacity in the world at the end of 2020 [18].

By 2050, human activity must result in net-zero greenhouse gas emissions to stop global warming [19]. Reducing CO₂ emissions from the energy industry and other energy-intensive industries like metallurgy, cement, and petrochemicals is the aim of CCS technology. CCS can cut CO₂ emissions to the atmosphere in modern conventional power plants by 80–90% when added to a plant without it. The initial generation of CCS technology involves energy-intensive amine-scrubbing. Examples of second and third generation CCS systems that have been suggested to reduce costs are carbonate looping and chemical looping combustion [19]. The industrial sector primarily uses four primary conventional carbon capture storage systems.

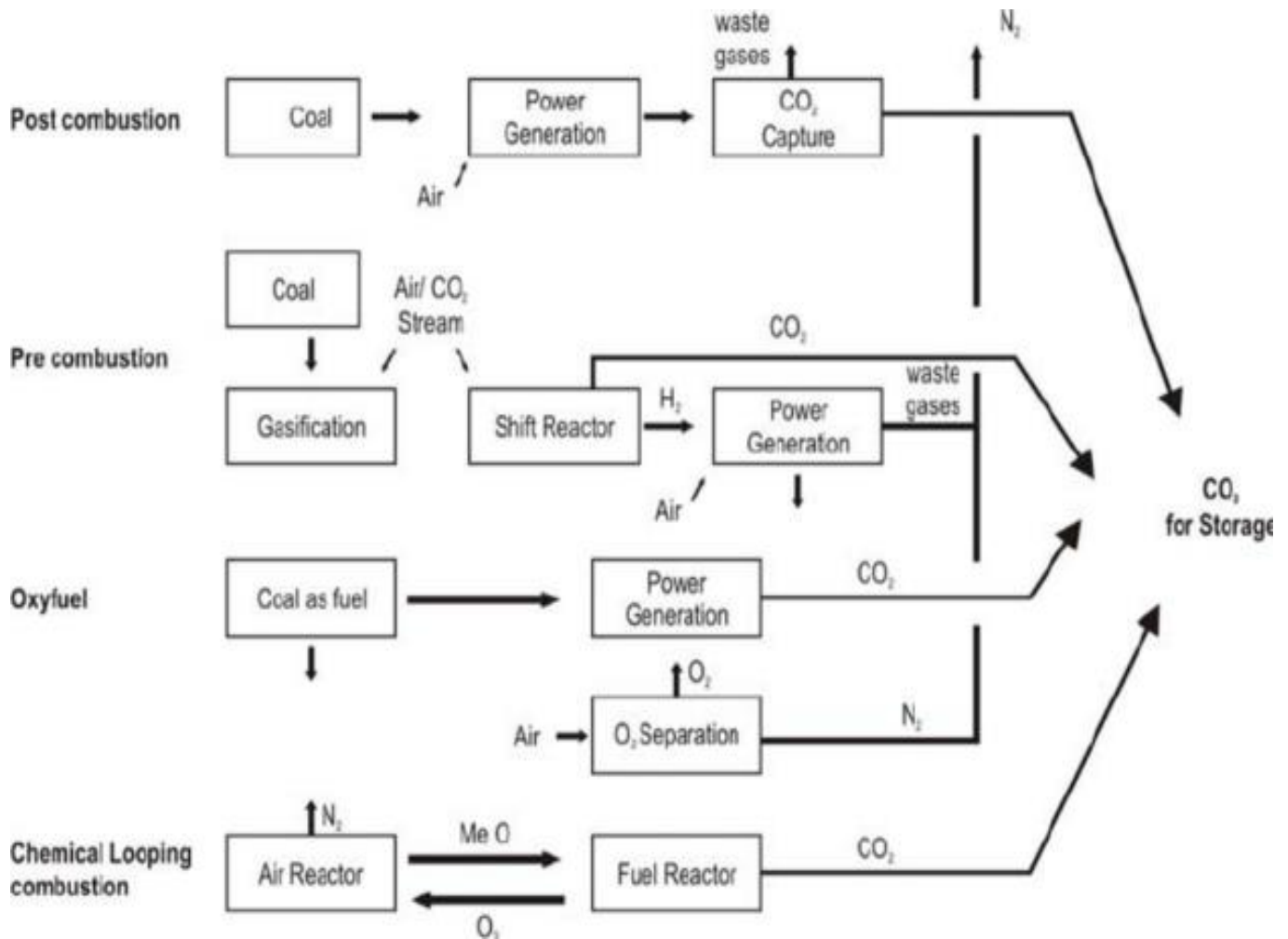


Figure 1-3. Comparison of different carbon capture technologies[20]

These technologies are stated below.

- Post combustion technology.
- Pre combustion technology
- Oxy-flame technology
- Chemical Looping technology

1.4 Pre combustion technology

Pre-combustion technology is one of the most widely researched technologies. Pre-combustion carbon capture method uses an air separation device to extract oxygen from the surrounding air, which reacts with the fuel. The main output of this procedure is called synthesis gas, or syngas. The syn gas is composed of hydrogen and carbon monoxide. Afterward, carbon monoxide from the syn gas is converted into CO_2 and H_2 by reacting with steam in a catalytic converter. The most common name for this reaction is the shift reaction, which involves the additional conversion of CO into CO_2 . Following that, the CO_2 is removed using chemical and physical procedures, producing fuel gas with a high hydrogen content. In numerous other chemical reactions, the CO_2 is retained and utilized as a raw material [21]. Because of the significant capital investment required and the amount of effort required to capture CO_2 with this technology, it is currently not developed enough to be applied at the industrial level.

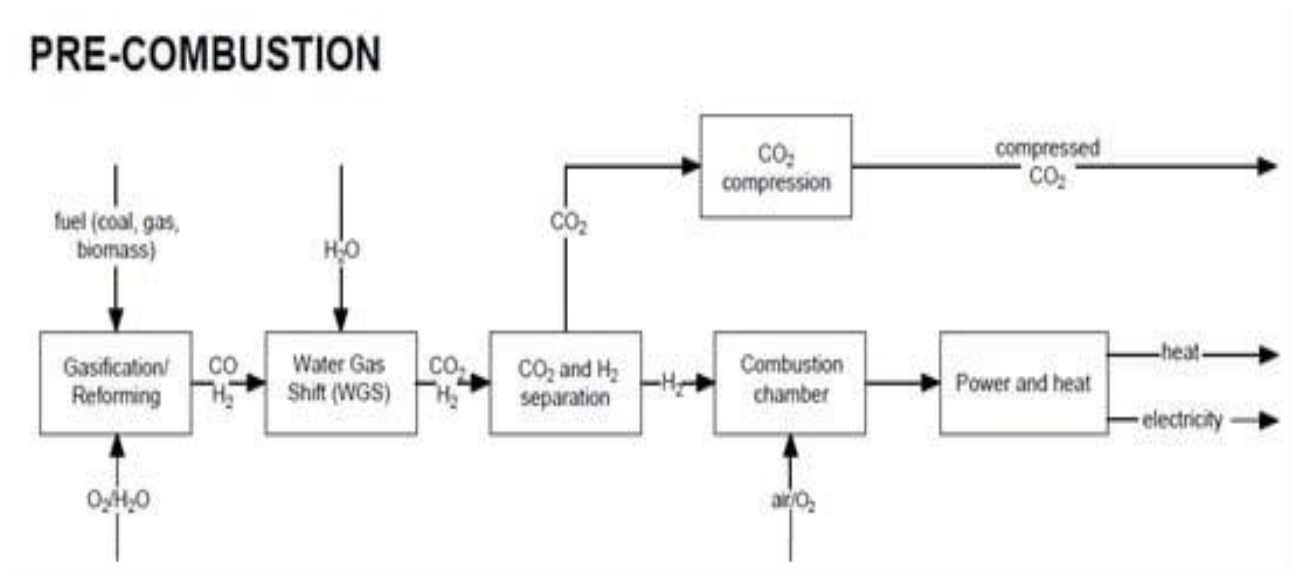


Figure 1-4. Block diagram of pre combustion technology[22]

1.5 Post Combustion Technology

This process uses membrane separation, adsorption, and absorption to remove CO₂ from the flue gases following the burning of fossil fuels. It is the only technology capable of retrofitting already-existing plants. The most challenging part of this technique is separating CO₂ from exhaust gases, which contain a significant amount of nitrogen N₂. One of the many benefits of post-combustion capture is that it may make use of current combustion systems without requiring significant modifications. It is simpler to implement post-combustion capture as a retrofit option for current facilities, in tandem with the other two options. The benefit is contingent upon the efficiency of the power-producing process. Because the separation stage—that is, carbon dioxide capture—requires a lot of electricity, it heavily influences the development cost of CCS. It makes up between 75 and 80 percent of the entire cost of CCS [23]. Numerous separation techniques may be applied to post-combustion capture. Among these are membranes, cryogenic separation, adsorption, physical absorption, and chemical absorption.

1.6 Oxy-Flame Combustion Technology

Oxy-flame carbon capture technology is the leading technology nowadays for the capturing of CO₂. This method includes burning fossil fuels in the existence of pure oxygen instead of air. This can be done to raise CO₂ concentrations in flue gases, which can then be isolated from the flue gases. The flue gases contain carbon dioxide and water. CO₂ can be separated by the process of dehydration and low by using a temperature purification process.

POST-COMBUSTION

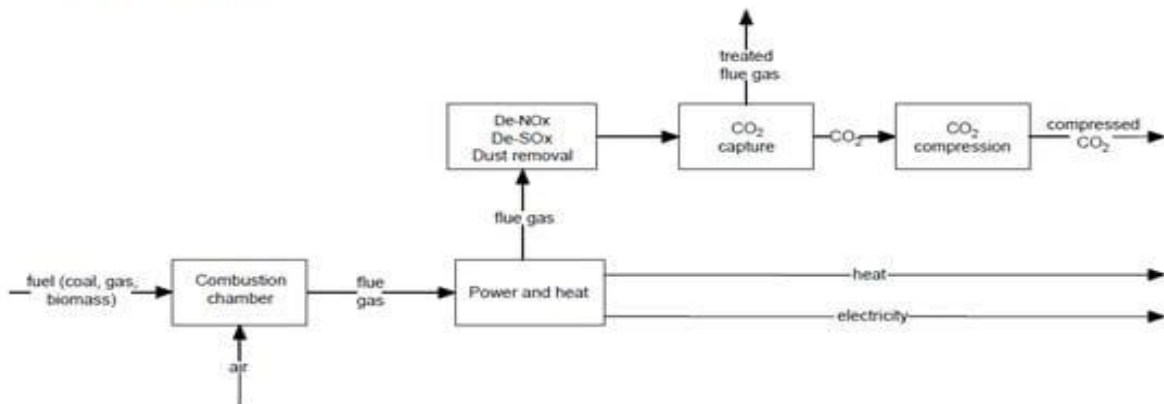


Figure 1-5. Block diagram of post-combustion technology [22]

It is superior to post-combustion carbon capture technology because it cannot contain N_2 in the flue gases like post-combustion technology, oxy flame only contains CO_2 and water, and it is free from nitrogen and its purification is easier. This method gives us the highest recovery of CO_2 and gives concentrated CO_2 with no N_2 present in the gas stream [24].

OXY-COMBUSTION

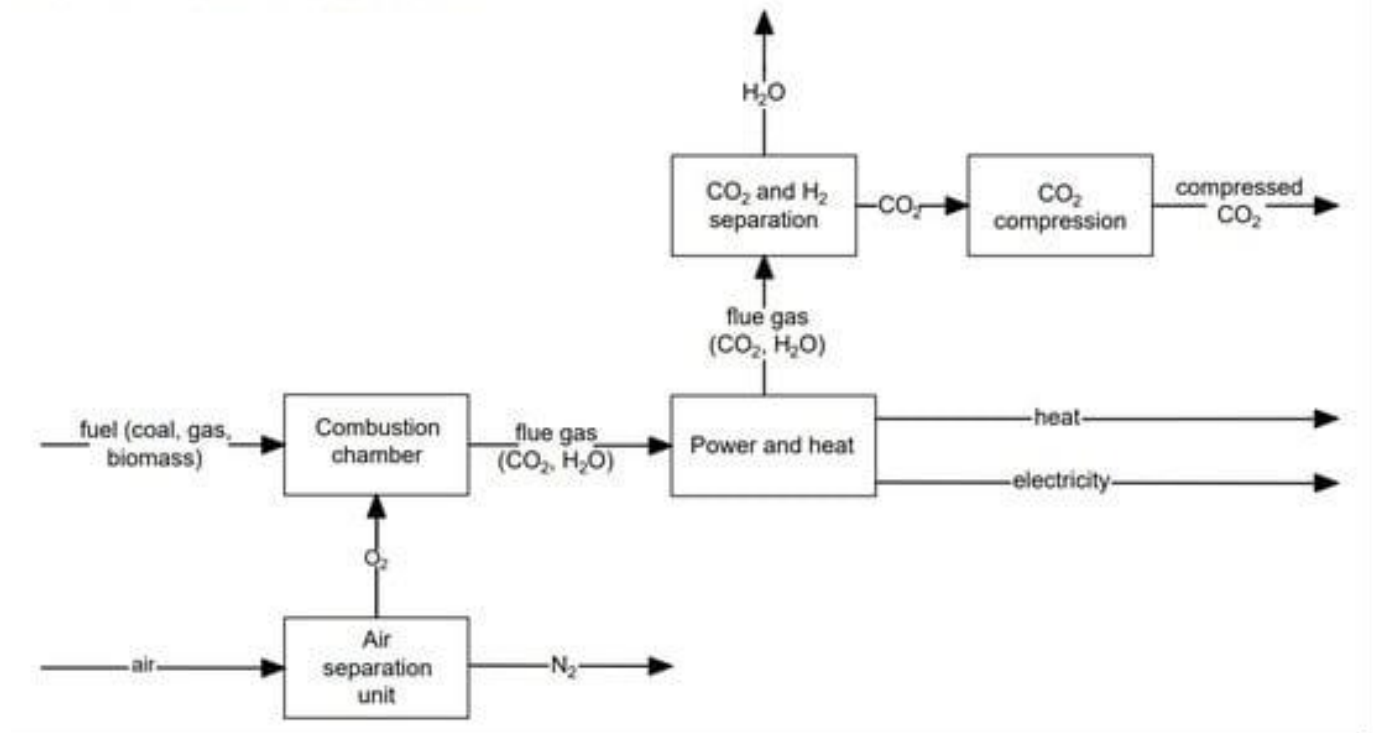


Figure 1-6. Block diagram of Oxy-combustion technology [22]

1.7 Chemical Looping Combustion Technology

One of the most promising carbon capture technologies is Chemical Looping Combustion (CLC) technology. The two reactors that make up the Chemical Looping Combustion technique are an air reactor and a fuel reactor. The oxygen carriers, which are typically fine metal particles, carry oxygen in both the air and the fuel reactor. Initially, the oxygen carriers are sent to the fuel reactor, where they burn up with the fuel and reduce to reduced metal (Me) or (MeO_{a-1}) , causing the reduction reaction to take place there. This reduced oxygen carrier is sent to the air reactor, where the air stream oxidizes it, returning it to its initial state (MeO_a) . The only advantage of this

loop is that flue gas only comprises CO₂ and water vapors rather than N₂ gas. After the water vapors are condensed and separated from the stream, a clean CO₂ stream was produced, which was then stored.

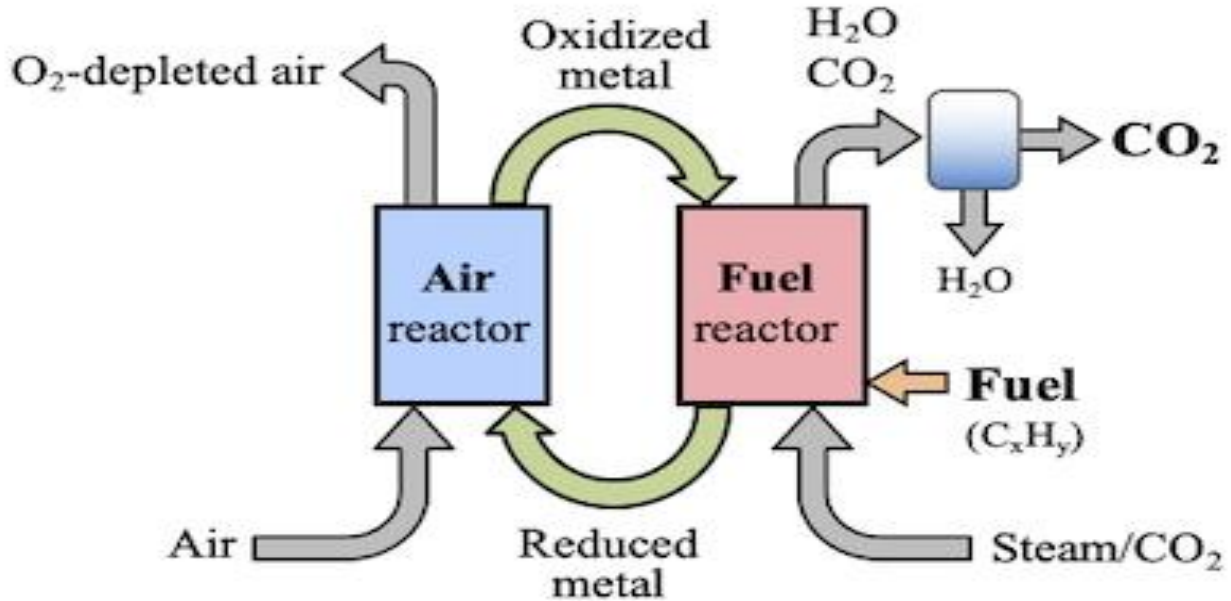


Figure 1-7. Schematic of chemical looping combustion technology [25]

Figure 8 displays the chemical looping combustion technology schematic. The transfer of oxygen from the oxygen carriers to the fuel, in a fashion that allows for direct contact between the fuel and the oxygen carrier, is the basis of the chemical looping process. With the aid of metal oxide, the fuel is first reduced to produce CO₂ and H₂O. The metal oxide (Me_xO_y) is then further reduced to produce the metal (Me) or the reduced form of metal Me_xO_{y-1}. Reaction (1) gives the generic reduction process that is applied globally if the fuel gas composition is expressed as C_nH_{2m}O_p. CO₂ and H₂O are present in the gas that is created following the initial reaction. Following that, the gas is filtered and any water in it condenses, producing a stream of CO₂ with a higher concentration. Later, this CO₂ gas stream is prepared for transportation and storage. This method's relationship to other carbon dioxide technologies is one of its advantages. The primary benefit of this approach is its inherent ability to separate CO₂; this eliminates the need for a separate unit, saves money on an additional air separation unit, and eliminates the additional energy consumption associated with a separation unit. Redox is the foundation of the chemical reaction

scheme used in chemical looping technology. The oxidation and reduction reactions are both a part of the chemical looping technology. Below are the chemical reactions that took place in the chemical looping technology. Both the metal and the reduced metal oxide are generated in reaction 1. It is then prepared to begin the next reaction by further oxidizing it with air in a two-step process. N₂ and the unreacted O₂ are present in the flue gas that is produced because of the reaction. Since the two phases make up the net chemical reaction, the combustion enthalpy is the same as in conventional combustion, which occurs in reaction 3 when the fuel burns in direct contact with airborne oxygen. This process yields a clean stream of CO₂ gas. As a result, the overall heat evolved during the chemical looping technology process is equal to that of traditional combustion techniques. [8]

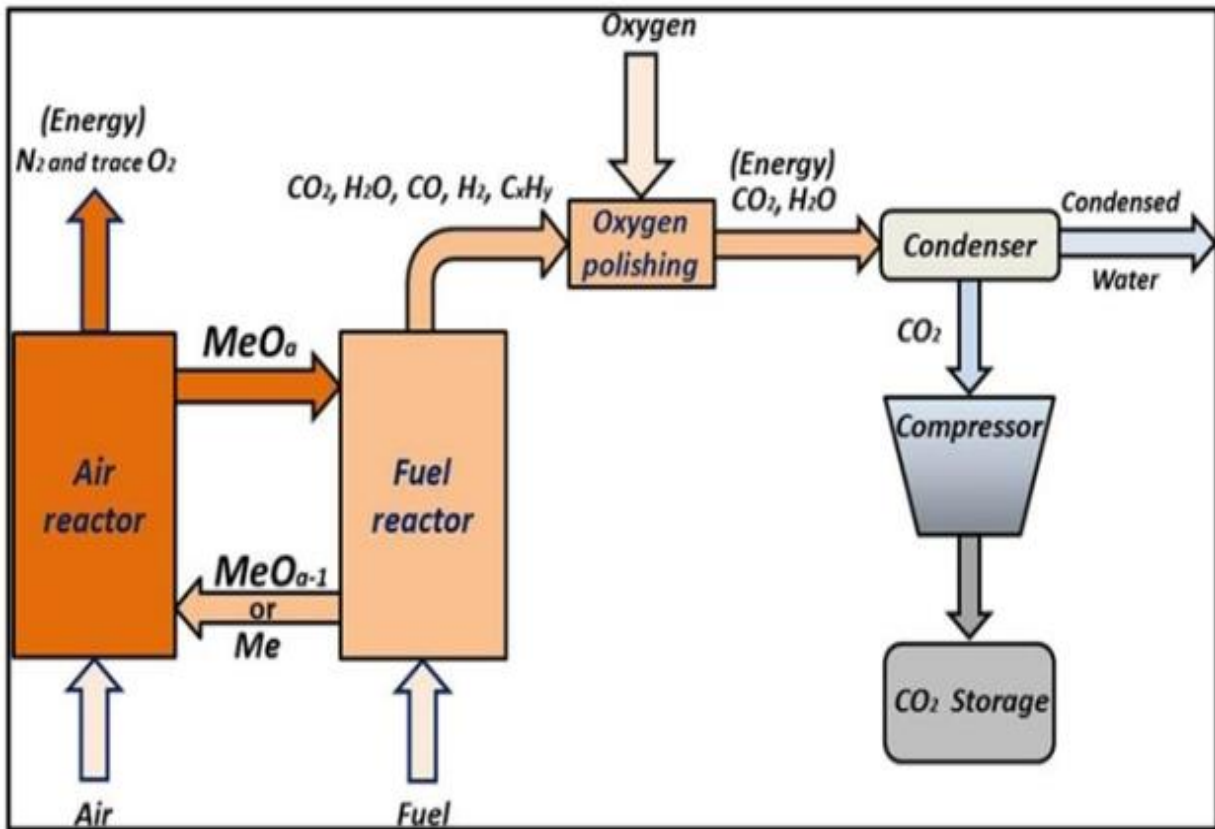
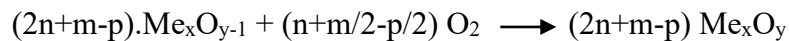
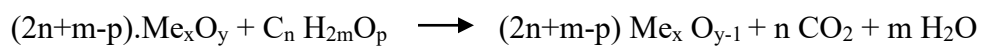


Figure 1-8. Schematic of chemical looping combustion technology [26]



The reactions demonstrate that a concentrated stream of CO₂ was created by condensing water vapors, and that reaction 2 regenerates the metal oxide that was present in reaction 1. This process also reduces the cost of employing metal oxide.

1.8 Separation Techniques

The technologies for CO₂ separation covered in the previous section include both chemical and physical techniques.

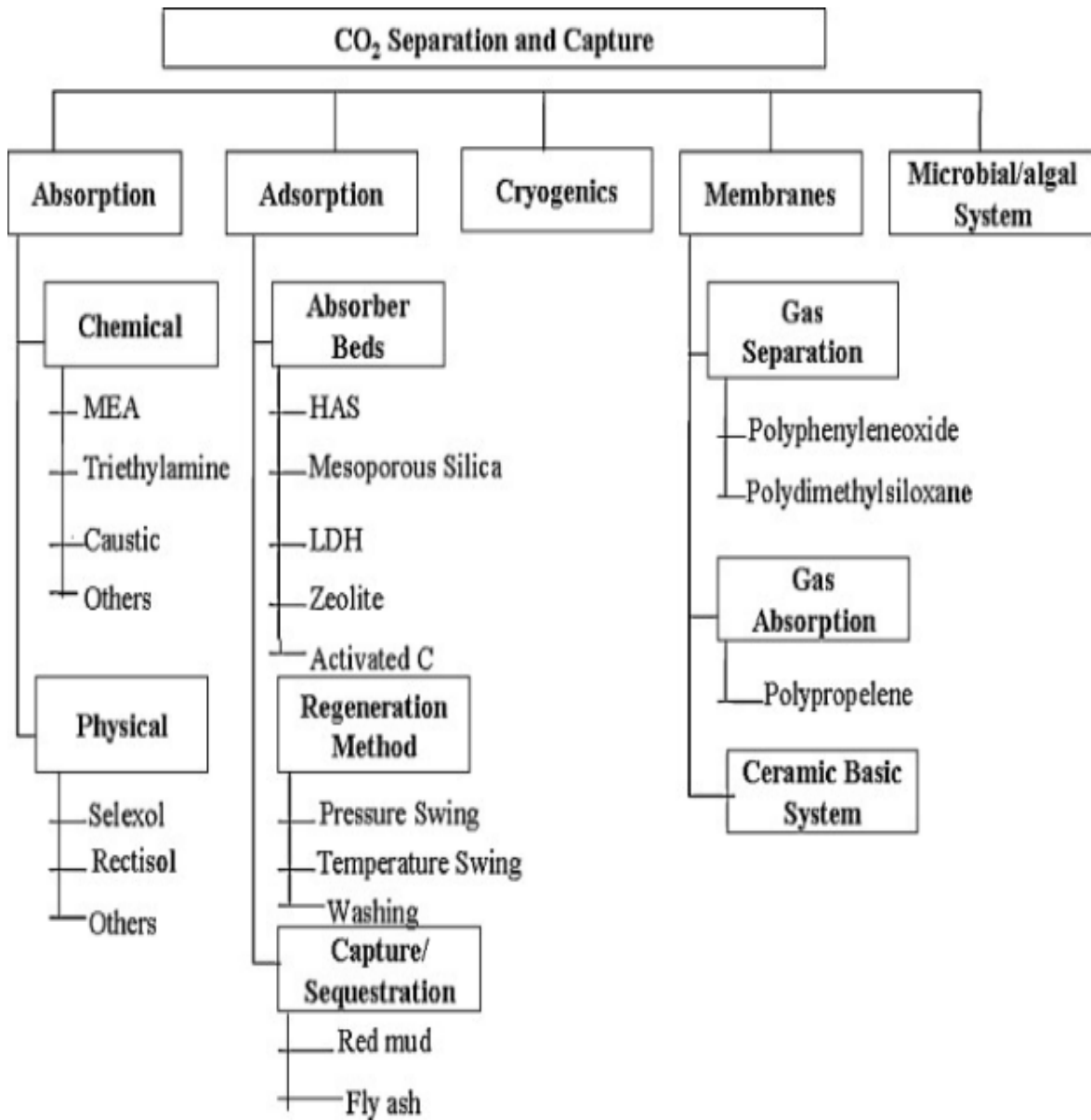


Figure 1-9. Techniques for CO₂ capture [27]

This analysis focuses on the most widely used procedures:

- Absorption
- Adsorption
- Cryogenic distillation.
- Gas separation membranes

There is also a hybrid system that uses membranes related to cryogenic distillation.

1.8.1 Absorption

The methods for capturing CO₂ through absorption are classified according to whether the solvent absorbs the sorbate being inert chemically without undergoing a chemical reaction, or whether the sorbate (CO₂) and the solvent undergo a chemical reaction that produces chemical compounds from which the CO₂ is later recovered. Chemical and physical absorption are the names given to these two different processes, respectively.

To capture CO₂, chemical absorption relies on an exothermic reaction between the gas stream's CO₂ and an absorbent, ideally at a low temperature. At a higher temperature, the reaction is subsequently reversed in a procedure known as "stripping" or "regeneration." At low partial pressure, chemical absorption is especially useful for CO₂ capture; the most common solvents used in this process are amine or carbonate solutions.

Amines are organic compounds that are produced from ammonia (NH₃) in which organic substituents or components replace one or more hydrogen atoms. The terms primary, secondary, and tertiary amines are used to describe these compounds, depending on the quantity of substituents. Methylamine (CH₃NH₂ or CH₅N), which has a methane (CH₃) group in place of one hydrogen atom, is the most basic primary amine. Primary, secondary, and tertiary amines are denoted, respectively, by R₁-NH₂, R₁R₂ -NH, and R₁ R₂ R₃ -N. This simplifies the nomenclature by replacing the organic group with R.

Physical absorption methods employ organic or inorganic physical solvents to absorb the components of acid gas rather than reacting with them chemically. Henry's law, which states that, the partial pressure of the gas in equilibrium with the solvent is proportional to the amount of gas

dissolved in unit volume of a solvent at a specific temperature, can be used to determine the CO₂ absorption by a solvent based on the vapor-liquid equilibrium of the mixture.[28]

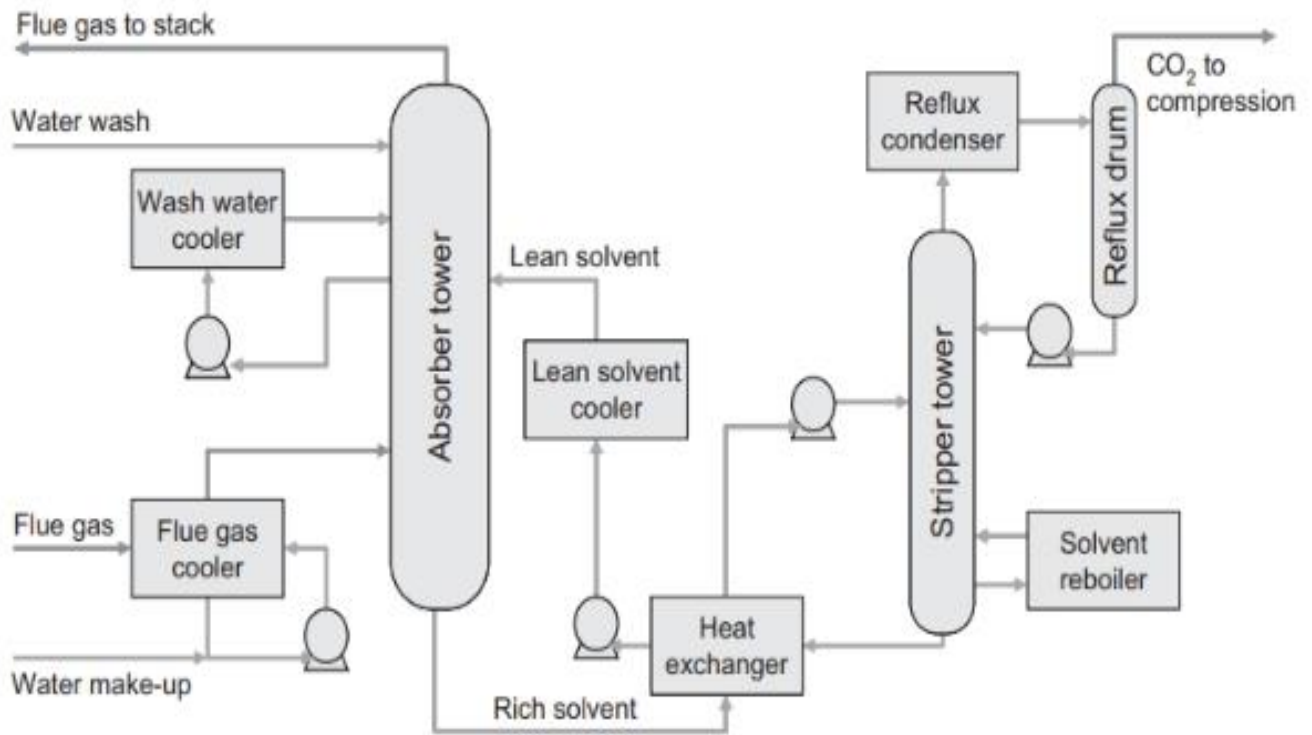


Figure 1-10. Process flow diagram of amine-based carbon capture through absorption [28]

1.8.2 Adsorption

Adsorbed atoms or molecules, often referred to as particles, stay on the surface of the sorbent in contrast to absorption, which occurs when the absorbed component (the sorbate) moves into the solvent's bulk and creates a solution. Comparable to absorption, however, the adsorbate's attachment to the surface might occur via a weaker physical attractive force (physical adsorption or physisorption) or a chemical bond (chemical adsorption or chemisorption).

Activated carbon exhibits the steepest adsorption isotherm and the highest CO₂ adsorption over most of the pressure range, reaching 8 mole per kg at 2 MPa. Nevertheless, there is a significant amount of hysteresis in the desorption isotherm, which lowers the working capacity to 2.2 mole per kg over the shown pressure range. Zeolite-13X exhibits a very low hysteresis and an intermediate adsorption capacity, but its working capacity is just 1.7 mole per kg due to the

isotherm's shallow gradient. The adsorption capacity of natural zeolite is the lowest, little over half that of activated carbon at 2 MPa. However, due to its steeper isotherm and comparatively low hysteresis, it has a working capacity of 2.3 mole per kg over this pressure range, which is slightly greater than that of activated carbon. Because physical sorbents have smaller binding strengths, they are usually utilized at lower temperatures and thus lower heat of adsorption, but chemical sorbents can maintain good capacity at higher temperatures because of their greater heats of adsorption. Thus, the distinction between low and high operating temperatures is typically reflected in the split between physical and chemical sorbents.[28]

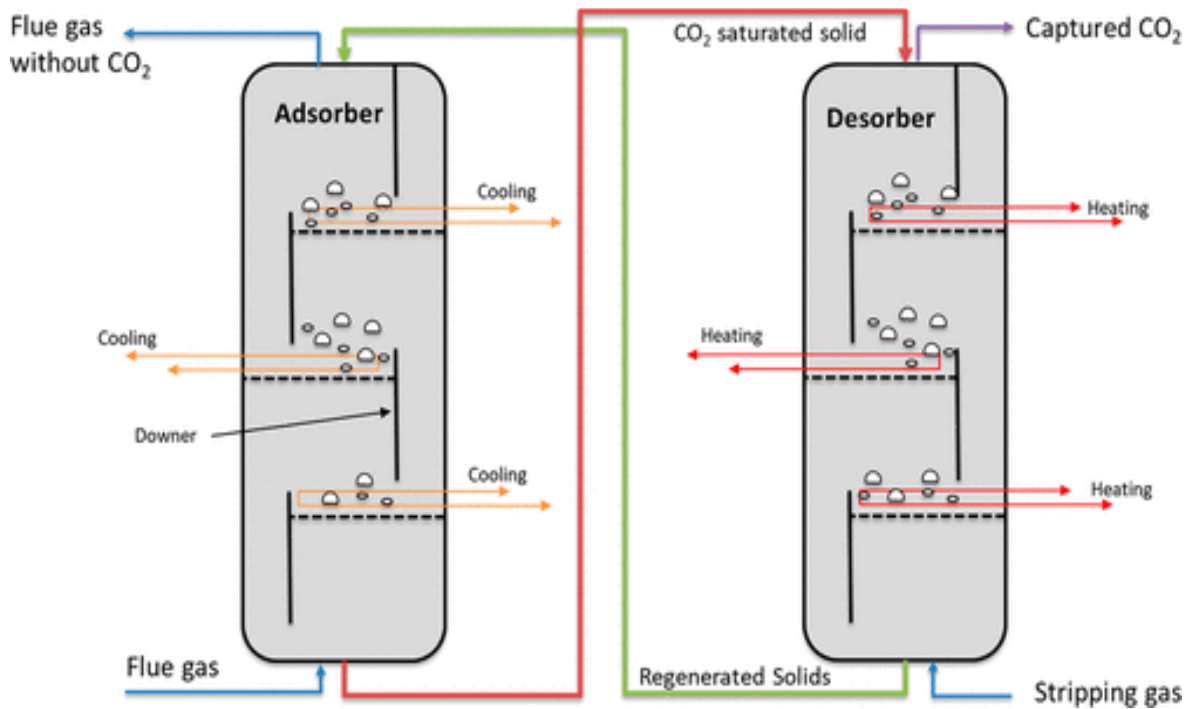


Figure 1-11. Multistage fluidized bed with downer and heat exchanger. [29]

1.8.3 Membrane Separation

The 1980s saw the development of techniques for the separation of hydrogen (from hydrotreaters in refineries, for example), oxygen and nitrogen, and carbon dioxide (CO₂) from natural gas. The latter was done either to process the natural gas to sales quality or for applications involving enhanced oil recovery (EOR). This marked the first use of membranes for gas separation. Membranes can be used for a variety of carbon capture tasks, such as CO₂ separation from post-combustion flue gases and hydrogen separation in precombustion capture systems. Many various

membrane techniques might be used; these include novel technologies that are being researched and developed, based on sophisticated materials, as well as established technologies that have already been used on an industrial basis. Membranes are either porous or nonporous, and porosity is the primary property that defines the process for transferring permeating molecules through them.

Viscosity dominates gas flow at the macropore scale, and as pore size decreases below the mean free path of gas molecules, diffusion takes over. Molecular sieving, where flow is mostly controlled by surface interaction with the pore walls, occurs when the pore size decreases below 10 \AA and approaches molecular dimensions. Molecular sieving gives way to a solution-diffusion transport process as the pore size reaches the 1 \AA scale. The sections that follow provide descriptions of these transport processes.[28]

1.8.4 Cryogenic Distillation

Two applications of distillation techniques relate to CCS: first, to produce oxygen through cryogenic air separation for oxyfuel combustion; second, to separate CO_2 from natural gas, either for the purpose of treating the gas to sales specifications or for reinjecting the CO_2 formed in an enhanced oil recovery (EOR) project.

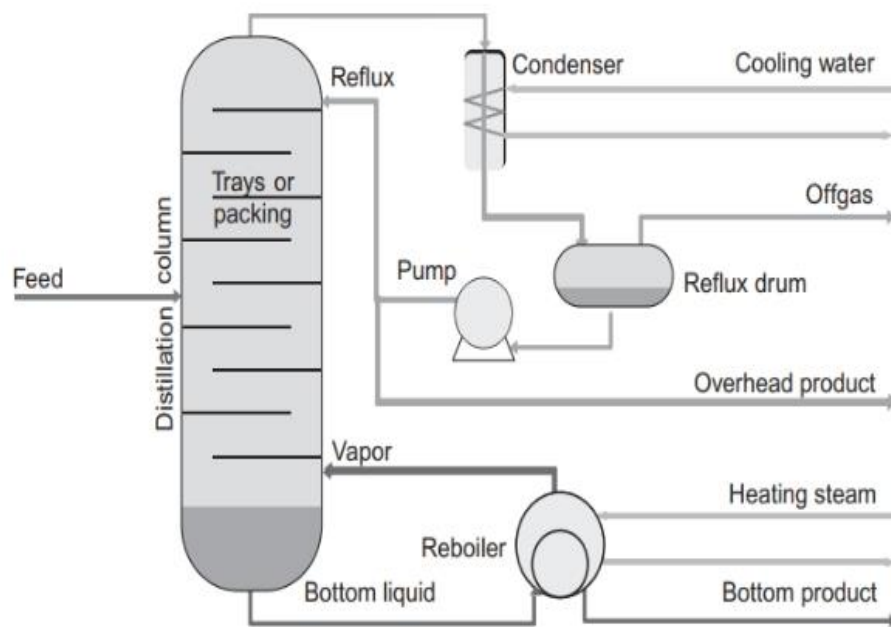


Figure 1-12. Cryogenic distillation column process. [28]

A distillation column's streamlined process flow is seen in Figure 13. The reflux stream lowers the boiling point of the mixture and maintains the less volatile component in the liquid phase by increasing the concentration of the volatile component in the upper part of the column in addition to cooling the top of the column. By doing this, the process of separation becomes more efficient and requires fewer trays to reach the desired level of separation. The practical design of a distillation process must also address the range of operating conditions that column performance must be maintained, such as potential changes in feed composition, feed rate, and ambient temperature. Issues that may lower the effectiveness of separation include:

- Entrainment: extra liquid is transported upward due to high vapor rates.
- Weeping: high liquid rates that descend excessively because of low vapor pressure
- Foaming: the expansion of liquid brought on by the retention of vapor bubbles in the liquid; this is typically caused by the feed stream's surfactant components.[28]

1.9 Adsorbents for Carbon Dioxide Capture

Now, the most advanced technology is carbon capture with adsorbents. Adsorbents come in a variety of forms and are employed to capture CO₂. Because of their large surface area, low cost, thermal stability, and high rate of CO₂ adsorption, adsorbents are the most widely utilized technology. Numerous adsorbent kinds are employed, such as metal-organic framework adsorbents, carbon-based adsorbents, silica-based adsorbents, alkali earth metals, and zeolite adsorbents. The only issue with carbon-based adsorbents is that they have a limited adsorption capacity, low surface area, and small pores. Despite being thermally stable, these adsorbents required less energy for the regeneration process. Zeolite adsorbents exhibit high adsorbent quality, good structure, and large pore sizes. However, these adsorbents have two drawbacks: as temperature rises, their adsorption decreases, and because of their high hydrophilicity, even very small amounts of moisture can deactivate them. These days, CO₂ from flue gas is also captured using solid adsorbents based on alkali earth metals. CO₂ capture from flue gas at high temperatures without the presence of water vapor sorbents has also been studied. In post-combustion procedures based on calcium, the alkali earth metal is utilized to create a concentrated stream of carbon

dioxide. Alkali earth metals, like CaO, can react reversibly with CO₂ to produce alkali earth metal carbonate, or CaCO₃, which is utilized in carbon capture methods such as pre- and post-combustion [30].

Zeolites are an important class of materials that have been the subject of extensive research for many years due to their unusual structures and exceptional qualities. Microporous aluminosilicate materials known as zeolites are composed of SiO₄ and AlO₄ crystalline frameworks that are joined tetrahedrally by oxygen atoms. These materials contain many interconnected cavities and channels with uniform pore sizes ranging from 0.3–1.0 nm, which are occupied by cations and water. The process of hydrothermal crystallization is the most often used to create zeolites. This is accomplished by using a primary source of silica and aluminate in a closed system with autogenous pressure and temperatures ranging from 60 to 240 °C for periods ranging from a few hours to a few days. The type of zeolite that is formed can be changed by adjusting the synthesis process's parameters, including the reactants, time and temperature of crystallization, molar ratio of the reaction mixture, and pH of the reaction mixture. Zeolites are distinguished by their large surface areas (600–800 m²/g), shape/size selectivity, and 400 °C thermal stability. Zeolites have found widespread use in the primary industrial chemical processes, including gas adsorption, catalysis, purification, ion exchange, drying agents, and detergents, due to their remarkable characteristics. There have also been reports of new, cutting-edge uses for zeolites in the areas of chemical sensors, green chemistry, medicine, nanotechnology, and H₂ storage. [31]

1.10 Introduction to Zeolites

Zeolites are hydrated aluminosilicate minerals composed of silica (SiO₄) and alumina (AlO₄) tetrahedra that are interconnected. Put another way, they are solids made of silicon, oxygen, and aluminum that have a somewhat open, three-dimensional crystal structure. Water molecules are trapped in the spaces between the metals, which include sodium, potassium, and magnesium, as well as alkali or alkaline-Earth metals. Zeolites are composed of a variety of crystalline formations with big open pores (also called cavities) arranged in a highly regular fashion and a size like that of tiny molecules.

Zeolites are incredibly stable solids that can withstand environmental conditions that would be difficult for many other materials to handle. Because they don't burn and have relatively high

melting points (over 1000°C or 1800°F), high heat doesn't concern them. They also don't oxidize in the air, dissolve in water or other inorganic solvents, or succumb to high pressures. They are not thought to be harmful if inhaled or come into touch with the skin, yet they may be carcinogenic (cause cancer) when they are fibrous. They're thought to have no negative effects on the environment because they're non-reactive and made of naturally occurring minerals. Zeolites sound boring, but that's not what makes them useful—they're stable and unreactive.

Zeolites' open, cage-like "framework" shape and ability to trap other molecules inside of it are what makes them so fascinating. This is the process by which water molecules and alkali or alkaline-Earth metal ions—positively charged atoms with an insufficient number of electrons, sometimes referred to as cations—become embedded in zeolite crystals, however, they may not stay there indefinitely. Zeolites can exchange other positively charged ions for the metal ions that were initially trapped inside of them; this process is officially referred to as cation exchange. Additionally, as discovered by Cronstedt more than 250 years ago, zeolites may readily absorb or lose water molecules (a process known as reversible dehydration). Zeolites are sometimes referred to as molecular sieves because of their regular, fixed-size holes that allow small molecules to flow through while trapping bigger ones.

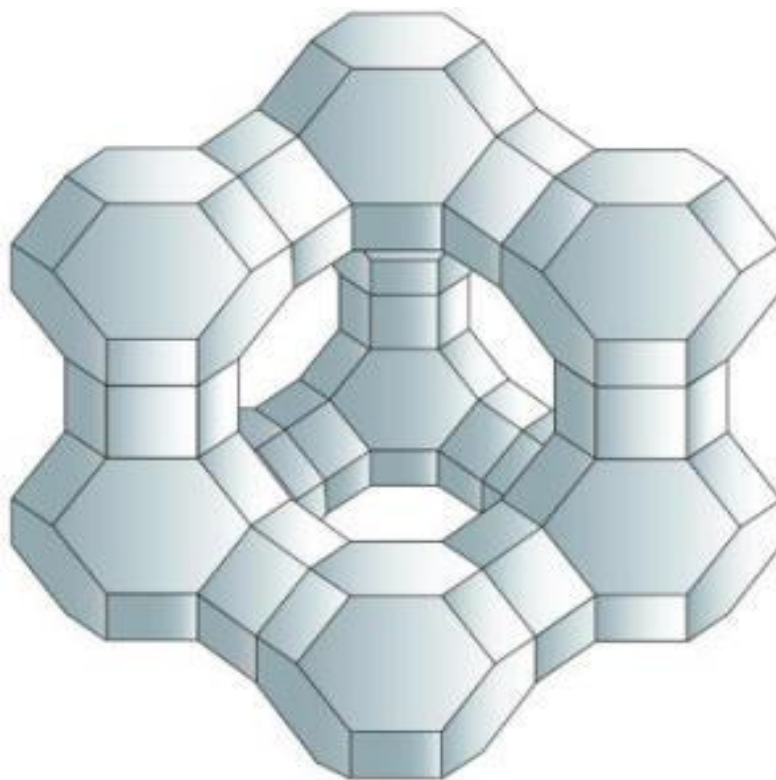


Figure 1-13. The pores in between the aluminum, silicon, and oxygen atoms in zeolites [32]

1.11 Synthesis of Zeolites

1.11.1 Hydrothermal Synthesis

In the simplest terms possible, a typical hydrothermal zeolite synthesis is as follows:

- A cation source is combined with amorphous reactants that contain silica and alumina, typically in a basic (high pH) media.
- A sealed autoclave is used to heat the aqueous reaction mixture, usually at reaction temperatures exceeding 100 °C.
- The reactants stay amorphous for a while after reaching the synthesis temperature.
- The crystalline zeolite product is detectable following the aforementioned "induction period."
- Almost all the amorphous material gradually gives way to a mass of zeolite crystals that are recovered through filtration, washing, and drying.

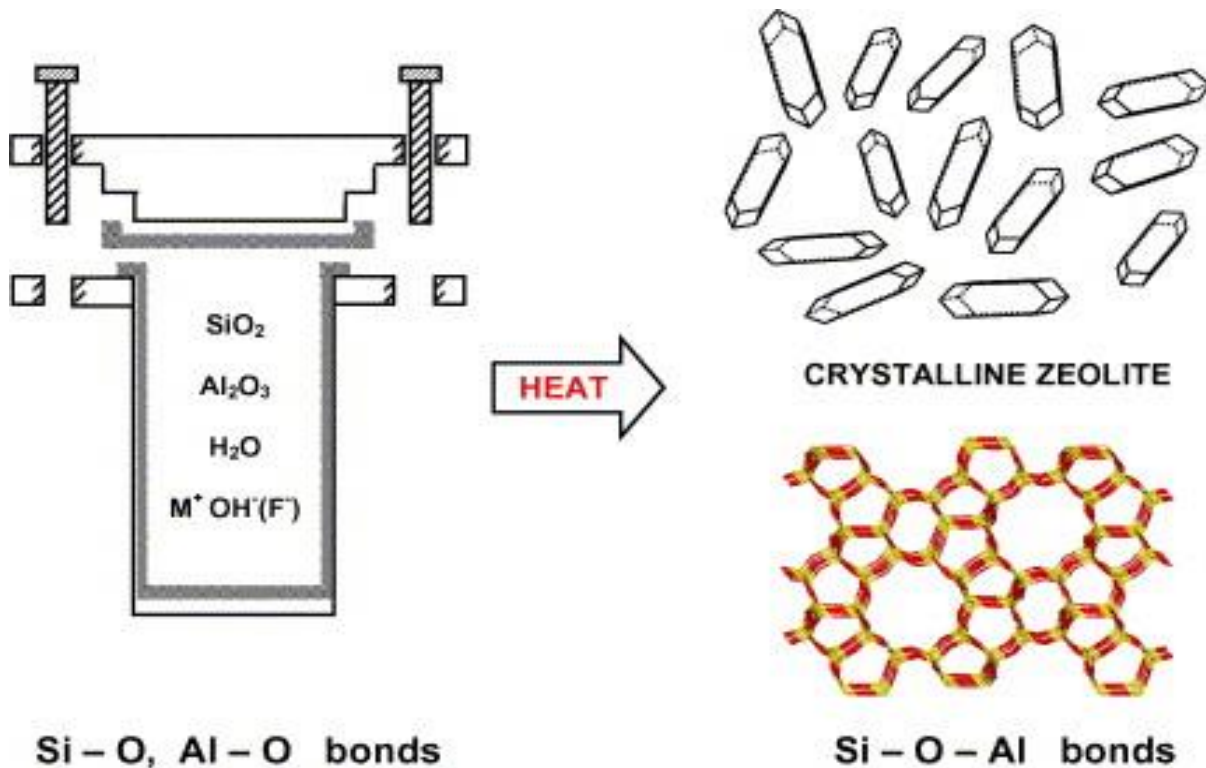


Figure 1-14. Hydrothermal method of zeolite synthesis [33]

Figure 15 provides a schematic illustration of this. The oxide form of the components (Si, Al) that will comprise the microporous framework is imported. These precursors are often amorphous and oxidic, containing Si O and Al O links. A "mineralizing" agent, usually an alkali metal hydroxide, is added to the hydrothermal reaction to produce the crystalline zeolite product (such as zeolite A), which has Si O Al links. No significant enthalpy change would be expected because the bond type of the product is extremely like that found in the precursor oxides. As a zeolite synthesis reaction has a rather tiny overall free energy change, the result is typically kinetically regulated.

In zeolite synthesis, where the desired product is often metastable, kinetic control has a pervasive impact. To prepare the necessary material consistently and to the same standard, a significant portion of the expertise in this crucial field for industry revolves around selecting the precise parameters for product optimization. The selection of beginning reagents will frequently be influenced by these factors. It is also very typical for the reagents to reflect some degree of pre-combination, as in the case of solid sodium aluminate or sodium silicate solution. These can include the simple oxides or hydroxides discussed above, such as precipitated silica or alumina trihydrate. These materials might be more advantageous in terms of cost or processing simplicity, but they might also provide the best paths to specific materials since reagent choice flexibility allows equilibria to be attacked from several angles. This could have kinetic advantages, e.g., a preference for one phase to nucleate over another in conditions when mixtures would ordinarily co-crystallize. The guidebook published by the International Zeolite Association's Synthesis Commission (IZA) provides a solid overview of the topic of practical zeolite synthesis. [33]

1.11.2 *Solvothermal method*

The overall term for the process of using a solvent to synthesize zeolites is "solvothermal synthetic method." Since water is by far the most important solvent, its use is defined by the term "hydrothermal." Nonetheless, a variety of organic solvents have been effectively employed for the synthesis of zeolite, including hydrocarbons, ethylene glycol, pyridine, and alcohols (methanol, ethanol, and pentanol). These molecular solvents generate a sizable autogenous pressure at high temperatures, just like water does. The solvent utilized in this procedure may have nonpolar, hydrophobic, or hydrophilic polar solvent characteristics. This word is designated as ionothermal when utilizing ionic solvents, often known as ionic liquids. Thus, all ionothermal and hydrothermal

techniques are essentially solvothermal techniques, but not all solvothermal techniques are. Although ionic is in the ionothermal synthesis process, the fundamental distinction between them is that solvents stay in molecule form in both solvothermal and hydrothermal synthesis methods. Ionic liquids' ionic nature reveals characteristics including low vapor pressures. Figure 16 depicts a general schematic representation of solvothermal processes.

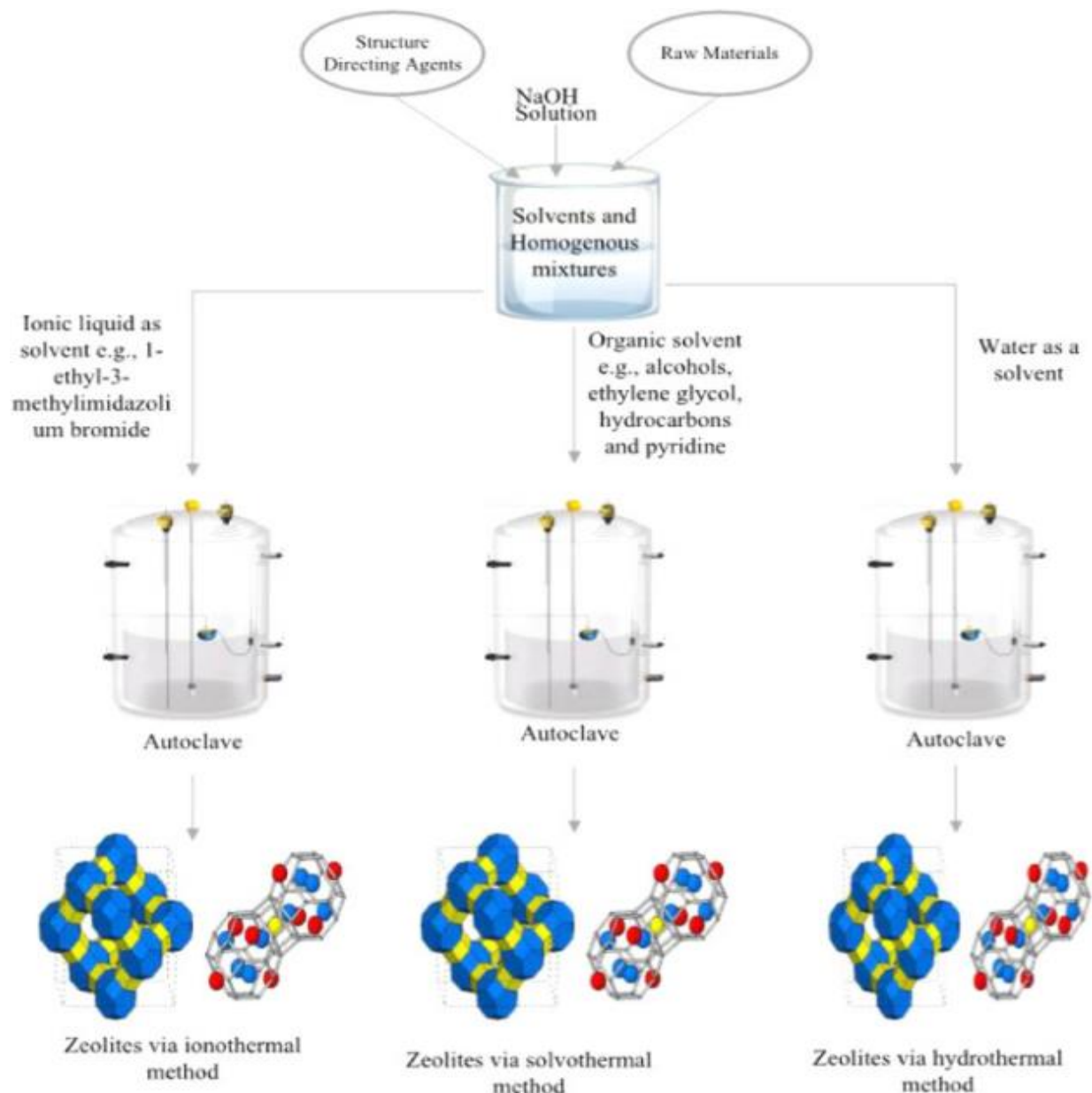


Figure 1-15. General schematic of all solvothermal methods (including hydrothermal and ionothermal) for the synthesis of zeolite. [34]

Solvothermal techniques rely on a variety of parameters, in addition to temperature and pressure. Therefore, by appropriately altering the parameters, this approach provides simple and accurate control over the final zeolite product's size, shape distribution, and crystalline structure. The solvothermal approach has been used in several prior attempts to synthesize zeolite. [34]

1.11.3 *Ionothermal method*

Ionic liquids are used in ionothermal synthesis, which is primarily based on low vapor pressure chemicals (Fig. 16). As a result, during the solidification process, ionic liquids function concurrently as the solvent and as a possible template or structure-directing agent. There is little difference between hydrothermal, solvothermal, and ionothermal processes; the only difference is the solvents used. As a result, the zeolite synthesis in these three approaches is similar. Cooper and colleagues' groundbreaking work in this field was published in 2004. Depending on the situation, they prepared a variety of unique materials using deep eutectic solvents (such as urea/choline chloride and 1-ethyl-3-methylimidazolium bromide). The primary benefit of this approach is that the solvent can function as a template or structure-directing agent. Additionally, because the solvent and template are the same species, removing the products is not too difficult once they are obtained. Furthermore, the ion thermal technique can form a crystalline phase and yield large-sized crystals. Additionally, the composition of crystals in growth can be easily controlled. However, the generation of hazardous compounds and extended operational duration are disadvantages. Zeolites have also been reported to be synthesized in several investigations. The zeolite scientific community has recently shown an increasing amount of interest in this approach. Numerous papers describe the use of this technique to create synthetic zeolites.[34]

1.11.4 *Sol-gel method*

A three-dimensional network structure is formed through a physicochemical process that begins with the production of an inorganic colloidal suspension (sol) and ends with the gelation of the sol in a continuous liquid phase (gel). The conversion of a solution system from a liquid "sol" phase to a solid "gel" phase is known as the "sol-gel process." Better technique control is possible with this process, leading to increased porosity and more consistent particle size. The effectiveness of this procedure can be affected by many things.

These are.

- pH
- Temperature
- Heating rate
- Hydrolysis rate.

This approach is the subject of numerous reports.

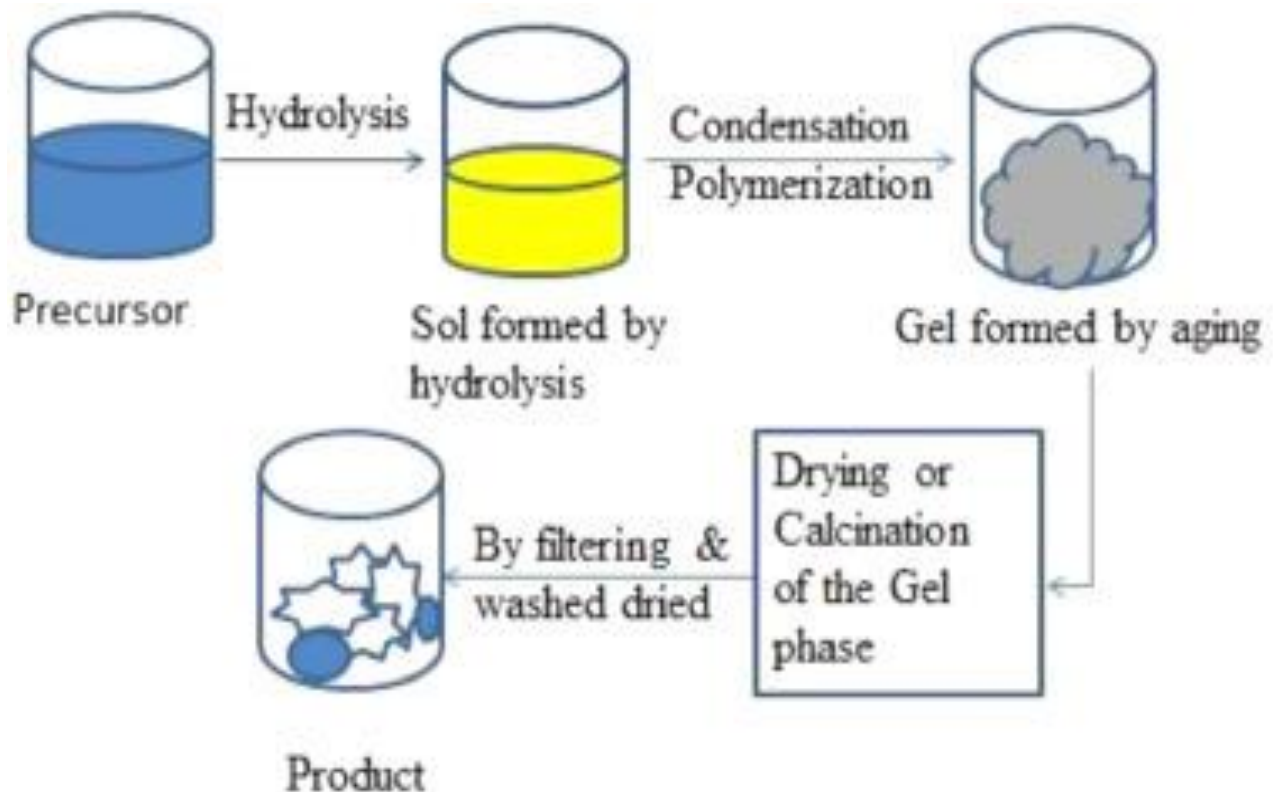


Figure 1-16. Sol-gel method for synthesis of zeolite. [34]

This method's main benefit is that it doesn't require any expensive or specialized equipment. Fig. 17 shows the steps of the sol-gel approach. Because of molecular mixing, this process produces a homogenous, high-quality product.[34]

1.12 Applications of Zeolites

Zeolites' inherent qualities, which include their porosity and structural diversity, uniform pore size and shape, cation mobility, and the hydrophobic and hydrophilic nature of the absorbates and absorbents, have led to a wide range of applications for the material, including absorbability,

membrane separation, coagulation activity, water purification, and antimicrobial activities. Zeolites are still used today to solve a wide range of industrial, scientific, and environmental problems.

1.12.1 Catalytic Properties

The existence of zeolites' active sites, often referred to as Brønsted acid, on the OH bridging framework between the silicon and aluminum channel, is what gives them their catalytic properties. A negative charge is produced on the lattice when trivalent elements take the place of Si atoms in the zeolite framework that must be counterbalanced by a positively charged counterion. A Brønsted acid site forms when a proton provides the charge balance. The sites are called bridging hydroxyl sites. The hydroxyl groups and Si-OH-Al sites act as a donor of protons.

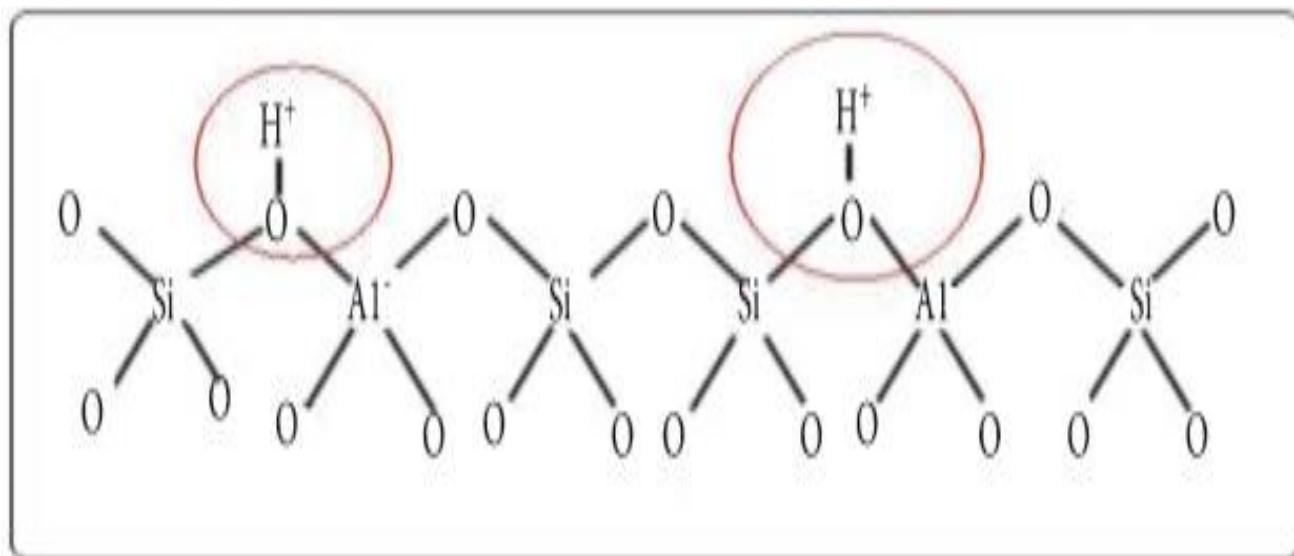


Figure 1 -17. Brønsted acid sites in zeolites framework [35]

Use of zeolite A as the heterogeneous catalyst in the esterification process, ethyl acetate was produced from acetic acid and ethanol. By removing undesirable molecules from the process during its equilibrium, zeolite, acting as a surfactant, is utilized to move the reaction toward the product (Figure 19). Water and ethyl acetate are produced by intramolecular dehydration that

occurs when the adsorbed acetic acid on the zeolite catalyst creates a chemical bond with the ethanol (Figure 19).

The authors did not address the factors that contribute to low catalytic rate and poor catalyst utilization, such as long diffusion paths and small pore sizes that decrease the catalytic process's transport efficiency, lessen the impact of diffusional restrictions, and increase the accessibility of big molecules to the active sites present in zeolite channels, all while maintaining high selectivity and catalytic activity.

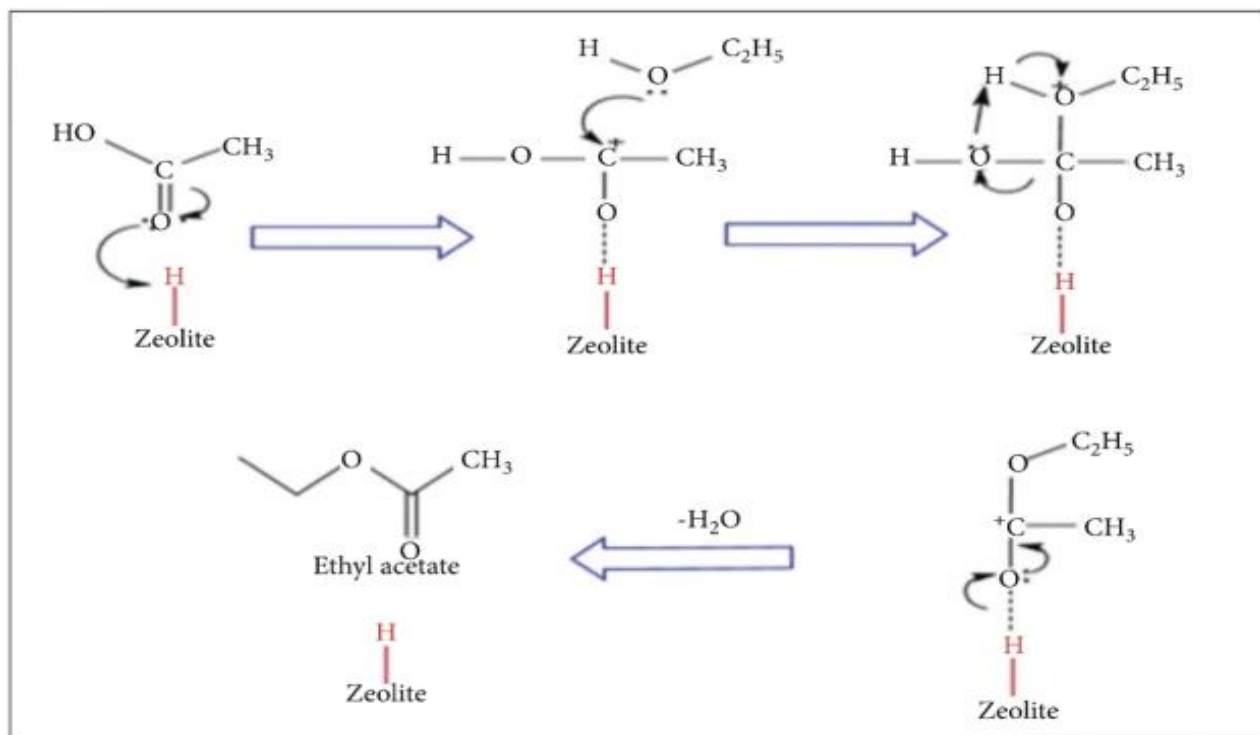


Figure 1-18. Vapor-phase acetic acid esterification with ethanol [35]

1.12.2 Adsorption

The adhering mechanism of the zeolite is affected by several factors, includes ion-exchanging activities, adsorbate form, adsorption equilibrium, adsorption selectivity rate, and adsorbent and adsorbate reactivity. Through adsorption kinetics, the ability of Zn exchangeable zeolite A, which was created, to effectively absorb methylene blue (MB) from solution. It is concluded that contact time had an impact on the adsorption of MB on Zn-exchanged zeolite A, with the adsorption equilibrium being reached in 180 minutes. As demonstrated, the synthesized

Zn-exchanged zeolite exhibits significant adsorption for methylene blue dye at optimal contact time. The authors did not, however, consider the impact of competing agents during MB adsorption. A dual-electronic adsorbent was used by several researchers, including, to modify zeolite adsorption for the removal of organic, cationic, and oxoanionic chemicals. Toxic contaminants are removed from wastewater using Na-H-zeolite which is an amphiphilic and dual-electronic adsorbent. Great ion exchange capacity zeolites exhibit great levels of selectivity during adsorption. [35]

1.12.3 *Ion Exchange Properties of Zeolites*

The AlO_4 and SiO_4 tetrahedra structures are the main building blocks of zeolites. They join via oxygen ions to form secondary building units (SBU), which are then joined to form a three-dimensional crystalline zeolite structure. Al replaces Si in the zeolite structure, causing a negative charge that is counterbalanced by alkaline and Earth alkaline metal cations. Na^+ , K^+ , Ca^{+2} , and Mg^{+2} are examples of active metal ions that balance the net negative charge that is formed on the ends of zeolites. As seen by the reaction below, these positively trapped ions are relatively loosely bound and easily exchangeable in a contact solution between zeolite (Z). Zeolites' ion exchange capabilities are extensively employed in detergents, wastewater treatment, and hard water purification. Cr (VI) and As (V) are extracted from the solution by substituting active metals for insoluble Cr and As ions. The ion exchange characteristics of the Georgian zeolite Phillip site, scolecite and analcime were studied by Tsitsishvili et al. Isotherms of ion exchange demonstrate the great selectivity of the Phillip site. The three natural zeolites found in Georgia— Phillip site, scolecite and analcime —are utilized as ion exchangers and can take the place of synthetic materials in regional environmental and industrial applications, according to the authors' conclusions.[35]

1.12.4 *Purification of Water*

Zeolites are utilized to purify wastewater from a variety of sources, such as waste liquids produced by metal finishing and agricultural, municipal, natural, and municipal waste that contains ions of metals Sb, Ni, Co, Zn, Pb, Cu and Cr. By exchanging with the cations on a zeolite's extra-framework exchange active sites, the dissolved cations are eliminated from water. To remove toxic metals from a variety of natural zeolites (chabsite, phitipsite, mordenite and clinoptilotite); even

when there are competing cations present, these zeolites exhibit great selectivity for the NH_4^+ ion. The scientists reported that the zeolite exchange sites remove harmful metal ions from water and replace them with cations that are acceptable to biology, including Na^+ , K^+ , Mg^{2+} , Ca^{2+} , or H^+ . It investigated the use of synthetic zeolites to remove heavy metals from motorway stormwater. Zeolite's ability to remove heavy metals is effective, but it depends on the pH of the solution.[35]

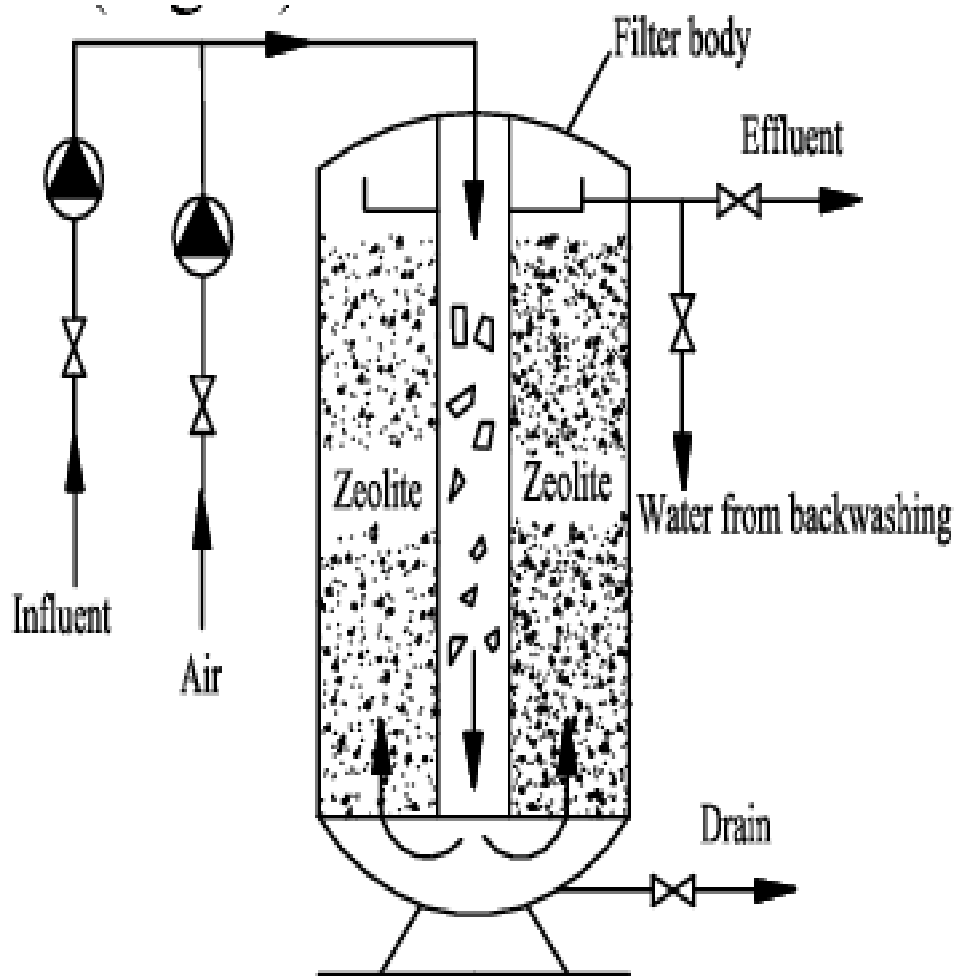


Figure 1.19 Zeolites use for water purification.

CHAPTER 2 LITERATURE REVIEW

(Bahmanzadegan et al., 2023). The goal of this work is to maximize the CO₂ adsorption capacity of 4A-zeolite, which is made from kaolin, by using structural alterations obtained via impregnation with diethanolamine (DEA) and tetraethylenepentamine (TEPA). Using a test apparatus, the modified zeolites' adsorption capability was evaluated at various pressures, temperatures, and amine concentrations. We find that the optimal working conditions for the 4A-DEA adsorbent are 25.270 °C, 8.870 bar of pressure, and 11.112 weight percent of amine, and that its ideal adsorption capacity is 579.468 mg/g. [36]

(Hedayati et al., 2023). The goal of this work is to explore different CO₂ adsorbents for temperature-pressure swing adsorption-based post-combustion capture of CO₂. Activated carbon (AC), clinoptilolite, three synthetic zeolites (13X, 4A and 5A), and a metal organic framework (MOF-MIL-53) are among these adsorbents. Adsorbents were tested with several gas mixes that mimicked a combustion exit stream (O₂/CO /N₂/CO₂/) to assess their performance and adsorption capacity of CO₂ throughout subsequent adsorption–desorption cycles at various circumstances (1–6 bar and 120–180°C). Excellent adsorption capacity of 4.3 mmolCO₂/g zeolite and highly stable performance across multiple cycles were demonstrated by the 13X zeolite[37]

(Cavallo et al., 2023). Both naturally occurring Clinoptilolite (Clino) and Linde-Type A (LTA) zeolite, were studied separately or following an ion-exchange method, and their CO₂ adsorption performances were compared to evaluate their potential use as solid adsorbents for Carbon Capture and Storage (CCS). While natural clino has intriguing CO₂ adsorption performances at medium-high temperatures (it is the most performant material at 423 K), LTA zeolites have superior CO₂ adsorption capacities at lower temperatures. [38]

(Najafi et al., 2023). By using a unique post-synthesis modification technique, different metals, such as transition metals (Cu²⁺ and Fe³⁺) and alkaline earth (Mg²⁺ and Ca²⁺), alkali (Na⁺, K⁺), and alkali (Na⁺, K⁺), were successfully added to the morphology of faujasite zeolites (X and Y). Zeolite X, is a faujasite zeolite with a lesser ratio of Si/Al, performs better in CO₂/N₂ and CO₂/CH₄ separation than zeolite Y, which has a greater ratio. KX had the largest diffusion coefficients for N₂ and CH₄, as well as the highest CO₂/N₂ and CO₂/CH₄ IAST selectivity in all the samples, with values of 61 and 152 at 100 kPa, respectively. Potassium metal that had been

added to the faujasite zeolites demonstrated potential as absorbents for the removal of CO₂ from the stream of natural gas and flue gas. [39]

(Zhao et al., 2023). The goal of the study is to create a series of commercial zeolite 13X particles (13X@MPC) with microporous carbon coatings through the pyrolysis of polyvinylidene fluoride (PVDF), where zeolite 13X beads are coated in a homogeneous microporous layer. After being covered in a layer of microporous carbon, zeolite 13X changes from hydrophilic to hydrophobic. 13X@MPC exhibits an optimized sample with a low H₂O uptake (157.1 cm³/g) half that of 13X (315.2 cm³/g) and a strong CO₂ uptake (76.2 cm³/g) comparable to 13X (80.5 cm³/g). Using the ideal adsorption solution theory, 215 is the expected optimal CO₂/N₂ selectivity. The innovative separation experiment confirms the exceptional capacity of 13X@MPC to collect carbon from wet flue gas. Under the same conditions, the zeolite 13X (6.8 cm³/g and 12.5) exhibits significantly higher CO₂/N₂ selectivity (56.2) and CO₂ capacity (26.5 cm³/g).[40]

(Cavenati et al., 2004). This study examined the adsorption of nitrogen and carbon dioxide on samples of Zeolite 13X and activated carbon. Zeolite 13X was found to be more appropriate for carbon dioxide separation due to its higher heat of adsorption and greater selectivity for carbon dioxide over nitrogen. Keeping in mind a few zeolite limitations, such as its hydrophilic nature, which will maintain its adsorption capacity.[7]

(Agata et al., 2023). To uncover the underlying adsorption physics, in-depth rod-level 3D numerical simulations are performed on 3D-printed zeolite-13X lattice structures. In particular, the current work focuses on how the utilization ratio, adsorption rate, and inlet air velocity all interact at the breakthrough time of a zeolite lattice structure. The findings imply that, to maximize the zeolite media's utilization while simultaneously optimizing the sorption rate for a quick adsorption process and breakthrough time, the inlet air velocity for a particular 3D-printed zeolite lattice structure must be carefully specified. Designing sophisticated 3D-printed zeolite structures for upcoming carbon dioxide removal systems requires an understanding of the concepts. [41]

(Panda, Kumar, et al., 2020). To create hierarchical zeolite 4A (HZ 4A) with certain textural features, microporosity was added in this study through post-synthesis alteration of binder which contains zeolite 4A groups through use of urea treatment. In comparison to Z4A bodies, HZ 4A-13 attained better CO₂ adsorption efficacy with reasonable CO₂ energy of regeneration due to the presence of mesopores, it provided less adsorption capacity of water (20% less), mid temperature

of desorption (13 °C less), less adsorption heat of CO₂ (14% less), and quick gas diffusion inside the pores in both sorption (30 s quicker) and desorption (91x quicker). [42]

(Hedlund et al., 2021). Steel monolithic supports with a microchannel width of 0.5 mm and a cell density of 1600 cpsi were used to cultivate uniform 13X films with 11 and 3 μm thickness. The rate-limiting step in the adsorption process was the transport of CO₂ in the thin zeolite layer, as indicated by numerical modelling. The mass transfer resistance of the 11 μm film is 100 times lower than that of zeolite 4A beads and 2.2 times lower than that of zeolite 13X pellets. It was demonstrated that gas film resistance, pressure drop, and axial dispersion were insignificant. [43]

(Davarpanah et al., 2020). This study looked at the low-cost zeolite clinoptilolite's adsorption capacity for absorbing carbon dioxide (CO₂) at a moderate temperature, which is emitted by industrial processes. At 293 K, Z13X's adsorption capacity was higher than that of bare and ion-exchanged clinoptilolite, but at a moderate temperature of 338 K, clinoptilolite showed the highest CO₂ uptake (i.e., 25% higher than Z13X). This characteristic seems consistent with the lower CO₂ adsorption isosteric heat on clinoptilolite in comparison to the other samples. [44]

(Panda, Singh, et al., 2020). A thorough analysis was conducted to determine how zeolite 4A bodies' physical and chemical modifications affected the properties of CO₂ adsorption. The amine impregnation method was used to accomplish the chemical modification, while the planetary ball mill was used to accomplish the physical change. Following milling, the surface area dropped by 53%, which resulted in a 28% decrease in the CO₂ adsorption capacity in Zeo-12 (milled zeolite 4A bodies). On the other hand, Zeo-00 (unmilled zeolite 4A bodies) and Zeo-12 showed a rise in CO₂ adsorption capacity of 10.45% and 46.23%, respectively, following chemical modification by isopropyl amine impregnation. Additionally, the CO₂ adsorption isotherm data was used to determine the Henry constant, which was shown to be improved by 2.92% and 130.79% in Zeo-00 and Zeo-12-IPA, respectively. [45]

(Hong et al., 2020). To compare the pore characteristics and adsorptive efficiency of monoliths containing the 13X zeolite or the metal organic framework MIL-101(Cr) for CO₂ collection, a comparative analysis was carried out. When compared to 13X zeolite monoliths, the MIL-101(Cr) monoliths CO₂ adsorption capacity is approximately 37% higher (because of mmol/g) at development and somewhat less (around 7%) at equilibria. It was discovered that MIL-101(Cr) monoliths were 1.5x effective at adsorbing CO₂ than zeolite 13X monoliths. The study examined

the impact of regeneration temperature on CO₂ sorption in zeolite 13X monolith and MIL-101(Cr). The findings indicated that an increase in regeneration temperature resulted in a greater capacity for CO₂ adsorption. In conclusion, the investigation shows that MIL-101(Cr) monoliths outperform zeolite 13X monoliths in CO₂ adsorption capabilities. [46]

(Ozturk et al., 2022). Comparative data about CO₂ capture between raw and amine-impregnated micro-, meso-, and microporous support materials is provided by this study. The immobilized liquids were diethanolamine (DEA) and monoethanolamine (MEA), Conversely, zeolite 4A (4A), activated carbon (AC), and pumice (P) served as the macro-, meso-, and microporous support materials. Amine loading increased the CO₂ collection efficiencies of pumice, activated carbon, and zeolite 4A by 19.1, 13.4, and 5.4 times for MEA and 8.8, 6.2, and 4.1 times for DEA, respectively. At 373 ± 2 K and 1 kPa, the CO₂ release rates from the DEA- and MEA-impregnated 4A, AC, and P were found to be 0.242, 0.580, and 0.670 mg respectively. During the cycle operation, the MEA-impregnated support components' CO₂ sorption capacities showed more negative impacts than the DEA-impregnated ones, and the effect increased from the micro toward the microporous support materials. [47]

(Murge et al., 2019). Tetra-ethylene pentaamine was impregnated in house-developed zeolite supports in this investigation to see if it might be used to increase CO₂ adsorption capability. The impact of temperature, Si/Al ratio, amine loading, and reactor pressure on CO₂ uptake capability was investigated. As the loading of amine and temperature of adsorption increased, a decreasing trend in CO₂ adsorption capability was noted. Zeolite-Y, also known as Z-Y-3 with a silica/alumina ratio of 2.25, demonstrated its highest adsorption capacity at 30 °C. Under atmospheric pressure, the obtained values were approximately 114 and 190 mg CO₂/g sorbent, respectively. [48]

CHAPTER 3 EXPERIMENTATION

This section describes the experiments that were conducted in various labs and includes a variety of appropriate synthesis techniques that were used to produce the required products. The synthesis methods used to create the intended product are covered in this section. The preparation of the synthesized zeolite 13X, 4A, and its monolith is discussed in this section.

3.1 Synthesis of Zeolite 13X

The zeolite 13x is synthesized in the laboratory, using the hydrothermal method.

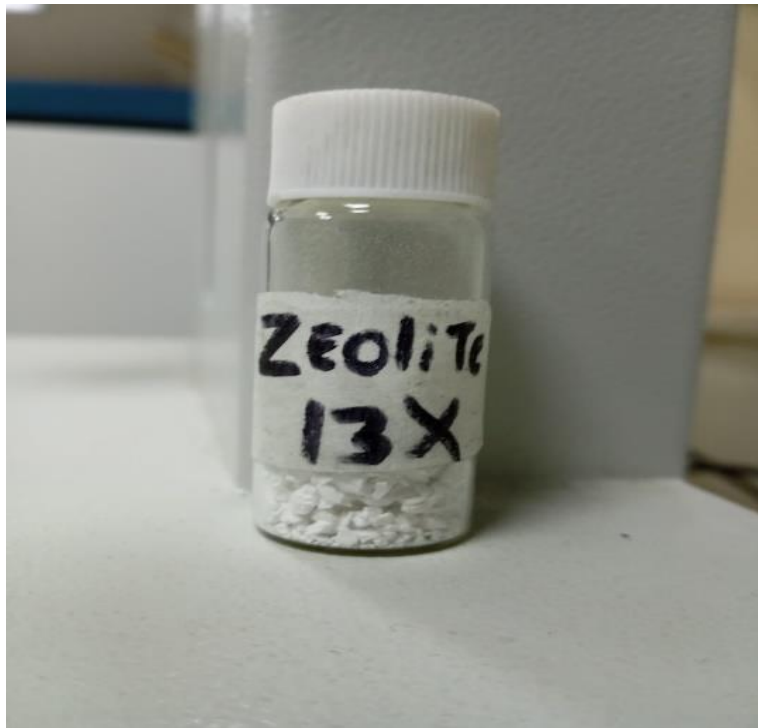


Figure 3-1. Zeolite 13X

3.1.1 Materials

Sodium Hydroxide (Sigma-Aldrich), Sodium Aluminate (Sigma-Aldrich), and Sodium Silicate (Sigma-Aldrich) are used in their original shape. Deionized water (DI) was utilized for dissolving materials, preparing gels, and washing purposes.

Table 1 shows the materials used in the synthesis properties.

Table 3-1. Chemicals used in the synthesis properties.

Sr. No	Chemicals	Molecular Weight (g/mol)	Boiling Point (°C)	Melting Point (°C)
1	Sodium Hydroxide	39.997	1388	323
2	Sodium Aluminate	81.970	Soluble in water	1650
3	Sodium Silicate	122.06	2355	1410

3.1.2 Method of Preparation

To synthesize zeolite 13X, a hydrothermal crystallization process is used. $3.5\text{Na}_2\text{O}:1\text{Al}_2\text{O}_3:2.9\text{SiO}_2:150\text{H}_2\text{O}$ is the hydrogel formula used to synthesize the zeolite 13X. To get 100g of the gel use 4.18g of sodium hydroxide, 5.23g of sodium aluminate, 20.21g of sodium silicate, and 70.48g of Deionized water (DI). First sodium hydroxide (NaOH) is dissolved in DI water, then the dissolved solution is divided into two half ratios and in one half add sodium Aluminate and in the other half add Sodium silicate, Now adds the silicate solution drop by drop to aluminate solution at 25°C to form a thick gel. The hydrogel was then stirred for 6h at moderated speed after that the sol-gel was aged overnight and crystallized in stainless steel Teflon for 14h at a temperature of $90\text{ }^\circ\text{C} \pm 5\text{ }^\circ\text{C}$. After Crystallization, remove the sample from Teflon and cool down at room temperature then wash the sample several times with DI water to maintain the PH value till 8. In final the solid gel is dried in an oven at a temperature of 250°C and proceed for the characterization.

3.2 Synthesis of zeolite 4A

Zeolite 4A is synthesized in the laboratory, using the hydrothermal method.

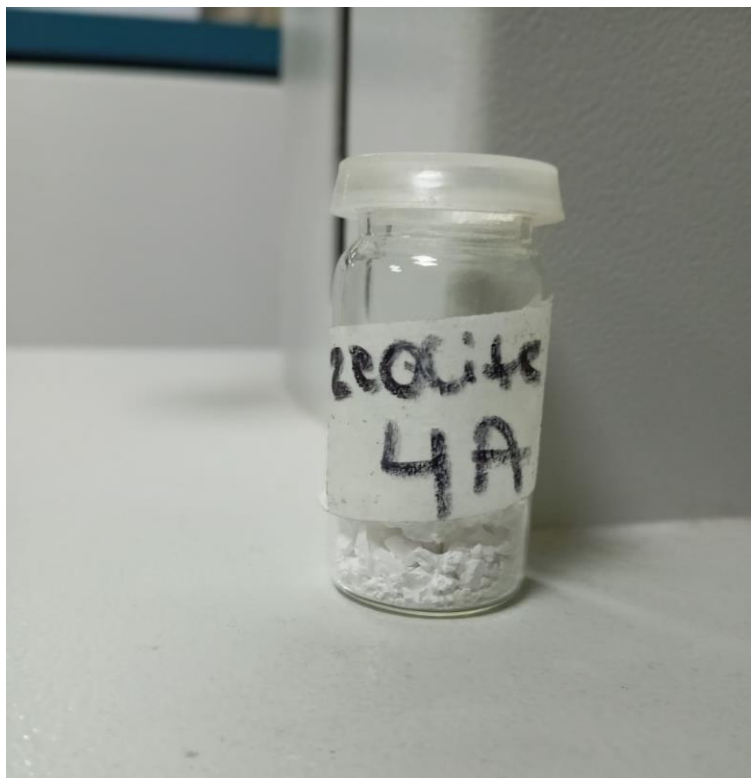


Figure 3-2. Zeolite 4A

3.2.1 *Materials*

Sodium Hydroxide (Sigma-Aldrich), Sodium Aluminate (Sigma-Aldrich), and Sodium Silicate (Sigma-Aldrich) are used in their original shape. Deionized water (DI) was utilized for dissolving materials, preparing gels, and washing purposes.

Table 1 shows the materials used in the synthesis properties.

3.2.2 *Method of Preparation*

A hydrothermal crystallization method is used for the synthesis of zeolite 4A by using the molar ratio $3.5\text{Na}_2\text{O}:1\text{Al}_2\text{O}_3:2\text{SiO}_2:150\text{H}_2\text{O}$. To get 100g of the gel use 4.9g of NaOH, 5.22 g of Sodium Aluminate, 14.18g of sodium silicate, and 75.69g of DI water. First sodium hydroxide (NaOH) is dissolved in DI water, then the dissolved solution is divided into two half ratios and in one half add sodium Aluminate and in the other half add Sodium silicate, Now adds the silicate solution drop by drop to aluminate solution at 25°C to form a thick gel. The hydrogel was then

stirred for 6h at moderated speed after that the sol-gel was aged overnight and crystallized in stainless steel Teflon for 14h at a temperature of $90\text{ }^{\circ}\text{C} \pm 5^{\circ}\text{C}$. After Crystallization, remove the sample from Teflon and cool down at room temperature then wash the sample several times with DI water to maintain the PH value till 8. In final the solid gel is dried in an oven at a temperature of 250°C and proceed for the characterization.

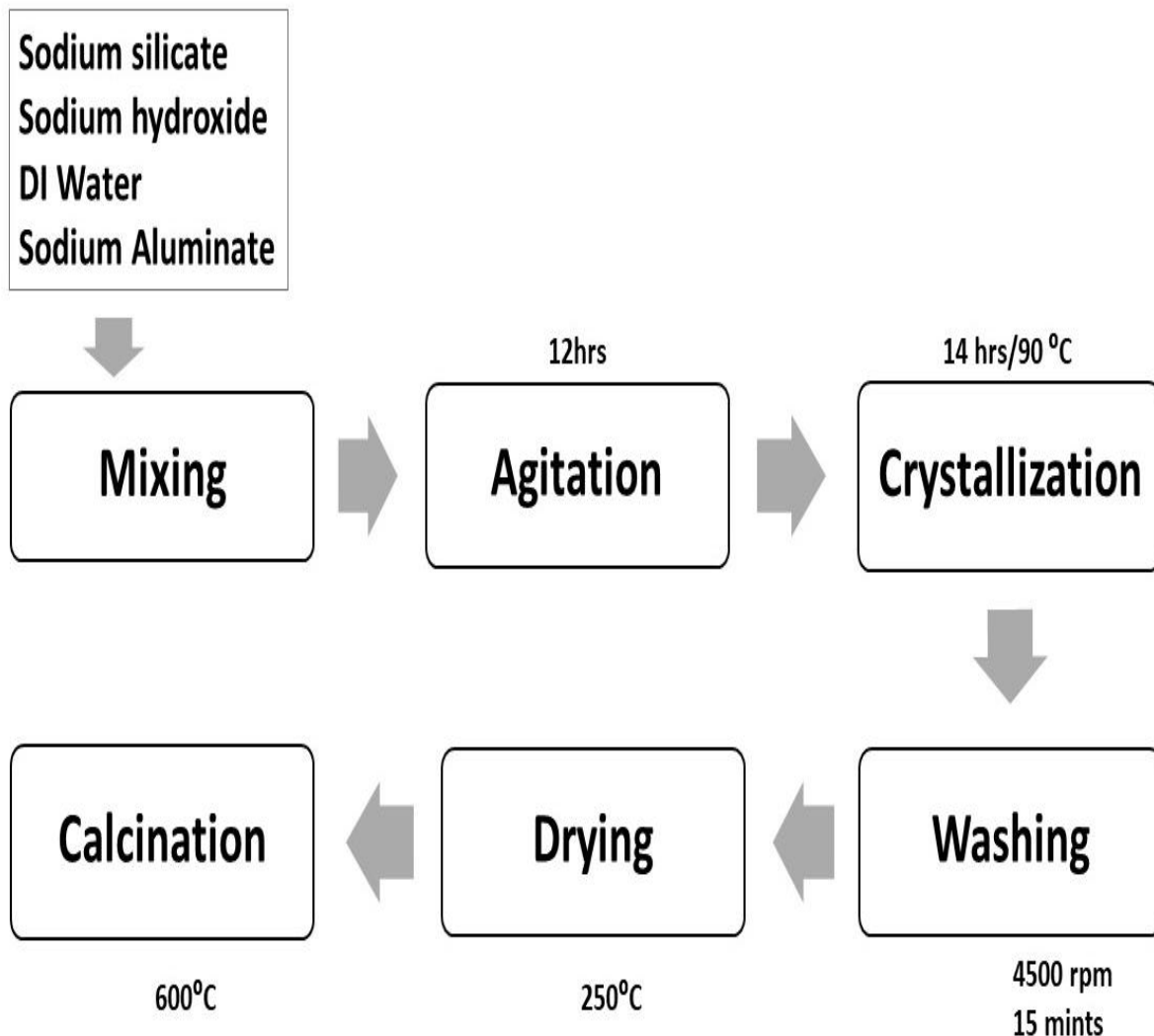


Figure 3-3 Schematic Of synthesis of zeolites.

3.3 Synthesis of Zeolite 13x Monolith

The zeolite 13X monolith is synthesized in the laboratory.

3.3.1 *Materials*

Table 3-2. Properties of chemicals used in synthesis.

Sr. No	Chemicals	Molecular Weight g/mol	Boiling Point (°C)	Melting Point (°C)
1	Zeolite 13X	318.399	330	1650
2	Humic Acid	227.1	774	350
3	Activated Carbon	12	600	3550

Zeolite 13X monolith, Activated Carbon, Humic Acid as a binder, Deionized Water (DI). Table 2 shows the properties of chemicals used in the synthesis of 13x monolith.

3.3.2 *Method of Preparation*

To synthesize the honeycomb monolith using zeolite 13X, Activated carbon and humic acid, 67%w/w of the zeolite 13X, 28%w/w of Activated Carbon and 5% w/w of Humic Acid as a binder. The solid product is mixed by using a ball mill to be sure that each solid component is spread equally. After that DI water is added slowly drop by drop until the solid weight composition of 80% has been obtained and mixed for 6h. The formed slurry is now dry at 85°C for 12 hours after drying the zeolite monolith is obtained. Calcination was the last process used to prepare the green honeycomb monolith. The final treatment was carried out in a vacuum furnace which was heated to 600°C and left on for 12 hours.

3.4 **Synthesis of zeolite 4A monolith**

The zeolite 4A monolith is synthesized in the laboratory.

3.4.1 *Materials*

Zeolite 4A monolith, Activated Carbon, Humic Acid as a binder, and Deionized Water (DI).

Table 3 shows the properties of chemicals used in the synthesis of 4A monolith.

Table 3-3. Chemical properties of materials used in the synthesis of zeolite 4A monolith.

Sr. No	Chemicals	Molecular Weight g/mol	Boiling Point (°C)	Melting Point (°C)
1	Zeolite 4A	318.399	716	1650
2	Humic Acid	227.1	774	350
3	Activated Carbon	12	600	3550

3.4.2 Method of Preparation

To synthesize the honeycomb monolith using zeolite 4A, Activated carbon and humic acid, 67%w/w of the zeolite 13x, 28%w/w of Activated Carbon and 5% w/w of Humic Acid as a binder. The solid product is mixed by using a ball mill to be sure that each solid component is spread equally. After that DI water is added slowly drop by drop until the solid weight composition of 80% has been obtained and mixed for 6h. The formed slurry is now dry at 85°C for 12 hours after drying the zeolite monolith is obtained. Calcination was the last process used to prepare the green honeycomb monolith. The final treatment was carried out in a vacuum furnace which was heated to 600°C and left on for 12 hours.

3.5 Synthesis of zeolite 13X and 4A monolith

The zeolite 13x and 4A monoliths are synthesized in the laboratory.

3.5.1 Materials

Zeolite 13X and 4A monolith, Activated Carbon, Humic Acid as a binder, and Deionized Water (DI).

Table 3.4. Chemical properties of materials used in the synthesis of zeolite 13X and 4A monolith.

Sr. No	Chemicals	Molecular Weight (g/mol)	Boiling Point (°C)	Melting Point (°C)
1	Zeolite 4A	318.399	716	1650
2	Zeolite 13X	318.399	716	1650
3	Humic Acid	227.1	774	350
4	Activated Carbon	12	600	3550

3.5.2 Method of Preparation

To synthesize the honeycomb monolith using zeolite 13X and 4A, Activated carbon and humic acid, 33.5%w/w of the zeolite 13x, 33.5%w/w of the zeolite 4A, 28%w/w of Activated Carbon and 5% w/w of Humic Acid as a binder. The solid product is mixed by using a ball mill to be sure that each solid component is spread equally. After that DI water is added slowly drop by drop until the solid weight composition of 80% has been obtained and mixed for 6h. The formed slurry is now dry at 85°C for 12 hours after drying the zeolite monolith is obtained. Calcination was the last process used to prepare the green honeycomb monolith. The final treatment was carried out in a vacuum furnace which was heated to 600°C and left on for 12 hours.

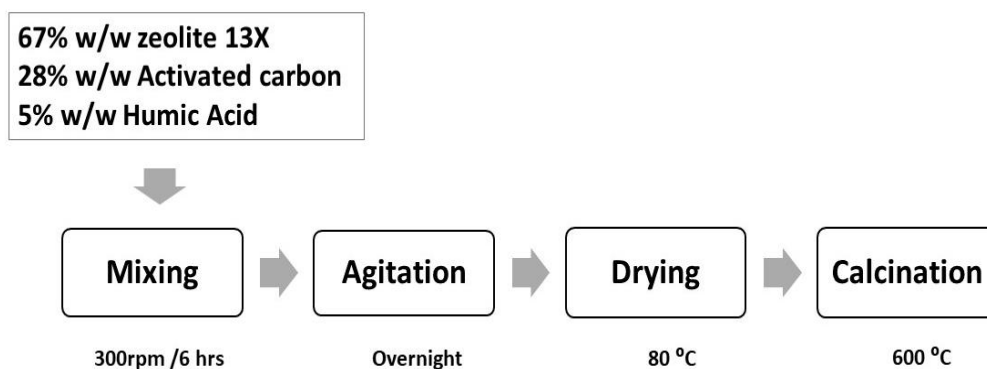


Figure 3-4 Schematic of Synthesis of Zeolite Monolith

CHAPTER 4 CHARACTERIZATION TECHNIQUES

Several methods have been used to characterize the sorbents. The methods that are employed are as follows:

- Scanning Electron Microscope (SEM)
- X-ray Diffraction (XRD)
- Fourier Transform Infrared Spectroscopy (FTIR)
- CO₂ capture study

4.1 Scanning Electron Microscope

Early in the 1950s, scanning electron microscopy was invented. The scanning system, detectors, electron column, vacuum system, display, and electronics control are the primary parts of scanning electron microscopy. The structure and morphology of the zeolite are examined using the SEM, an analytical tool. The scanning electron microscope (SEM) that has been utilized has a resolution of roughly 4 nm and a magnification capability of roughly 10–150,000X. It operates on a very basic idea. There are two cathode ray tubes in it. The sample is placed into the first cathode ray tube, and a high-energy electron beam is fired at its surface. The detector then receives the signal from the bombardment and converts it into a voltage. The second cathode ray tube component receives these voltage signals now, and it displays them on the display. An image is created on a CRT display by the operation of both CRTs, point by point. Concurrent signals are produced by backscattered electrons, secondary electrons, and X-ray detectors; these signals are used to create SEM images. Using a scanning electron microscope (SEM), one can do investigations such as energy dispersive X-ray spectroscopy (EDX), back scattered electron (BSE), and SEI in less than five minutes. Scanning electron microscopy operates at a very high speed. With the right instruction, scanning electron microscopy is a simple and easy technique to use. [49]

We can learn about morphology, topography, and composition through scanning electron microscopy. It is also capable of identifying crystalline formations, providing qualitative assessments, and detecting and looking into fractures. SEM analysis is referred to as "nondestructive" since no volume loss has been seen during the production of X-rays by electron

contact. This is because the electrons interact with the sample only on its surface, preventing sample penetration and enabling repeated material study. The SEM's schematic and key components—the electron gun, anode, magnetic lens, scanning coils, secondary electron detector, TV scanner, and magnetic lens—are depicted in figure 22.

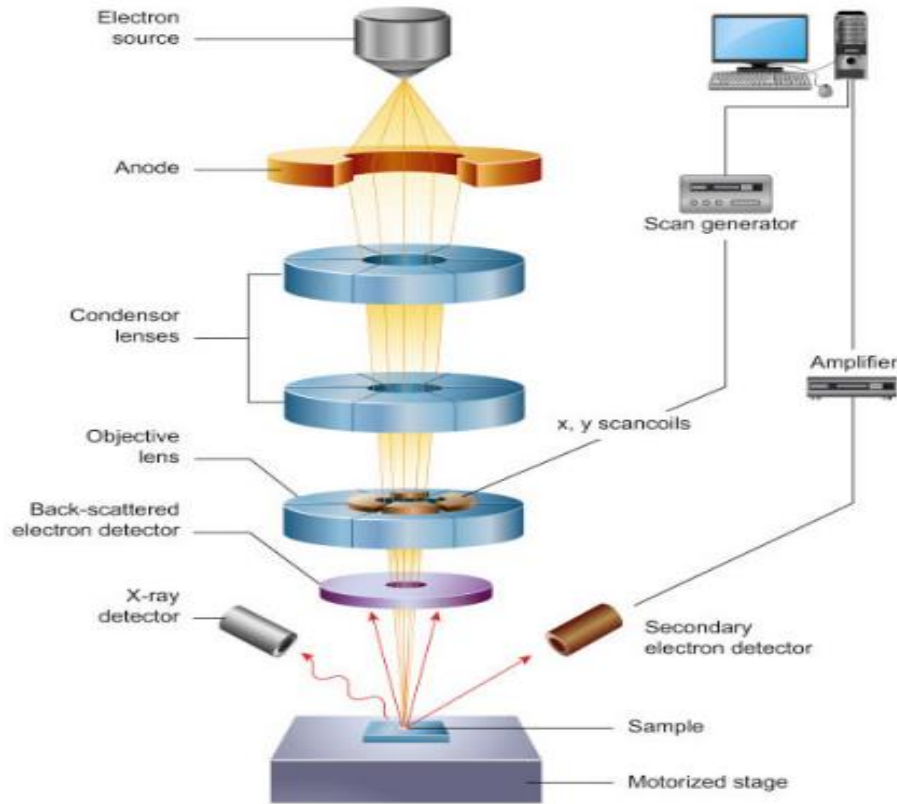


Figure 4-1. Schematic of SEM [49]

4.2 X-Ray Diffraction

By calculating the average distances (atomic spacing) between atomic layers and rows, X-ray diffraction (XRD) provides an analytical tool for revealing the crystalline or phase structures of solid objects. Crystallite size, phase purity, phase identity, crystallinity, lattice parameters, and crystal structure may all be inferred from XRD pattern data. With a wavelength of approximately 1 \AA , X-rays are electromagnetic radiations that are longer than γ -rays but shorter than ultraviolet radiation. The three primary parts of XRD are the detector, sample holder, and X-ray tube. The fundamental idea behind XRD technology is the interference that occurs between a sample and monochromatic X-rays. A cathode ray tube produces X-rays when it charges an electron beam at

high energy and targets a typical copper target. The inner electron shell of the sample material may become dislodged because of the interaction of these high-energy electrons. This ionization process yields distinctive X-ray spectra. An X-ray diffractometer was used to study the sample crystals that had been triggered by zeolites. The material for analysis is uniformly fine-grained. The d-spacing between structural layers at a given angle can be found via XRD. In line with Bragg's law.

$$n\lambda = 2d \sin\theta \quad (4.1)$$

Bragg's law is commonly applied to crystal diffraction and makes the diffraction process easy to grasp. We may determine the crystallite size of the crystals by applying the Debye-Scherrer equation. Every crystalline material has a unique X-ray pattern that is used to identify it, much like a fingerprint.[50]

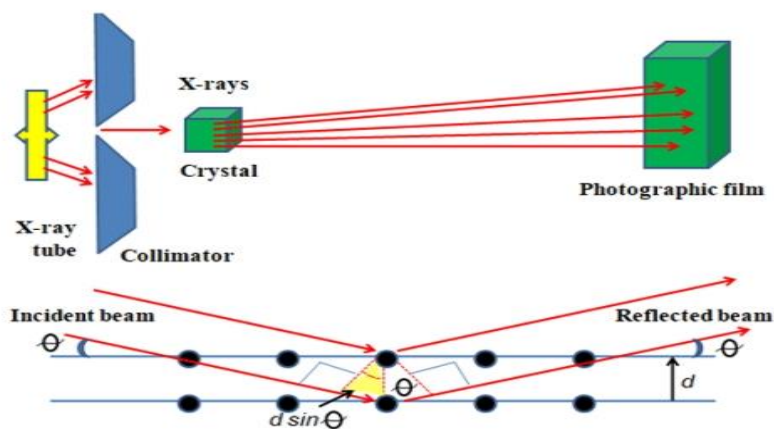


Figure 4-2. Working principle of XRD[50]

4.3 Fourier Transform Infrared spectroscopy (FTIR)

An analytical method called Fourier transform infrared spectroscopy, or FTIR, can be used to determine the kind of chemical bonds that are present in a molecule or to offer information about the vibrational characteristics of functional groups. It is applied to sample analysis, both qualitative and quantitative. The fundamental idea behind FTIR is that when a sample interacts significantly

with electromagnetic radiation, a change in dipole moment must happen because of the molecule vibrating and becoming IR active or of distinct vibrational states being excited.[51]

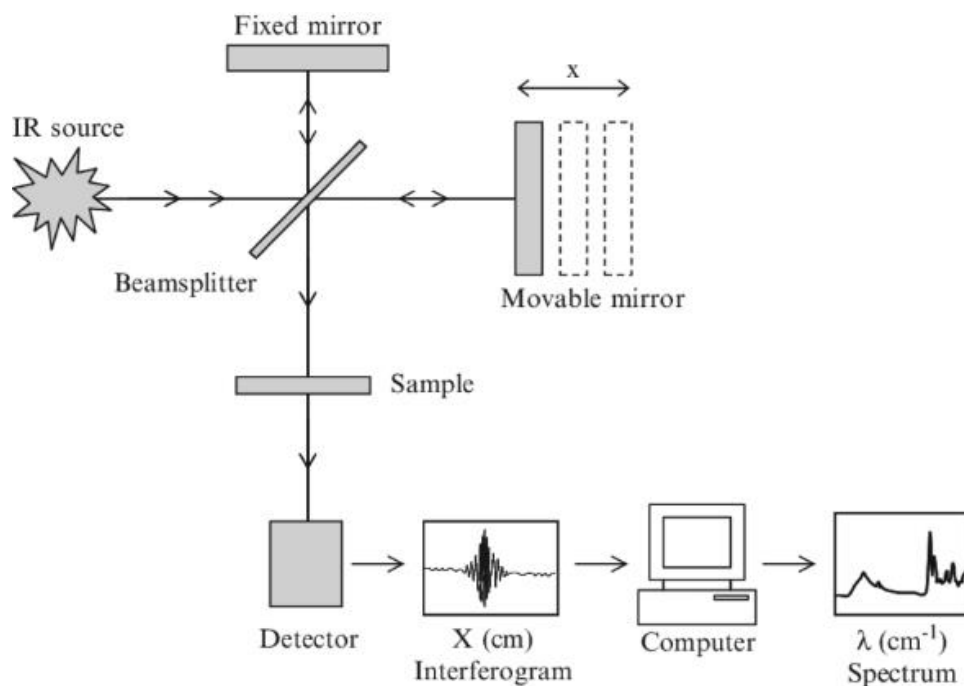


Figure 4-3. Schematic of FTIR [51]

Covalent bonds are in a constant state of vibration or flexible. Stretching or bending—symmetric or asymmetric—can occur during vibration. The resultant infrared spectrum is a plot of frequency and transmittance expressed in wavenumbers. Since oxygen and hydrogen do not absorb infrared light, they are IR inactive molecules. For the examination of the metal-organic framework, an FTIR instrument (Perkin Elmer, Spectrum 100) with a wavenumber range of 450cm^{-1} to 4000cm^{-1} was available. The FTIR apparatus is filled with pelletized zeolite. Less than ten minutes were spent on the analysis, which was conducted at room temperature.

4.4 BET

The specific surface area of materials, particularly porous materials like catalysts, adsorbents, and powders, may be measured using the Brunauer-Emmett-Teller (BET) theory. In 1938, Stephen Brunauer, Edward Teller, and Paul Hugh Emmett created it. The BET theory's primary objective is to calculate a material's surface area by examining the physical adsorption of gas molecules onto its surface. It is commonly used to characterize the porosity and surface area of materials in material science, chemistry, and chemical engineering. The quantity of gas absorbed

on the surface of a solid substance at various relative pressures is measured using the BET technique. Because it forms a monolayer on the material's surface at very low temperatures and pressures, gases like nitrogen are often utilized. The specific surface area is then determined using the BET equation and the resulting adsorption isotherm. Through the analysis of gas adsorption isotherms, the BET theory provides a useful tool for estimating the surface area of materials. In many applications, including the design and optimization of catalysts, adsorbents, and other materials with high surface area requirements, this knowledge is essential.

The BET equation gives a way to compute the specific surface area by connecting the quantity of gas adsorbed to the relative pressure. The formula is as follows:

$$\frac{P}{V(P_i - P)} = \frac{c-1}{V_m * c} + \frac{1}{V_m P_i} \quad (4.2)$$

- P represents the equilibrium pressure.
- P_i represents the saturation pressure of adsorbate.
- V is volume of absorbed gas.
- V_m is the monolayer capacity.
- There is a constant c that is associated with the adsorption energy.

4.5 CO₂ Capture Study

A high-pressure adsorption chamber specifically developed for this purpose has been used to conduct adsorption investigations on zeolites and monoliths at different pressures. Because of its construction, the adsorption rig will be able to tolerate high pressure and temperatures. The CO₂ cylinder that makes up the adsorption rig is attached to the module using tubes. The CO₂ gas utilized in the adsorption analysis was found to be 99.9 percent pure. Mass flow controllers assisted in increasing the outflow stream rate from the gas containers. Throughout the experiment, a heating tape will be required to keep the temperature constant. The temperature of the inner column will be ascertained using a thermocouple instrument that has been put at the base of the column. To ensure maximum control over environmental interaction and to remove the possibility of air contamination, the complete adsorption system was contained in a glove box. To ascertain the

synthesized zeolites' CO₂ adsorption capacity, CO₂ adsorption studies must be performed. Before the adsorption experiment begins, the entire apparatus needs to be cleaned. Purge gas was produced using nitrogen. The nitrogen must circulate in the adsorption rig for approximately two hours to get rid of the undesirable pollutants. The CO₂ adsorption setup schematic is displayed in figure 25.

The treatment that takes place in an adsorption setup is as follows:

Zone I is where the sample degasses. If this function is enabled, the software will automatically complete the cooling air charging, vacuum evacuation, and charging end processes. After the degassing process is complete, remove the sample cell, weigh it, and reinstall it on the side of the analysis ports. Once the sample cells are put in Zone II, verify the matching numbers. Will not affect data and degassing procedures if the "normal temp, name, mass, and sample value" fields are left empty. There are two stages in Zone III. Simply heating the sample to remove moisture is the first step. The operator could input the desired delay time as well as the ideal degassing temperature and duration. The heating plus vacuum step is the second. Zone IV: can remain vacant.

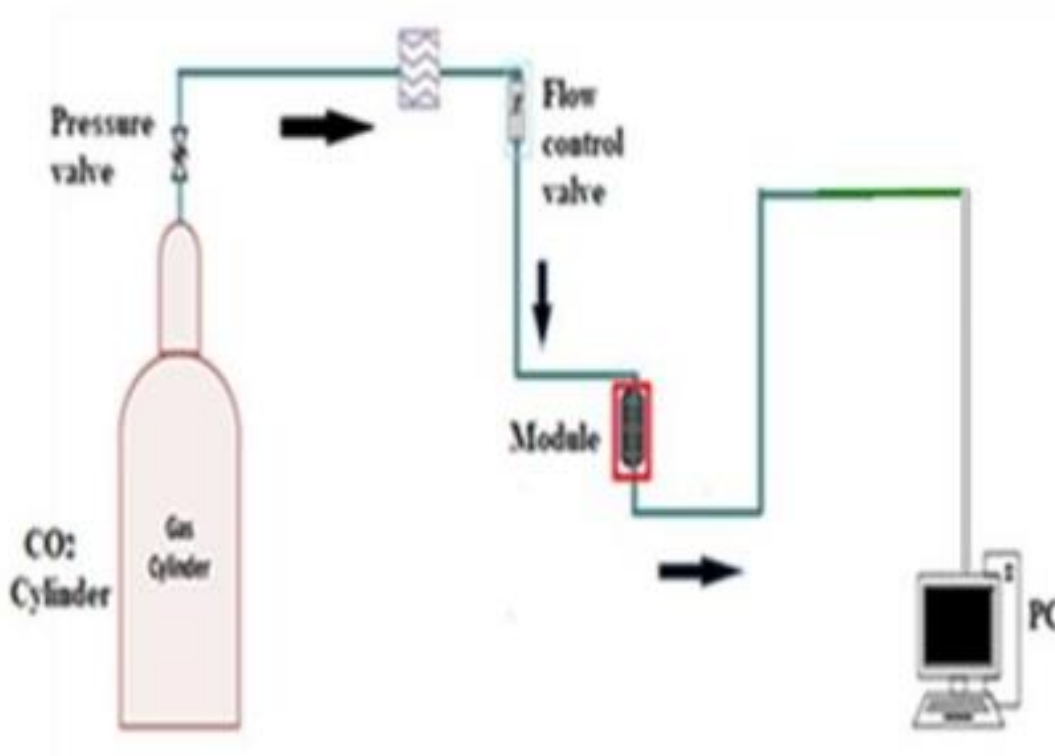


Figure 4-4. Process of CO₂ adsorption [52]

4.6 Particle Size Analyzer

The collective term for the technical processes or laboratory methods used to ascertain the size range, mean, or average size of the fragments in a liquid sample or powder is particle size analysis, measurement, or simply particle sizing. Particle size analysis is often performed at particle technology labs and is a component of particle science.

The devices known as Particle Size Analyzers (PSA) are operated to measure particle sizes. They are based on various techniques which include particle gravitational settling, particle light scattering (Rayleigh and Mie scattering), high-definition picture processing, and Brownian motion analysis. Many industries, including the chemical, culinary, mining, forestry, agricultural, cosmetics, aggregate, energy, and pharmaceutical sectors, may place a high value on particle size.

Because light scattering-based particle size measurement makes optical sample characterization very simple, it is widely used in a broad range of sectors, including polymer, food, pharmaceutical, and cosmetic manufacturing, to enhance product quality control. Numerous developments in light scattering methods for particle characterization have occurred in recent years.

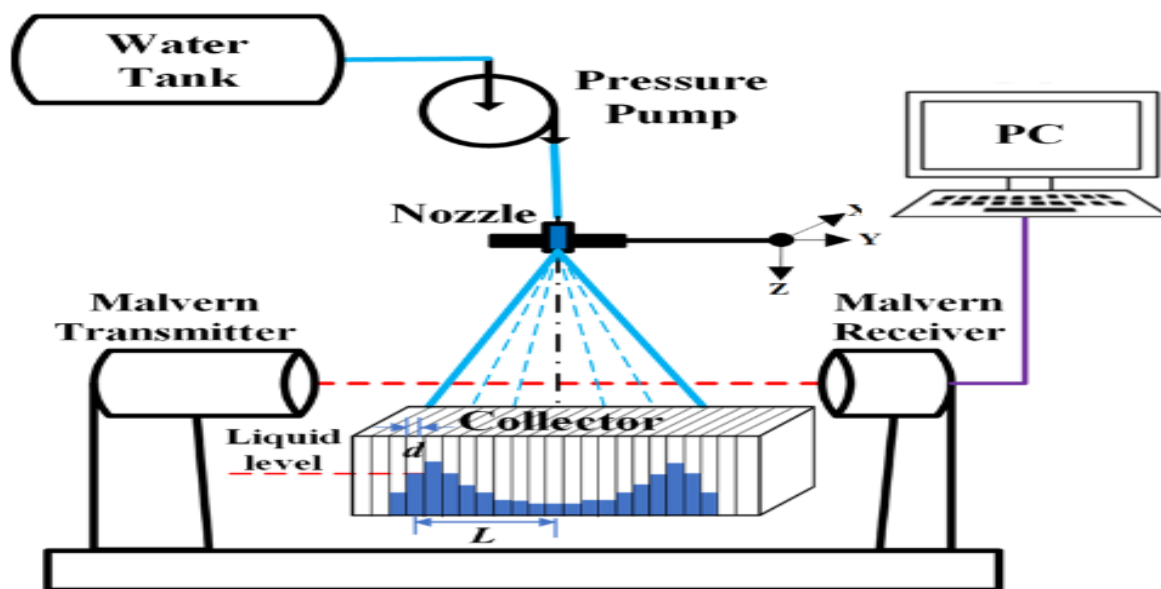


Figure 4-5. Schematic of Malvern particle size analyzer system

CHAPTER 5 RESULTS AND DISCUSSIONS

This chapter goes into elaborate detail on the outcomes that were obtained.

5.1 Characterization Techniques

X-ray diffraction (XRD), scanning electron microscopy (SEM), BET analysis, particle size analyzer, and Fourier transform infrared (FTIR) are a few examples of spectroscopies. We investigated our samples using these characterization methods to get a deeper understanding of their characteristics, structure, and morphology. The formation and shape of the samples were examined using the XRD, SEM, particle size analyzer, and BET methods; the functional groups and forms of bonds contained in our specimens have been determined using the FTIR technique. Variations in pressure conditions were used to carry out the CO₂ adsorption analysis. Every sample has been run through CO₂ studies. The detailed results resulting from the CO₂ capture studies and the characterization methods for each sample are presented below.

5.2 Scanning Electron Microscope

The purpose of scanning electron microscopy (SEM) is to determine the morphology and structure of materials. The samples are first dried under a vacuum before being subjected to the SEM. Following this, the dried samples are coated with gold and with support from the sputter coater to prevent material charging. The SEM images of zeolites and their monolith composites were taken at different magnifications of 0.5 μ m, 1 μ m, and 5 μ m to get a detailed study of the crystal structure and morphology.

The SEM descriptions of zeolite 13X, 4A, and its monolith composites were obtained, and each sample morphology is discussed below. The SEM images show a variety of different structures, the perfect geometry is not seen in some of the images.

5.2.1 SEM Image of zeolite 13X

To better depict the structure of each synthesized zeolite, several sizes of SEM images of 13X zeolite are displayed in Figure 5.1. The large variety of crystal sizes, which are made up of

uneven surfaces and nonuniform particles, are shown in Figure. As is the situation for FAU-type framework structures, the composite containing 95 weight percent 13X Zeolite has octahedral particle shape. This attests to the effective synthesis of this kind of zeolite.

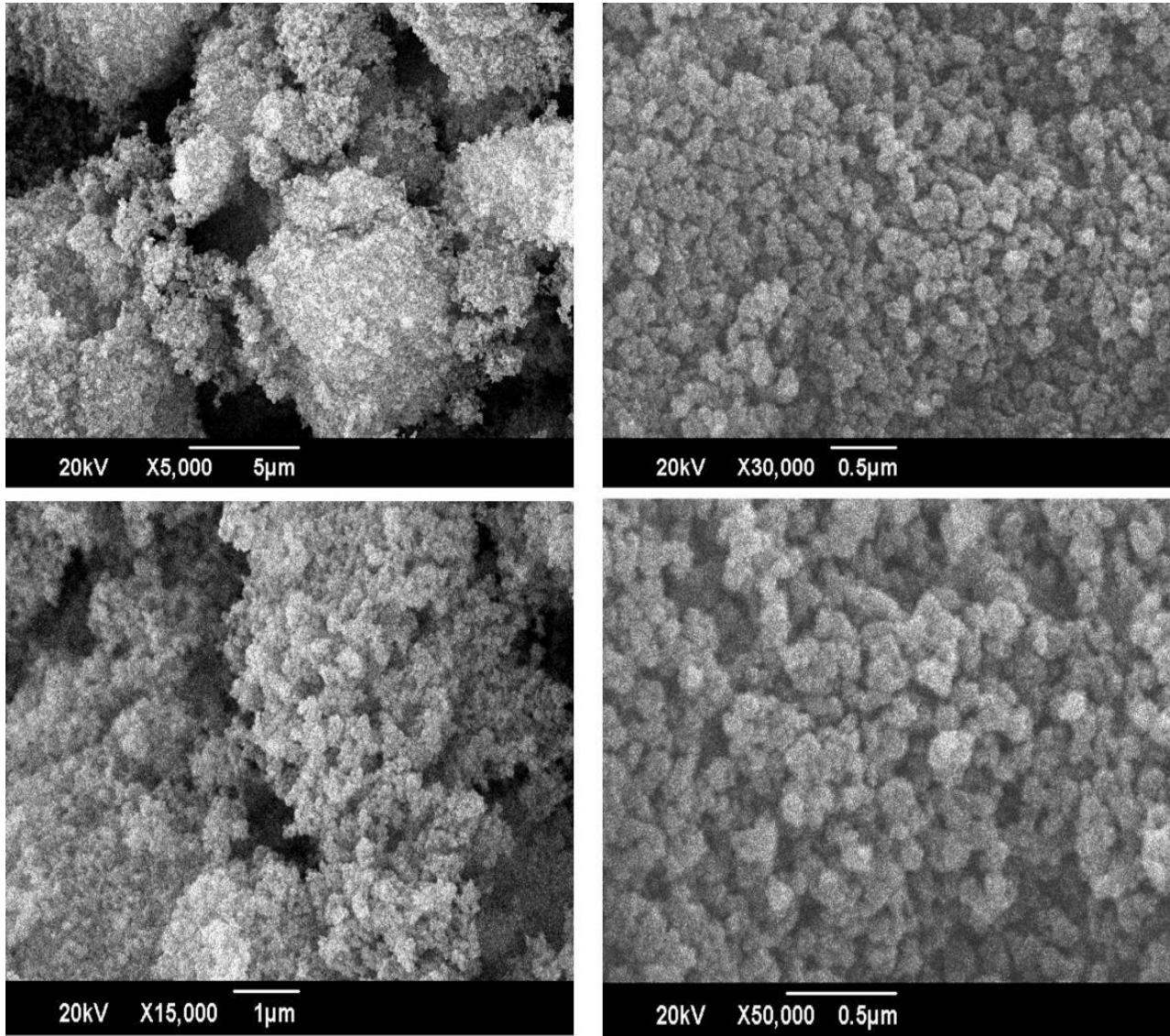


Figure 5-1. SEM Images Of 13X Zeolite at 0.5μm, 1μm and 5μm

5.2.2 SEM Image of Zeolite 4A

Figure 5.2 presented the SEM image of zeolite 4A at different magnification. For the Zeolites 4A, a cubic morphology with rounded corners and edges is seen, confirming the samples' high pure phase and crystallinity.

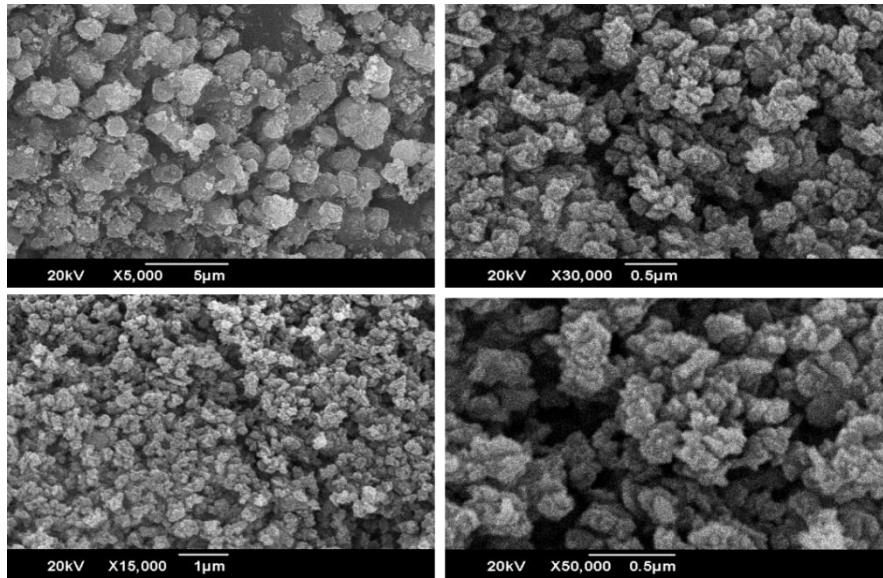


Figure 5-2. SEM image of zeolite 4A

5.2.3 SEM Image of zeolite monolith 13X at 0.5μm, 1μm, 5μm.

Using SEM micrographs, the composite's morphology was examined. The result shown in figure 5.3 presents an image of zeolite 13X monolith. It is feasible to see significant amounts of activated carbon and a huge amount of zeolite crystal, indicating significant heterogeneity. The energy spectrum of 13X monolith shown in figure 5.4 shows the presence of the characteristic elements.

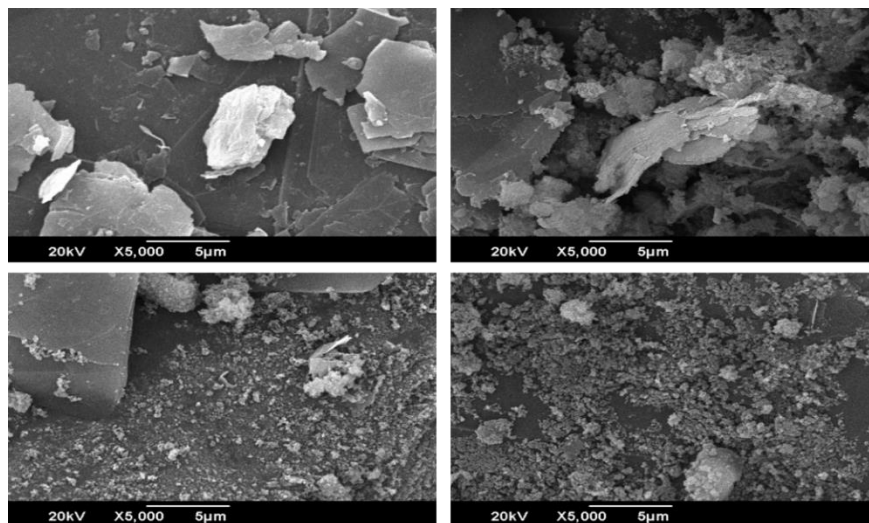


Figure 5-3. SEM Image of zeolite monolith 13X at 0.5μm, 1μm,5μm.

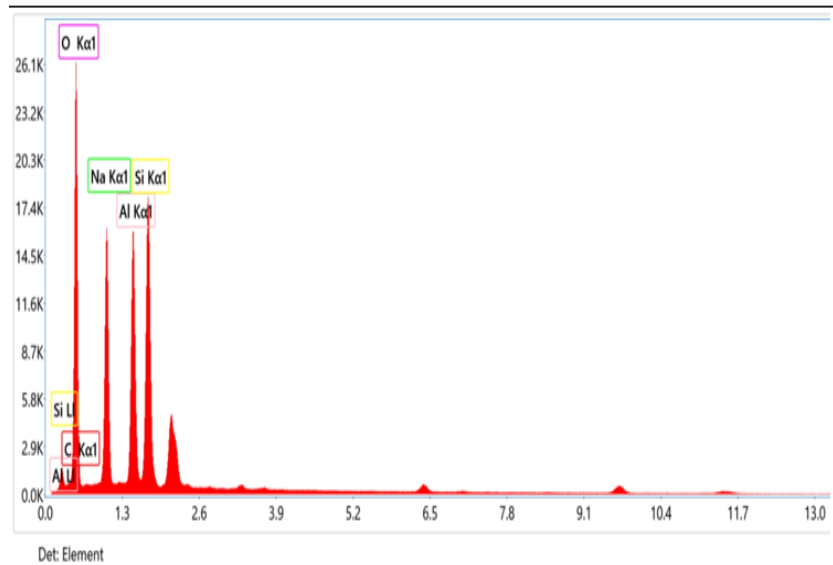


Figure 5-4. EDX OF Zeolite 13X Monolith

5.2.4 SEM Image of zeolite monolith 4A, at 0.5 μ m, 1 μ m, 5 μ m.

The zeolite 4A monolith SEM image is presented in figure 5.4 to demonstrate the inner and monolith surface of the sample, respectively. Considerable heterogeneity may be seen, as shown by the observable presence of zeolite crystal, and activated carbon.

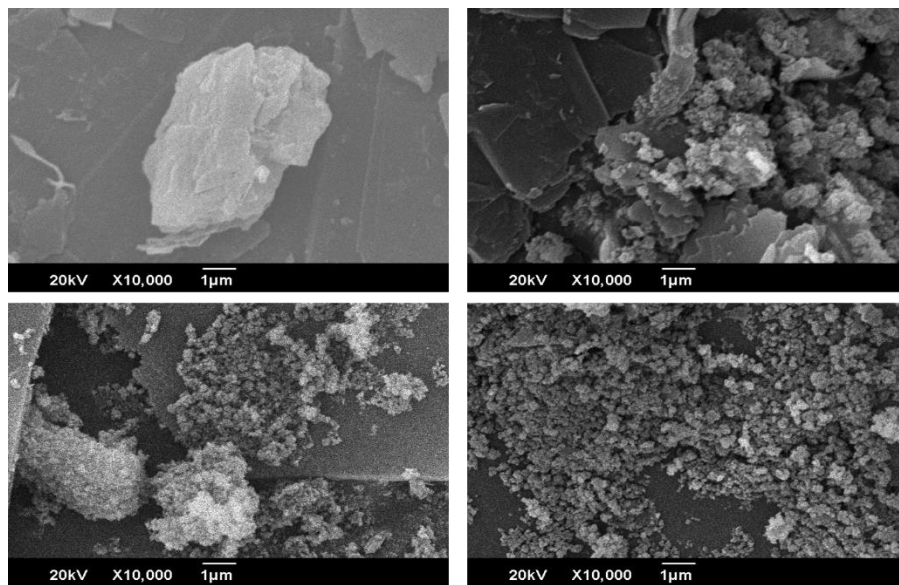


Figure 5-5. SEM Image of zeolite monolith 4A at 0.5 μ m, 1 μ m, 5 μ m.

5.2.5 SEM Image of zeolite monolith 13X+4A, at 0.5 μ m, 1 μ m, 5 μ m.

The zeolite 13X+4A monolith at 0.5 μ m, 1 μ m, 5 μ m magnifications in figure 5.5 show demonstrations of the sample's inner and monolith surface, respectively. It is feasible to see significant amounts of activated carbon and a huge amount of zeolite crystal, indicating significant heterogeneity. In figure 5.6 show energy dispersive spectrum respectively shows the combined monolith a part of zeolite crystals, so the presence of oxygen, sodium (Na), Aluminum (Al), silicon (Si), and small portion of carbon (c) are the characteristic elements of zeolite monoliths. In figure 5.7 shows energy dispersive spectrum of activated carbon in which carbon (C) and oxygen (O) is the key component of activated carbon.

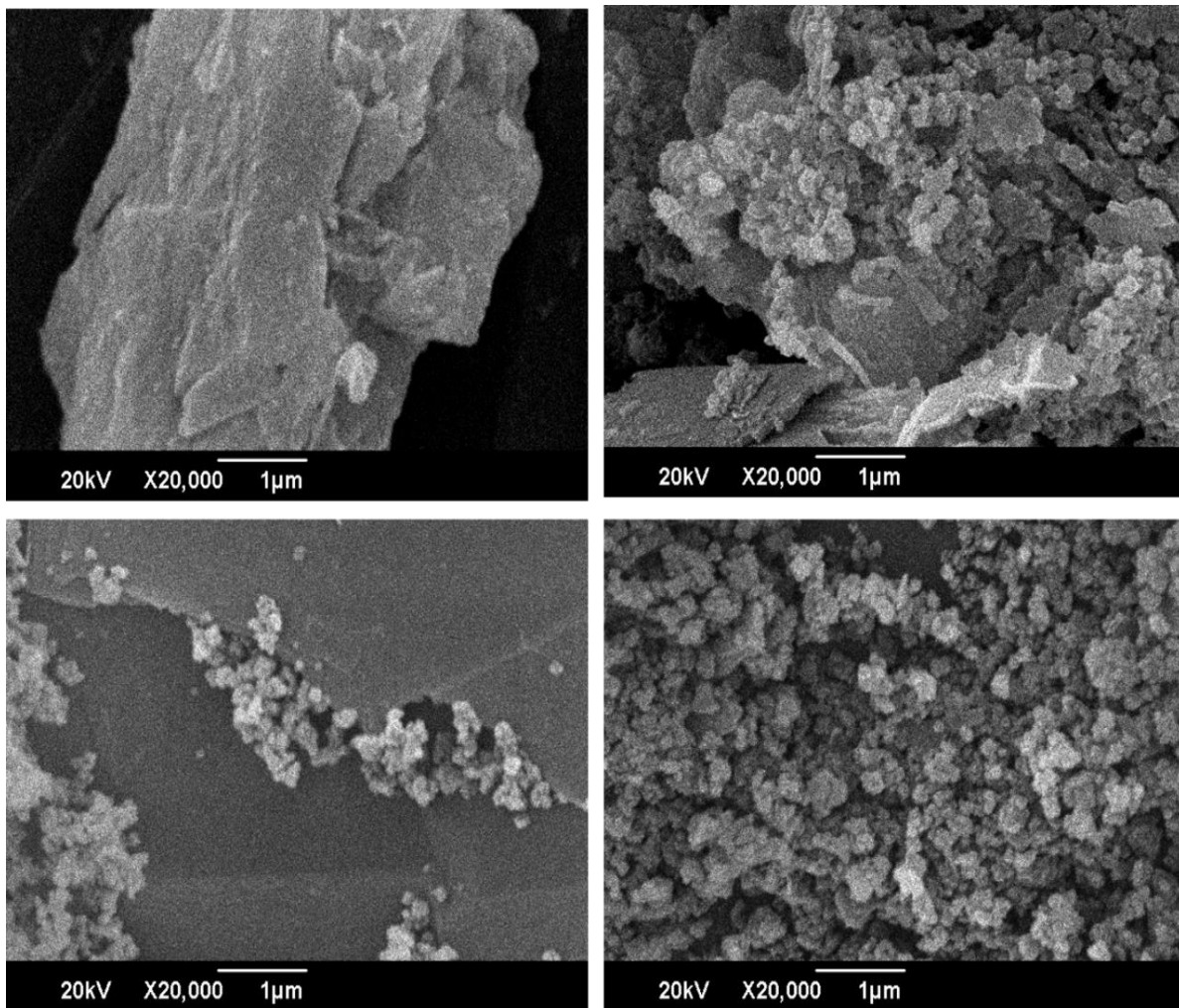


Figure 5-6. SEM Image of zeolite monolith 13X, 4A, and combine 13x+4A at 0.5 μ m, 1 μ m, 5 μ m.

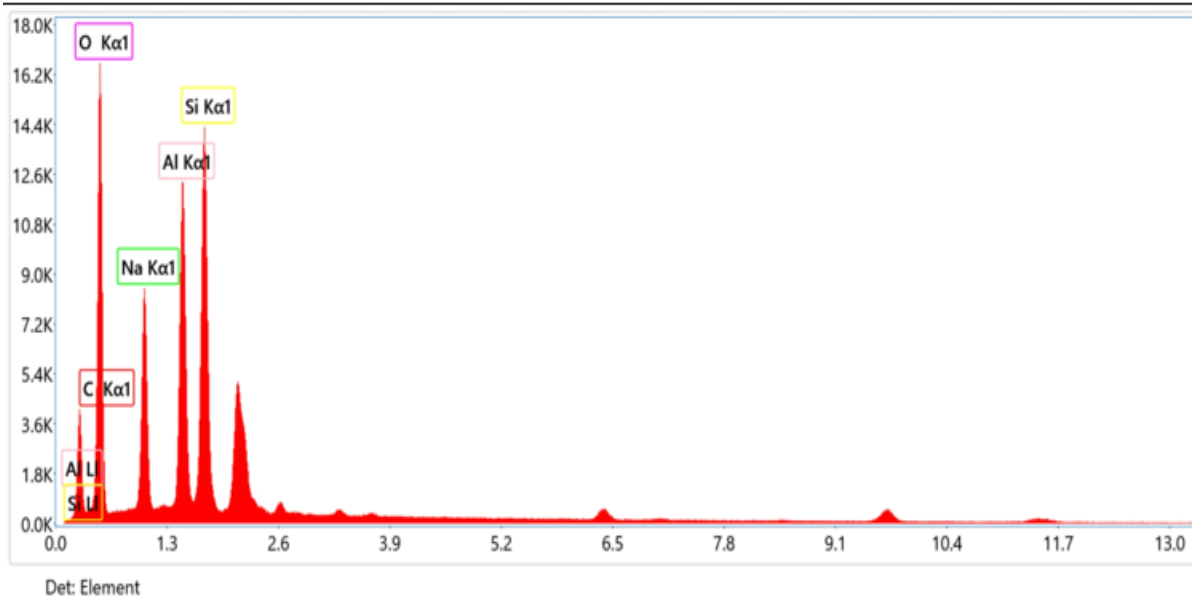


Figure 5-7. EDX of 13X and 4A monolith

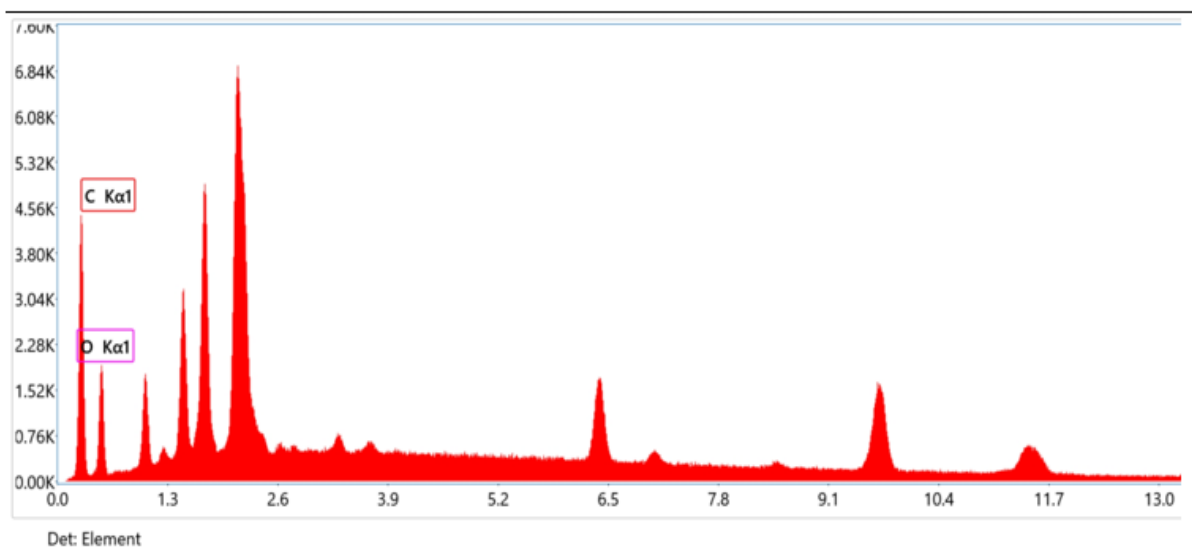


Figure 5-8. EDX of Activated carbon

5.3 BET

The specific surface area of materials, particularly porous materials like catalysts, adsorbents, and powders, may be measured using the Brunauer-Emmett-Teller (BET) theory. In 1938, Stephen Brunauer, Edward Teller, and Paul Hugh Emmett created it. The BET theory's

primary objective is to calculate a material's surface area by examining the physical adsorption of gas molecules onto its surface. It is commonly used to characterize the porosity and surface area of materials in material science, chemistry, and chemical engineering. The quantity of gas absorbed on the surface of a solid substance at various relative pressures is measured using the BET technique. Because it forms a monolayer on the material's surface at very low temperatures and pressures, gases like nitrogen are often utilized. The specific surface area is then determined using the BET equation and the resulting adsorption isotherm. Through the analysis of gas adsorption isotherms, the BET theory provides a useful tool for estimating the surface area of materials. In many applications, including the design and optimization of catalysts, adsorbents, and other materials with high surface area requirements, this knowledge is essential. In table 5 shown the bet data of the zeolites and its composite monoliths

Table 5-1. Physical Properties of adsorbents (SA: surface area, PV: pore volume and APD: average pore diameter)

Adsorbents	SA(m²/g)	PV (cm³/g)	APD(nm)
4A monolith	6.2560	0.019368	12.38
13X monolith	30.9321	0.106776	13.80
13X+4A monolith	11.8287	0.039781	13.45
Activated carbon	2.6996	0.008544	12.65

The physical properties of zeolites and their monoliths and activated carbon are given in table 1.

1. The BET surface area of 4A monolith, 13X monolith, 13X+4A monolith and Activated carbon are 6.25, 30.93, 11.82 and 2.69 m²g⁻¹, respectively. All the monoliths had considerably higher surface area than the reference activated carbon. While the 13X monolith had the highest surface area.

2. In adsorption processes, the pore diameter of adsorbents plays a key role in adsorption capacity, selectivity, and rate of adsorption. Amongst the four samples, the 13X monoliths have the highest diameter.
3. Pore volume is an important factor in considering the capacity of adsorber to absorb molecules. The adsorption capacity will be quite low if the pore volume is too small. The 13X monolith had the highest pore volume amongst the studied monoliths.
4. All the monoliths had better physical properties than activated carbon. While the 13X monoliths had the highest pore volume, average pore diameter and surface area.

5.4 Particle Size Analyzer

The mean particle size of synthesized zeolite particles was measured through the particle size analyzer. The mean particle size of the 13X and 4A zeolites are 21.5 μm and 3.12 μm . The distribution of particle sizes is given in figures 5.8 and 5.9. The particle size of the 4A zeolite is shown as unfluctuating, in comparison to 13X where the size of particles has a wide range.

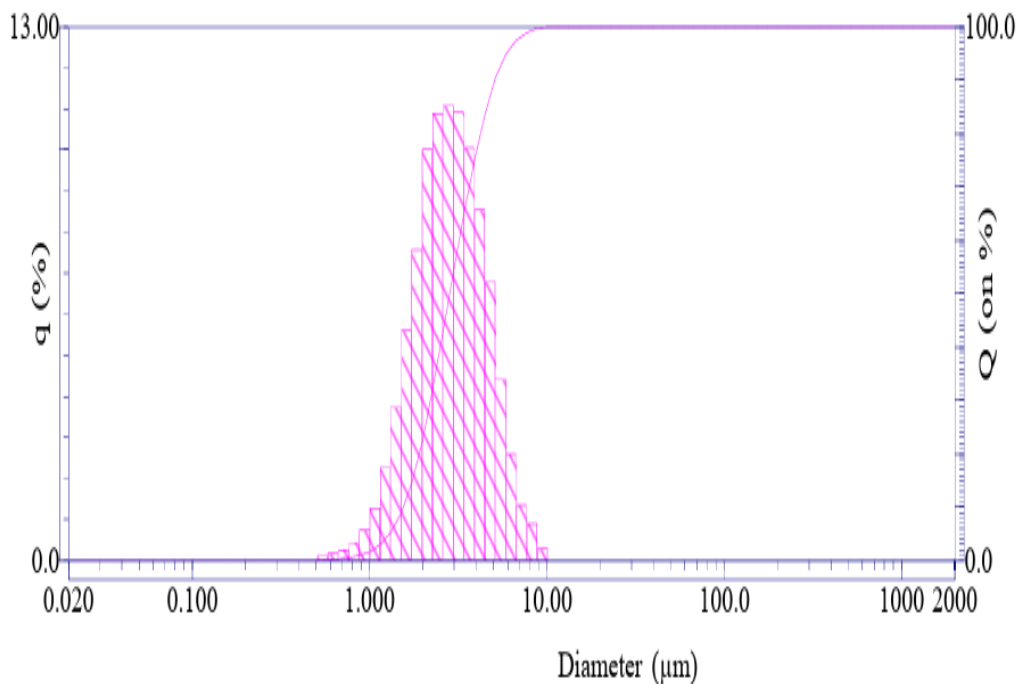


Figure 5-9. Size distribution of particle sizes of synthesized 4A zeolite

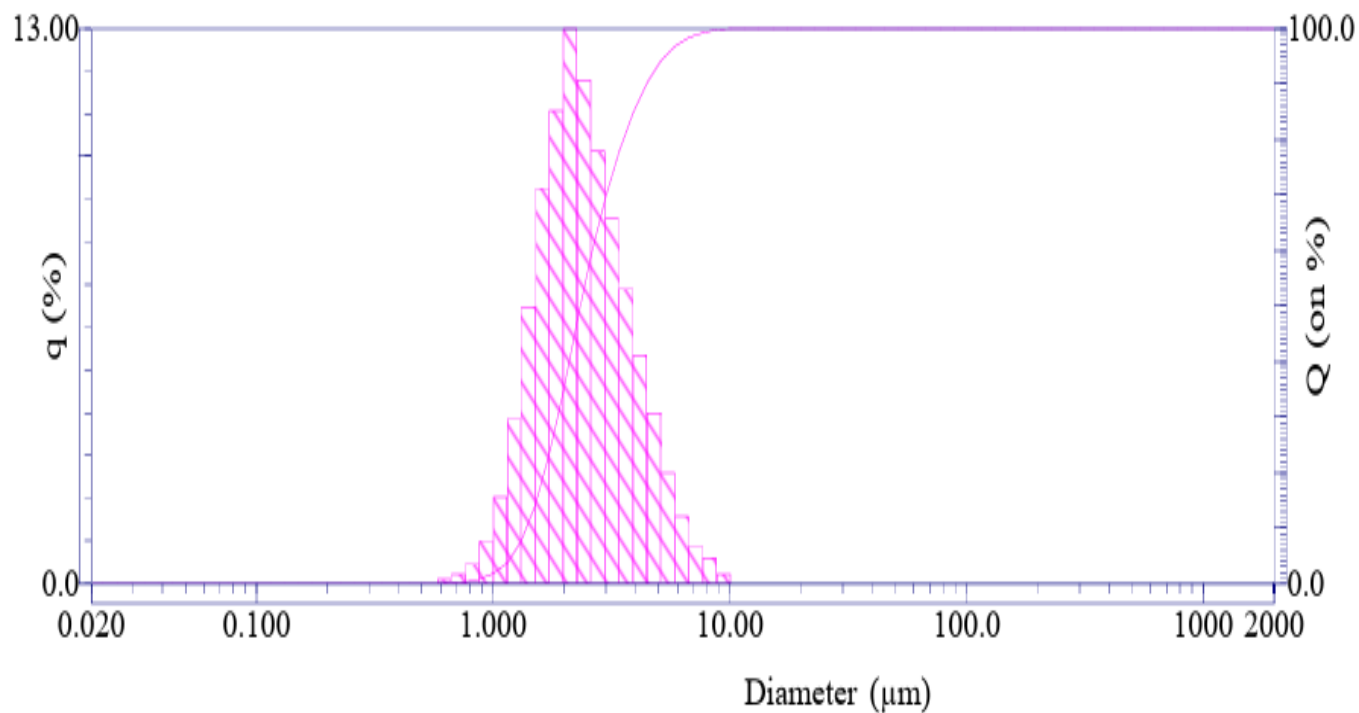


Figure 5-10. Size distribution of particle sizes of synthesized 13X zeolite

5.5 Fourier Transform Infrared spectroscopy (FTIR)

The results of the FTIR analysis demonstrate the various functional groups and bond types that are present in the samples. We form pellets out of our samples prior to FTIR analysis. Pellets were put inside the FTIR. A spectrogram is the output of the FTIR analysis. This shows a graph of transmittance in % and wave number in cm^{-1} from 500 to 4000 cm^{-1} . Fourier transforms infrared spectroscopy of the zeolite 4A, 13X zeolite, and its monoliths are shown in Figure 5.10. The observed bands of (735 cm^{-1}) zeolite 13X, zeolite 4A and its monolith correspond to the 13X Zeolite's symmetric stretching mode ($\leftarrow \text{O T O} \rightarrow$), where the T is either Si or Al. In symmetric stretching mode, peaks 735 cm^{-1} are attributed to internal tetrahedral stretch of zeolites and its monoliths are accredited to external linkage symmetric stretch. The peaks at (981 cm^{-1}) or (978 cm^{-1}) correspond to a asymmetric stretch. The peaks seen at 1650 cm^{-1} or 1643 cm^{-1} are concerned with water molecule H-O-H bending mode. Strong bands at 3433 cm^{-1} and 3443 cm^{-1} are caused by the water molecules in the composite's O-H stretching mode. The results of the characteristic zeolite 13X, 4A and its monoliths shown as a literature [53]

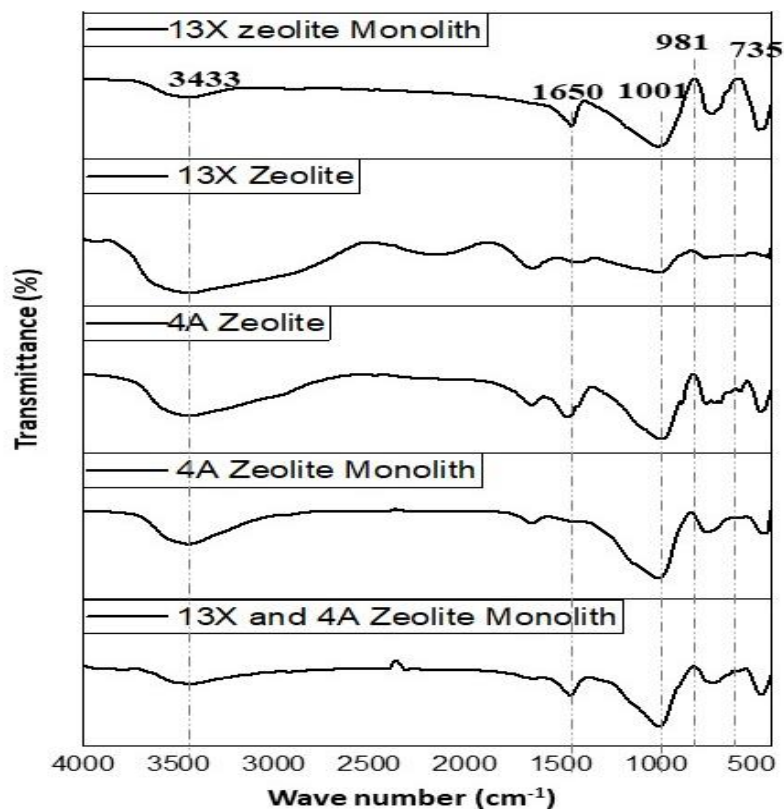


Figure 5-11. Combined FTIR of zeolites and its monoliths

5.6 X-Ray Diffraction

The XRD analysis was performed to determine the phase of the crystalline adsorbent and to determine its composition within the range of 2θ between 0° and 60° . Confirmation of the nature, planer structure, materials, and functioning were achieved using XRD analysis. XRD is typically the initial investigation to identify the purity and kind of zeolite. Using XRD analysis, the crystal phase of the generated samples was determined. Strong peaks, which are consistent with previously published studies like the peaks, show that the produced zeolites have great crystallinity. at $2\theta = 6.1^\circ, 10^\circ, 15.5^\circ, 20.1^\circ, 23.3^\circ, 26.7^\circ, 29.3^\circ, 30.5^\circ, 31.0^\circ,$ and 32.1° [54] show the formation of zeolite 13X in figure 5.11 show in hkl plans values. Furthermore, the primary peaks for the zeolite 4A produced material were seen at $2\theta = 7.18^\circ, 10.17^\circ, 12.46^\circ, 16.11^\circ, 21.6^\circ, 23.99^\circ, 27.11^\circ,$ and 29.94° , which is shown in figure 5.11 in hkl plan values. These figures align with the zeolite 4A reported quantities.

In figure 42 show the zeolite 13X monolith, Zeolite 4A monolith , zeolite 13X+4A monolith xrd patterns in which the hkl values of the synthesized monolith from zeolite 13X ,Zeolite 4A and activated carbon shown at 002 hkl value of activated carbon , (111) show the presence of the zeolite13x and plan (004) shows the zeolite 4A composition in the combine it also show both zeolite peaks are present and consistent with the result in literature. The results of the monoliths are overlapped with those of the zeolite 13X, zeolite 4A and activated carbon as shown in figure 5.12 as the major peak of the activated carbon is (002) are crystal plan of the activated carbon whereas the peak at (511) shows the impurity in the activated carbon with th presence of iron oxide.[53]

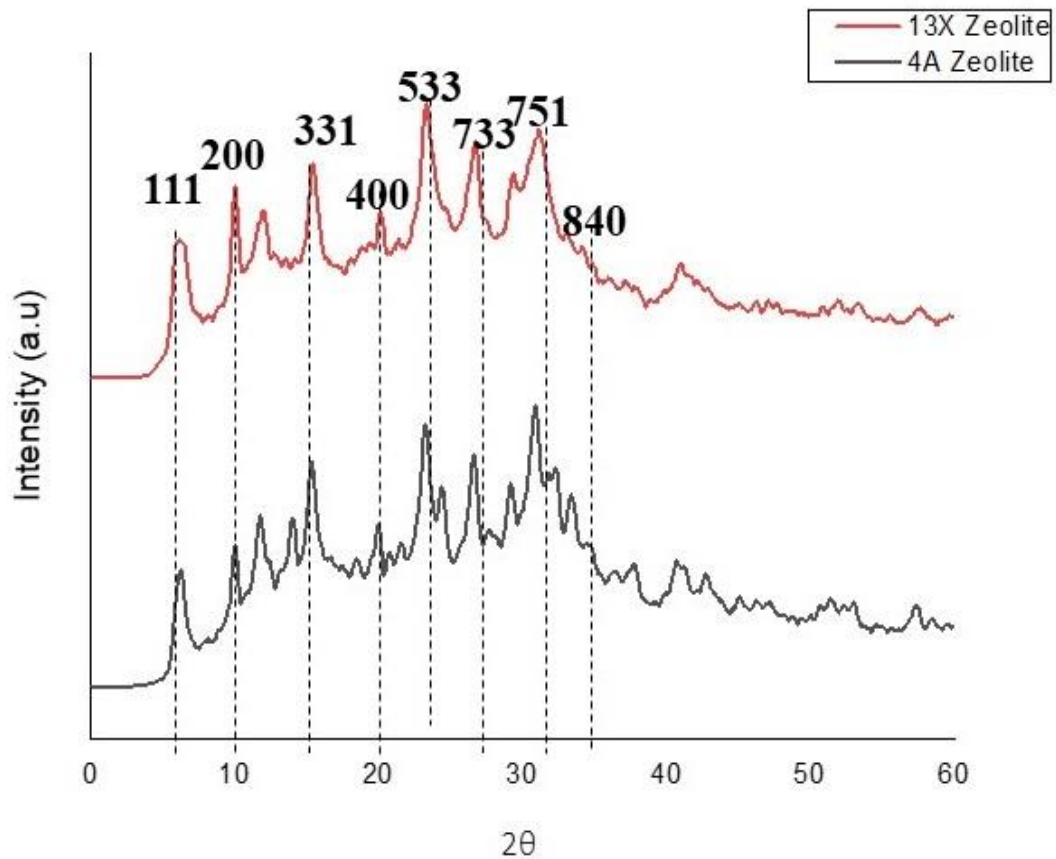


Figure 5-12. XRD of Zeolites

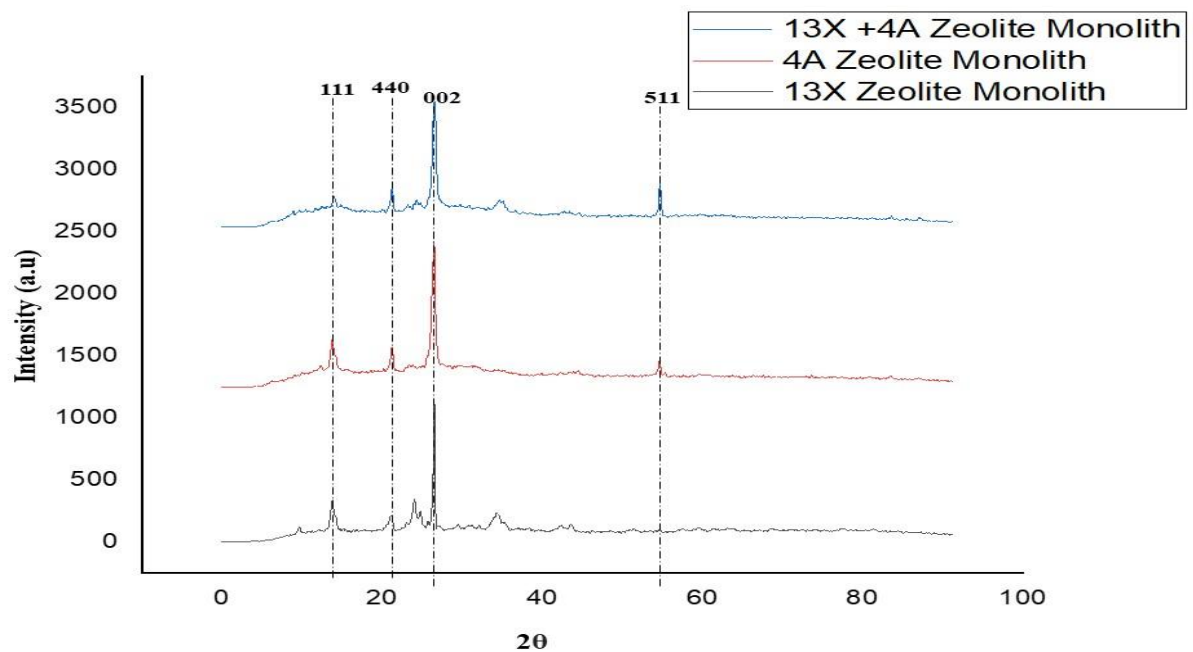


Figure 5-13. XRD of Zeolite Monoliths

5.7 CO₂ Adsorption study

The sample was inserted straight into the system as a powder. To remove any extra molecules and moisture content from the samples, they were heated to 100 degrees Celsius in a vacuum oven for over a day. The materials were degassed for 10 hours at a high temperature of 150 °C under vacuum to prepare them for the CO₂ adsorption study experiment. The temperature and pressure range for the adsorption studies were 298 K and 0–16 bar, respectively. After analyzing and importing the generated adsorption isotherms into Origin, graphs can be created.

The procedure for filling the sample is as follows. The sample's weight must first be determined using an analytical balance. Once the weight of the sample required for testing has been determined, take the measured sample, and make sure all necessary accessories are ready before filling samples. These accessories include a funnel, sample cell, screw rod, screwdriver, filling blocks, and filter foam. Measure the sample cell when it is empty. Take the funnel, place it inside the sample cell, and then add samples. Following the sample cell's fill, we weigh the sample

cell once again and subtract the difference between the sample-filled and empty cells to get the sample's weight. This gives us the sample's weight inside the sample cell. Once the samples are full, insert a single screw rod. To screw the rod, use the screwdriver. Prior to filling the last block, fill in the filter foam and a few filling blocks after screwing. Fill in the last filling block at the very end. Keep the filling block within the sample cell.

The process for testing samples is as follows.

M1 stands for the weight of a single empty cell. To lessen the chance of testing mistakes, fill in the sample using a funnel, making sure to fill in at least 0.08g of the sample. The sample cells should be installed in the proper places. Activate the pneumatic valve regulator and adjust the knob to set the output pressure to 0.5 MPa. Switch on the analyzer's power. To start the pretreatment procedure, open the analyzer and choose "setup" in the sample pretreatment zone. Remove the sample units and designate the sample weight as M2-M1 after the sample cells have been pretreated and weighed. Next, to start testing, connect the weighted sample cells to the analysis ports.

5.7.1 *Adsorption & Desorption Isotherms of Zeolite 13X*

The adsorption isotherms of the zeolite 13X are shown in the figure below. Both the desorption and the adsorption isotherms increase in a downward and upward direction, respectively. The adsorption analysis takes place between 0 and 16 bar of pressure at 45 °C. The graph, which displays the adsorption and desorption curves, is located between the CO₂ pressure (bar) and the CO₂ quantity adsorbed or desorbed (mmol/g).

As the pressure begins to rise from 0 to 2 bar, a little quantity of CO₂ is first adsorbed. The adsorption practically becomes persistent as the pressure rises; it is minimal in the 2 to 5 bar pressure range, so it becomes constant; and there is hardly any variation in the adsorption. Pressures greater than 6 bar result in an increase in the adsorption. Any pressure between 8 and 15 bar causes the adsorption to rise steadily. Adsorption increases between pressures of 12 and 15 bar, and when adsorption grows within this pressure range, there is a notable and abrupt increase in adsorption. At 15 pressure, this sample's CO₂ adsorption is 2.94 mmol/g.

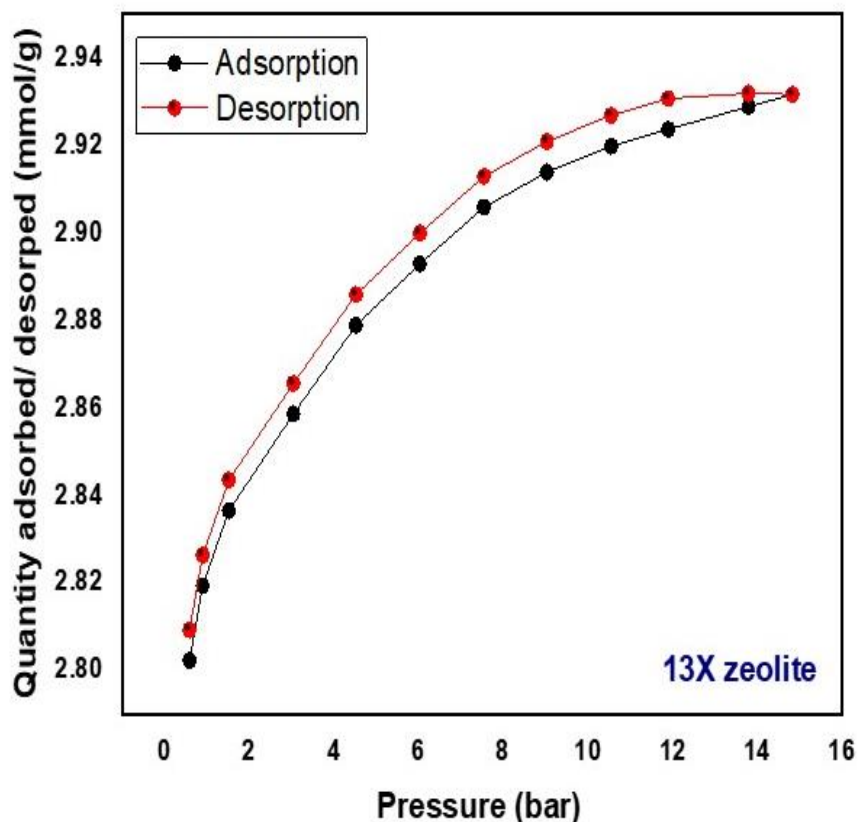


Figure 5-14. Adsorption/Desorption Isotherm of zeolite 13X

As per the desorption strategy, depressurization occurs whenever the pressure begins to decrease from 15 bar. The desorption curves follow the same general tendency as the adsorption curves. A large amount of CO₂ is absorbed during the same process when the pressure decreases from 15 to 11 bar. Desorption takes place when the additional pressure drops from 11 to 6 bar, as seen by the shift in the curve. when the pressure drops even lower, the curve becomes linear, and at 0.3 bar, the line becomes straight. Overall, 2.94 mmol/g of desorption was accomplished before stopping at 0.3 bar. This results in almost complete desorption.

5.7.2 Adsorption & Desorption Isotherms of Zeolite 4A

The adsorption/desorption isotherms of zeolite 4A are shown in the graph below. The desorption isotherm increases in a downward direction, whereas the adsorption isotherm increases in an ascending direction. The pressure range for the adsorption analysis is 0–15 bar, and it takes place at 45 °C. Demonstrates the sorption and desorption curves, with the graph centered between

the CO₂ pressure (bar) and the CO₂ amount absorbed/desorbed (mmol/g). For the examination of the CO₂ adsorption investigation, a 0.45g sample of Zeolite 4A composite is used.

Adsorption increases significantly when pressure rises from 0 to 2 bars at first; it increases with increasing pressure from 2 to 5 bars, reaches a plateau between 5 and 7 bars, and then experiences a dramatic spike from 8 to 11 bars, along with an increase in adsorption from 2.5 to 2.7 mmol/g. There is a linear trend in the rate of adsorption beginning at 13 bars of pressure and continuing continuously between 11 and 13 bars of pressure and there is an abrupt and rapid rise in adsorption; now when the pressure hits 13 bar, the adsorption is 2.9 mmol/g. At 13 bar of pressure, zeolite 4A absorbs at a rate of 2.9 mmol/g.

According to the desorption pattern, depressurization happens when the pressure begins to drop from 15 bar, and in zeolite 4A, there is a linear trend; as the pressure begins to drop from 15 bar, desorption begins, and it continues to grow. Between 12 and 6 bar, desorption is somewhat more pronounced. There is a good match between the adsorption line's trend and the desorption line. Desorption of CO₂ decreases with decreasing pressure from 8 bar to 0.5 bar, and then stops altogether. There was no loss of solubility and a detection limit of 0.0 mmol/g.

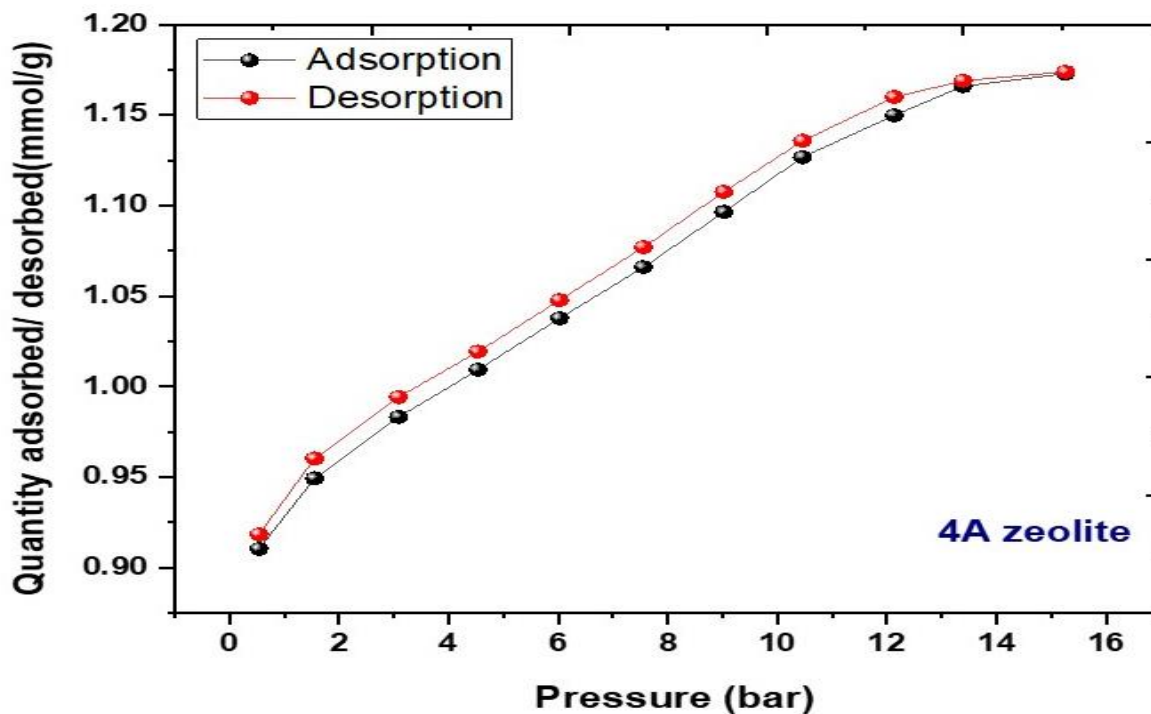


Figure 5-15. Adsorption/Desorption isotherm of Zeolite 4A

5.7.3 Adsorption & Desorption Isotherms of Zeolite 13X Monolith

The adsorption/desorption isotherms of the zeolite 13X monolith are shown in the picture. The desorption isotherm increases in a descending direction whereas the adsorption isotherm grows upward. The adsorption analysis takes place between 0 and 16 bar of pressure at 45 °C. The graph displays the adsorption and desorption curves, and it is positioned between the CO₂ pressure (bar) and the CO₂ amount that has been absorbed or desorbed (mmol/g). The CO₂ adsorption research investigation uses a 0.45g sample of the zeolite 13X monolith composite.

As the graph illustrates, adsorption begins at the beginning of the process when the pressure starts to build a range of 0 to 3 bars. As the pressure increases from 3 to 7 bar, the line becomes linear, and the rate of adsorption continues to grow. The quantity of CO₂ that has been taken in rises from 7 to 14 bar as the pressure rises. From 3.56 mmol/g to 3.64 mmol/g, the quantity of CO₂ adsorbed rises. Adsorption increases even further at pressures between 14 and 15 bar, when a large amount of CO₂ has been adsorbed.

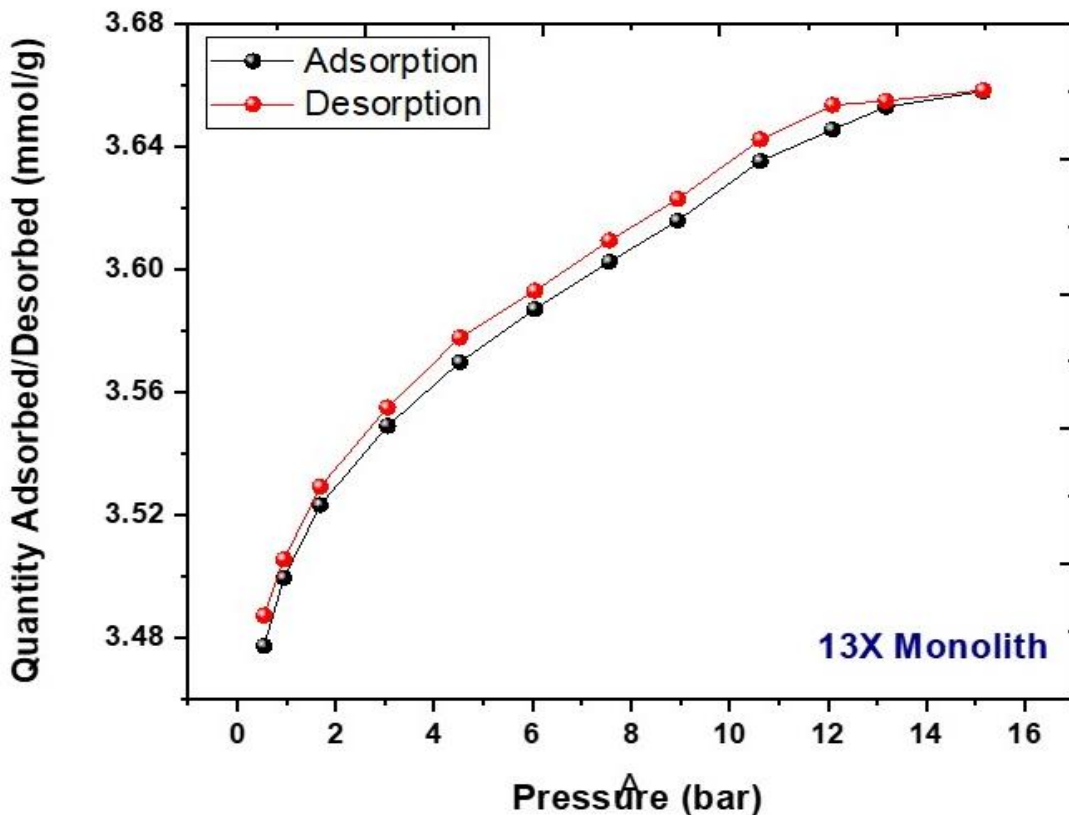


Figure 5-16. Adsorption/Desorption Isotherm of zeolite 13X Monolith

Adsorption of CO₂ at 15 bars is 3.68 mmol/g for this material. The adsorption of this sample increases and produces a much better outcome at a pressure of 15 bar compared to the Zeolite 13x sample. The Monolith ability to absorb the additional CO₂ is shown by the adsorption isotherm's rising trend.

When the pressure starts to decrease from 15 bar, depressurization occurs, as shown by the desorption pattern. After a large amount of CO₂ has been desorbed, the desorption isotherm appears as the pressure decreases from 15 to 11 bar.

At these pressures, the adsorption isotherm is at its sweet spot; however, when the pressure drops even lower, between 11 and 8 bar, the desorption isotherm almost straightens out, and desorbed CO₂ is little. Any residual CO₂ has been adsorbed as the pressure drops from 4 bar to 0.4 bar. At 0.4 bar of pressure, the desorption was determined to be 3.68 mmol/g and completed.

5.7.4 *Adsorption & Desorption Isotherms of Zeolite 4A Monolith*

The adsorption/desorption isotherms of the zeolite 4A monolith are shown in the figure below. Both the desorption and the adsorption isotherms increase in a downward and upward direction, respectively. The adsorption analysis takes place between 0 and 16 bar of pressure at 45 °C. It displays the adsorption and desorption curves, with the graph situated between the CO₂ pressure (bar) and the CO₂ amount absorbed or desorbed (mmol/g). To analyze the CO₂ adsorption investigation, a 0.45g sample of zeolite 4A monolith is employed.

As soon as the pressure increases from 0 to 2 bar, adsorption starts, and the quantity of CO₂ adsorbed increases virtually continuously and linearly. An increase in pressure from 2 to 8 bar may allow us to see a little rise in CO₂ adsorbed. Once again, we see a constant linear adsorption as the pressure increases from 8 to 11 bar, while adsorption happens at a much lower rate when the pressure increases from 11 to 15 bar. Maximum adsorption occurs at a pressure of 15 bar, with a specificity of 2.05 mmol/g. This material adsorbed 2.50 mmol/g of CO₂ at 15 bars. At a pressure of 15 bar, this sample's adsorption gives much less value compared to the prior one.

Depressurization begins at pressures below 15 bar, according to the desorption pattern. A drop in pressure from 15 to 11 bar triggers desorption. As a result of a substantial quantity of CO₂ being adsorbed, the desorption isotherm is seen.

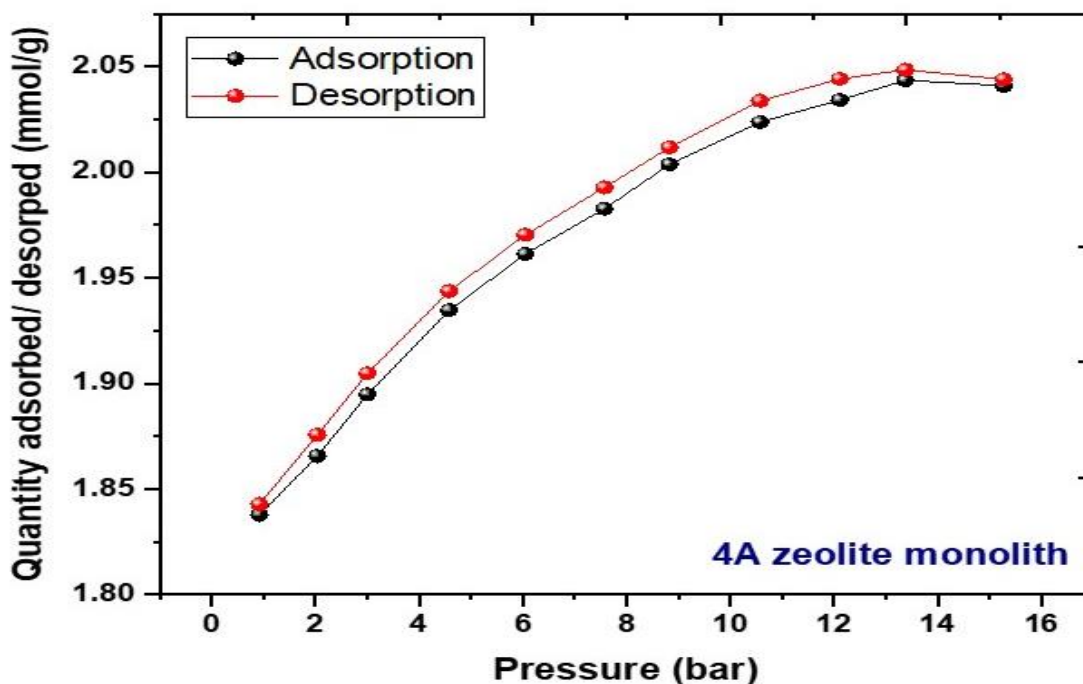


Figure 5-17. Adsorption/Desorption Isotherm of zeolite 4A monolith

It is situated on the adsorption isotherm, this pressure range is where the desorption isotherm largely flattens out; further reductions in pressure, from 11 to 8 bar, result in little desorbed CO₂. The remaining CO₂ has been adsorbed as the pressure drops from 4 bar to 0.5 bar. Desorption was found to terminate at 0.5 bar of pressure and a concentration of 2.05 mmol/g.

5.7.5 Adsorption & Desorption Isotherms of Zeolite 13X + 4A Monolith

The zeolite 13X+4A monolith's adsorption/desorption isotherms are shown in the image below. Both the desorption and the adsorption isotherms increase in a downward and upward direction, respectively. The pressure range for the adsorption analysis is 0–16 bar, and it takes place at 45 °C. It displays the adsorption and desorption curves, with the graph situated between the CO₂ pressure (bar) and the CO₂ amount absorbed or desorbed (mmol/g). For the examination of the CO₂ adsorption investigation, a 0.45g sample of the zeolite 13X+4A monolith is used. When pressure increases from 0 to 5 bar, adsorption increases. From 5 to 10 bars, it exhibits linear behaviors. From 10 to 12 bar, pressure increases even more, from 12 to 15 bar it increases more than usual single zeolite monoliths, where 4.90 mmol/g of CO₂ is absorbed overall.

When the pressure starts to fall below 15 bar, depressurization occurs, as seen in the desorption pattern. A noteworthy straight-line desorption occurs when the depressurization happens between 15 and 9 bar. Within this pressure range, As the pressure decreases further from 9-5 bar, a considerable quantity of CO₂ has been desorbed. Upon additional pressure reduction from 4-0 bar, almost all the CO₂ has been adsorbed. Stopping the desorption at 0.5 bar. The tendency of the desorption isotherm is the same as the adsorption isotherm. The isotherms for desorption have a nearly linear pattern. The result for the desorption was 4.90 mmol/g. In contrast to the composites discussed earlier, the adsorption and desorption of CO₂ for zeolite and its monoliths have less adsorption rate than the combine one.

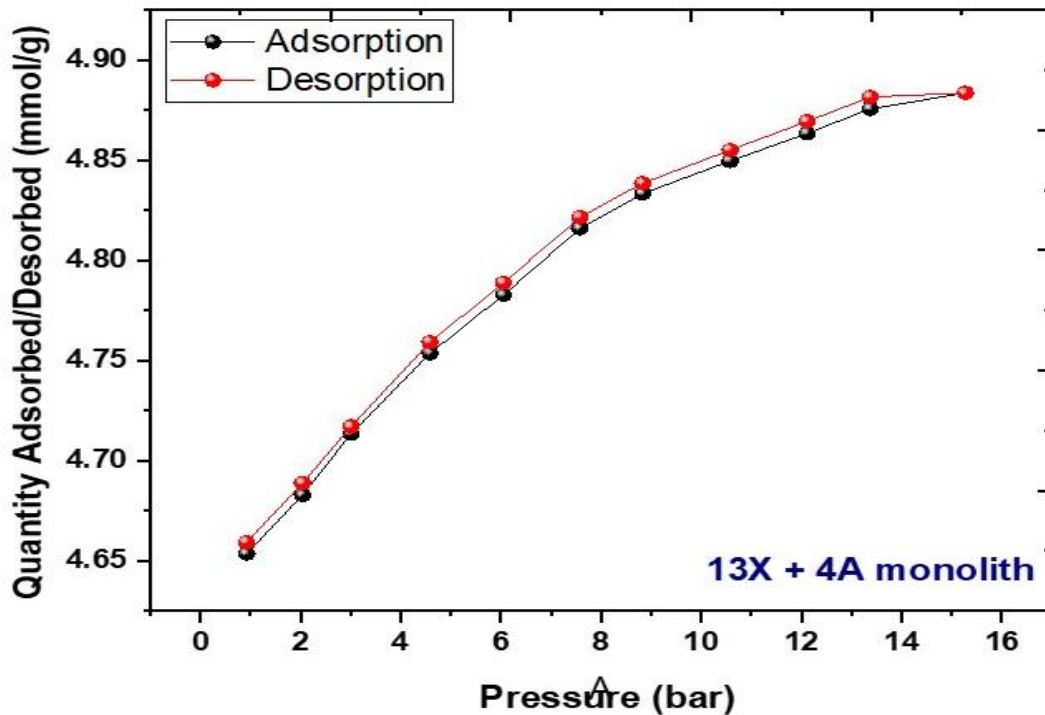


Figure 5-18. Adsorption/Desorption Isotherm of zeolite 13X +4A Monolith

The zeolite and its monolith generally have good adsorption capacity at even high pressure and monolith are shown in table good desorption. The zeolite 13X+4A monolith shows maximum capacity of 4.90 mmol/g CO₂ adsorption and zeolite 4A show less desorption capacity as 1.2mmol/g because of the Variations in the CO₂ adsorption capabilities of zeolite 4A are caused by variances in surface area, pore size, CO₂ molecular size, ion exchange capacity, and other structural

parameters. Synergistic effects arise from the combination, creating a material with a broader range of pore sizes that enhances the accommodation of various gas molecules. By increasing the surface area. The overall adsorption capabilities are enhanced and the number of active sites accessible for gas adsorption is increased by the combination. The combined monolith is more successful in targeted gas separation applications because the mixed zeolites increase selectivity for certain gases.

Better mass transfer and gas diffusion are made possible by the monolith structure, which accelerates adsorption kinetics and enhances overall performance. The monolith structure may be customized to operate optimally in a variety of gas purification or separation procedures.

Table 5-2. Summary of CO₂ adsorption analysis

Sr No	Zeolite and Monolith	Adsorption mmol/g
1	Zeolite 13X	2.94
2	Zeolite 4A	1.20
3	Zeolite 13X Monolith	3.68
4	Zeolite 4A Monolith	2.50
5	Zeolite 13X+4A Monolith	4.90

5.7.6 Comparison with literature

The table below compares our study with the literature and demonstrates that, when compared to the literature, our samples such as zeolite 13x ,4A and its monoliths have the greatest adsorption capacity and the largest adsorption capacity for the CO₂ gas. Our sample does not exhibit the constant line at the end of the isotherm, which indicates that monolith have moisture content somehow and still have the capacity to adsorb more CO₂. In contrast, the isotherms in the literature demonstrate that at high pressure, the adsorption lines become constant at the end of the isotherm, indicating that adsorbents get saturated and lose their ability to absorb more CO₂. Our investigations, which were conducted at a temperature of 45 degrees Celsius and a pressure range of 0 to 16 bar, demonstrate the strong adsorption capabilities of our composites, particularly our 3 weight percent composites, which exhibit the maximum CO₂ adsorption among the other

manufactured samples. As we have reviewed the literature, our findings therefore provide a complete justification for the earlier experiment conducted by other scientists. The literature show that the zeolite 13X+4A monolith have good adsorption capacity at even high pressure, this combined monolith shown 4.9mmol/good CO₂ adsorption due to high pore size abundant surface area, the ability to exchange ions, and other structural capabilities. The combined monolith has mixed zeolites that increases the selectivity for adsorption.

Table 5-3. Comparison table of zeolites and its monoliths

Sr. No.	Materials	Conditions	Adsorption	Ref.
1	Zeolite 13X	45 °C, 1-16bar	2.7	[55]
2	Mesoporous alumina	1-2 bar 25°C	1.2	[56]
3	Zeolite 13X+4A Monolith	45 c, 1-16bar	4.90	This work
4	Zeolite 4A Monolith	45 °C, 1-16bar	2.50	This work
5	Zeolite 13X Monolith	45 °C, 1-16bar	3.68	This work
6	Zeolite 4A	45 °C, 1-16bar	1.20	This work
7	Zeolite 13X	45 °C, 1-16bar	2.94	This work

CHAPTER 6 CONCLUSIONS AND RECOMMENDATION

This work aimed on the fabrication, characterization, and adsorption analysis of 13X and 4A zeolites, monolith synthesized using these zeolites and their mixture. Energy resources like fossil fuels with high CO₂ emissions contribute a lot to global climate change. Zeolites have the potential towards carbon capture, because of their large surface area, specific pore sizes, low cost, and molecular sieving ability. Hydrothermal preparation of the zeolites and monoliths was carried out. The samples were examined utilizing a variety of identifying methods, including XRD, SEM, FTIR, and BET. The FTIR study comprehensively identifies all functional groups present in our samples. The SEM images distinctly show the 2D framework and sheets of MOFs. The BET and particle size analyzer were used to see the physical properties of the particles. The results of XRD and FTIR were compared correctly with literature for the verification. The zeolites have a cubic shape with rounded corners and edges, indicating that they are pure phase and have a high degree of crystallinity. The particle size was seen to have a wide range which was also seen in SEM images for zeolite 13X. Zeolite 13x and its combined monolith showed a presence of oxygen, sodium (Na), Aluminum (Al), silicon (Si), and small portion of carbon (C) are the characteristic elements of zeolite monoliths. The adsorption capacity of carbon dioxide zeolites was checked using high pressure sorption analyzer. In general monoliths presented good adsorption capacity for carbon dioxide. Zeolite 13X+4A had the highest molar adsorption of 4.90mmol/g amongst the five studied samples. The monolith of zeolite 4A and 13X had the adsorption capacity of 2.50 and 3.68 mmol/g, respectively. While the 4A and 13X had an adsorption capacity of 1.20 and 2.94 mmol/g, respectively. The adsorption of carbon dioxide increased in each case with the increase in pressure because of higher collisions. The general trend shows a steep gradient to start with and then a gradual decrease in steepness until a uniform state is reached, which indicates saturation.

6.1 Future Recommendations

- Zeolite monoliths are used in energy storage applications, such as adsorption-based heat storage or gas storage for energy systems.
- Zeolite monoliths can serve as effective catalysts in various chemical reactions.

- Zeolite monoliths could be employed for water treatment, including the removal of contaminants such as heavy metals, organic pollutants, and ions.

REFERENCES

- [1] E. Wang et al., "Enhanced CO₂ capture by binary systems of pyridinium-based ionic liquids and porous ZIF-8 particles," vol. 128, pp. 415-423, 2019.
- [2] C. Chou, "Carbon dioxide separation and capture for global warming mitigation," *J. Adv. Eng. Technol*, vol. 1, pp. 2348–2931, 2013.
- [3] S. A. Rackley, "Overview of carbon capture and storage," *Carbon Capture and Storage*, pp. 23–36, 2017.
- [4] H. Yang *et al.*, "Progress in carbon dioxide separation and capture: A review," *Journal of environmental sciences*, vol. 20, no. 1, pp. 14–27, 2008.
- [5] J. Liu, P. K. Thallapally, B. P. McGrail, D. R. Brown, and J. Liu, "Progress in adsorption-based CO₂ capture by metal–organic frameworks," *Chem Soc Rev*, vol. 41, no. 6, pp. 2308–2322, 2012.
- [6] R. M. Barrer, "Zeolites and clay minerals as sorbents and molecular sieves," (*No Title*), 1978.
- [7] S. Cavenati, C. A. Grande, and A. E. Rodrigues, "Adsorption equilibrium of methane, carbon dioxide, and nitrogen on zeolite 13X at high pressures," *J Chem Eng Data*, vol. 49, no. 4, pp. 1095–1101, 2004.
- [8] R. Xu, W. Pang, J. Yu, Q. Huo, and J. Chen, *Chemistry of zeolites and related porous materials: synthesis and structure*. John Wiley & Sons, 2009.
- [9] N. Huang and B. Feng, "Facile synthesis of PEI-GO@ ZIF-8 hybrid material for CO₂ capture," vol. 43, no. 4, pp. 2224-2231, 2018
- [10] G. Petrecca, "Energy Conversion and Management," *Cham: Springer International Publishing*, 2014.

- [11] F. N. Tubiello, M. Salvatore, S. Rossi, A. Ferrara, N. Fitton, and P. Smith, "The FAOSTAT database of greenhouse gas emissions from agriculture," *Environmental Research Letters*, vol. 8, no. 1, p. 015009, 2013.
- [12] D. Nong, P. Simshauser, and D. B. Nguyen, "Greenhouse gas emissions vs CO₂ emissions: Comparative analysis of a global carbon tax," *Appl Energy*, vol. 298, p. 117223, 2021.
- [13] M. N. Dudin, E. E. Frolova, O. V. Protopopova, O. Mamedov, and S. V. Odintsov, "Study of innovative technologies in the energy industry: nontraditional and renewable energy sources," *Entrepreneurship and Sustainability Issues*, vol. 6, no. 4, p. 1704, 2019.
- [14] M. A. Clark *et al.*, "Global food system emissions could preclude achieving the 1.5 and 2 C climate change targets," *Science (1979)*, vol. 370, no. 6517, pp. 705–708, 2020.
- [15] B. Furukawa, K. E. Cordova, M. O’Keeffe, and O. Yaghi, "The chemistry and applications of metal-organic frameworks," vol. 341, no. 6149, p. 1230444, 2013.
- [16] G. -S. Zhai, L. Cao, and X.-H. Xia, "Synthesis of graphitic carbon nitride through pyrolysis of melamine and its electrocatalysis for oxygen reduction reaction," *Chinese Chemical Letters*, vol. 24, no. 2, pp. 103-106, 2013.
- [17] J. Yuan *et al.*, "Graphite carbon nitride nanosheets decorated with ZIF-8 nanoparticles: effects of the preparation method and their special hybrid structures on the photocatalytic performance," vol. 762, pp. 98-108, 2018.
- [18] US Department of energy, "Energy Storage Grand Challenge: Energy Storage Market Report," 2020.
- [19] I. Casas, J. Schell, R. Blom, M. J. S. Mazzotti, and P. Technology, "MOF and UiO-67/MCM-41 adsorbents for pre-combustion CO₂ capture by PSA: Breakthrough experiments and process design," vol. 112, pp. 34-48, 2013.
- [20] M. Goel, "Carbon capture and storage, energy future and sustainable development: Indian perspective," *Carbon Capture and Storage. Narosa Publishing House, New Delhi*, pp. 3–14, 2008.

- [21] I. Sreedhar, R. Aniruddha, and S. Malik, "Carbon capture using amine modified porous carbons derived from starch" *SN Appl Sci*, vol. 1, pp. 1–11, 2019.
- [22] K. C. N. S. and Tomasz K. Paweł Madejski, "Methods and Techniques for CO₂ Capture: Review of Potential Solutions and Applications in Modern Energy Technologies," 2022.
- [23] J. Park, D. Yuan, K. T. Pham, J.-R. Li, A. Yakovenko, and H.-C. Zhou, "Reversible alteration of CO₂ adsorption upon photochemical or thermal treatment in a metal–organic framework," *J Am Chem Soc*, vol. 134, no. 1, pp. 99–102, 2012.
- [24] A. Dhakshinamoorthy and H. Garcia, "Catalysis by metal nanoparticles embedded on metal–organic frameworks," *Chem Soc Rev*, vol. 41, no. 15, pp. 5262–5284, 2012.
- [25] K. Haque. Jun, and S. Jhung, "Adsorptive removal of methyl orange and methylene blue from aqueous solution with a metal-organic framework material, iron terephthalate (MOF-235)," vol. 185, no. 1, pp. 507-511, 2011.
- [26] S. Abuelgasim, W. Wang, and A. Abdalazeez, "A brief review for chemical looping combustion as a promising CO₂ capture technology: Fundamentals and progress," *Science of The Total Environment*, vol. 764, p. 142892, 2021.
- [27] A. Kaithwas, M. Prasad, A. Kulshreshtha, and S. Verma, "Industrial wastes derived solid adsorbents for CO₂ capture: A mini review," *Chemical Engineering Research and Design*, vol. 90, no. 10, pp. 1632–1641, 2012.
- [28] S. A. Rackley, "Overview of carbon capture and storage," *Carbon Capture and Storage*, pp. 23–36, 2017.
- [29] C. Dhoke, A. Zaabout, S. Cloete, and S. Amini, "Review on Reactor Configurations for Adsorption-Based CO₂ Capture," *Ind Eng Chem Res*, vol. 60, no. 10, pp. 3779–3798, Mar. 2021.
- [30] Q. Wang, J. Luo, Z. Zhong, and A. Borgna, "CO₂ capture by solid adsorbents and their applications: current status and new trends," *Energy Environ Sci*, vol. 4, no. 1, pp. 42–55, 2011.

- [31] D. G. Boer, J. Langerak, and P. P. Pescarmona, "Zeolites as Selective Adsorbents for CO₂ Separation," *ACS Appl Energy Mater*, vol. 6, no. 5, pp. 2634–2656, Mar. 2023.
- [32] C. Kempahanumakkagari, K. Vellingiri, A. Deep, E. E. Kwon, N. Bolan, and Kim, "Metal–organic framework composites as electrocatalysts for electrochemical sensing applications," vol. 357, pp. 105-129, 2018.
- [33] C. S. Cundy and P. A. Cox, "The hydrothermal synthesis of zeolites: Precursors, intermediates and reaction mechanism," *Microporous and Mesoporous Materials*, vol. 82, no. 1, pp. 1–78, 2005.
- [34] A. Khaleque *et al.*, "Zeolite synthesis from low-cost materials and environmental applications: A review," *Environmental Advances*, vol. 2, p. 100019, 2020.
- [35] T. Derbe, S. Temesgen, and M. Bitew, "A short review on synthesis, characterization, and applications of zeolites," *Advances in Materials Science and Engineering*, vol. 2021, pp. 1–17, 2021.
- [36] F. Bahmanzadegan, M. A. Pordsari, and A. Ghaemi, "Improving the efficiency of 4A-zeolite synthesized from kaolin by amine functionalization for CO₂ capture," *Sci Rep*, vol. 13, no. 1, p. 12533, 2023.
- [37] A. Hedayati, B. A. Delica, S. Perez-Gil, and S. Prieto-Fernandez, "Evaluation of high-performance adsorbents for separation of CO₂ from industrial effluent gases," *Greenhouse Gases: Science and Technology*, vol. 13, no. 2, pp. 216–226, 2023.
- [38] M. Cavallo, M. Dosa, N. G. Porcaro, F. Bonino, M. Piumetti, and V. Crocellà, "Shaped natural and synthetic zeolites for CO₂ capture in a wide temperature range," *Journal of CO₂ Utilization*, vol. 67, p. 102335, 2023.
- [39] A. M. Najafi, S. Soltanali, and H. Ghassabzadeh, "Enhancing the CO₂, CH₄, and N₂ adsorption and kinetic performance on FAU zeolites for CO₂ capture from flue gas by metal incorporation technique," *Chemical Engineering Journal*, vol. 468, p. 143719, 2023.
- [40] T. Zhao *et al.*, "Microporous carbon coated zeolite particles for efficient carbon capture from wet flue gas," *Sep Purif Technol*, vol. 317, p. 123762, 2023.

- [41] N. Agata, P. Agrawal, J. Cesarano, M. Niehaus, T.-M. J. Richardson, and S. Bigham, "Carbon Dioxide Adsorption Process of 3D Zeolite-13X Structures: A Numerical Study," 2023 International Conference on Environmental Systems, 2023.
- [42] D. Panda, E. A. Kumar, and S. K. Singh, "Introducing mesoporosity in zeolite 4A bodies for Rapid CO₂ capture," *Journal of CO₂ Utilization*, vol. 40, p. 101223, 2020.
- [43] J. Hedlund, G. Garcia, M. Balsamo, M. Zhou, and J. Mouzon, "Microchannel zeolite 13X adsorbent with high CO₂ separation performance," *Sep Purif Technol*, vol. 277, p. 119483, 2021.
- [44] E. Davarpanah *et al.*, "CO₂ capture on natural zeolite clinoptilolite: Effect of temperature and role of the adsorption sites," *J Environ Manage*, vol. 275, p. 111229, 2020.
- [45] D. Panda, S. K. Singh, and E. Anil Kumar, "Surface Remodelling of Zeolite 4A Bodies for CO₂ Capture: A Case Study," in *Advances in Energy Research, Vol. 2: Selected Papers from ICAER 2017*, Springer, 2020, pp. 541–549.
- [46] W. Y. Hong, S. P. Perera, and A. D. Burrows, "Comparison of MIL-101 (Cr) metal-organic framework and 13X zeolite monoliths for CO₂ capture," *Microporous and Mesoporous Materials*, vol. 308, p. 110525, 2020.
- [47] B. Ozturk, S. Demiral, and H. A. Ozen, "Adsorptive capture of CO₂ by amine-impregnated activated carbon, pumice, and zeolite 4A," *Greenhouse Gases: Science and Technology*, vol. 12, no. 5, pp. 602–615, 2022.
- [48] P. Murge, S. Dinda, and S. Roy, "Zeolite-Based Sorbent for CO₂ Capture: Preparation and Performance Evaluation," *Langmuir*, vol. 35, no. 46, pp. 14751–14760, Nov. 2019.
- [49] N. Li *et al.*, "Porous metal-organic frameworks for gas storage and separation: Status and challenges," vol. 1, no. 1, p. 100006, 2019.
- [50] J. Epp, "X-ray diffraction (XRD) techniques for materials characterization," in *Materials characterization using nondestructive evaluation (NDE) methods*, Elsevier, 2016, pp. 81–124.

- [51] Z. Chen, K. Adil, Ł. J. Weseliński, Y. Belmabkhout, and M. Eddaoudi, "A supermolecular building layer approach for gas separation and storage applications: The eea and rtl platforms for CO₂ capture and hydrocarbon separation," vol. 3, no. 12, pp. 6276-6281, 2015.
- [52] N. Z. Zulkurnai, U. Md Ali, N. Ibrahim, and N. Manan, "Carbon Dioxide Capture by Deep Eutectic Solvent Impregnated Sea Mango Activated Carbon," *E3S Web of Conferences*, vol. 34, p. 02030, Jan. 2018.
- [53] P. Wang, Q. Sun, Y. Zhang, and J. Cao, "Synthesis of Zeolite 4A from Kaolin and Its Adsorption Equilibrium of Carbon Dioxide," *Materials*, vol. 12, p. 1536, May 2019, doi: 10.3390/ma12091536.
- [54] J. B. Higgins, *Collection of simulated XRD powder patterns for zeolites*. Elsevier Science & Technology, 2007.
- [55] E. Davarpanah *et al.*, "CO₂ capture on natural zeolite clinoptilolite: Effect of temperature and role of the adsorption sites," *J Environ Manage*, vol. 275, p. 111229, 2020.
- [56] C. Chen and W.-S. Ahn, "CO₂ capture using mesoporous alumina prepared by a sol-gel process," *Chemical Engineering Journal*, vol. 166, no. 2, pp. 646–651, 2011.